Soft Matter

REVIEW

View Article Online
View Journal | View Issue

Cite this: *Soft Matter*, 2024, **20**, 2635

Dilute polyelectrolyte solutions: recent progress and open questions†

Carlos G. Lopez, ‡*[a] Atsushi Matsumoto *[b] and Amy Q. Shen *[c]

Received 9th April 2023,
Accepted 22nd November 2023

DOI: 10.1039/d3sm00468f

rsc.li/soft-matter-journal

Polyelectrolytes are a class of polymers possessing ionic groups on their repeating units. Since counterions can dissociate from the polymer backbone, polyelectrolyte chains are strongly influenced by electrostatic interactions. As a result, the physical properties of polyelectrolyte solutions are significantly different from those of electrically neutral polymers. The aim of this article is to highlight key results and some outstanding questions in the polyelectrolyte research from recent literature. We focus on the influence of electrostatics on conformational and hydrodynamic properties of polyelectrolyte chains. A compilation of experimental results from the literature reveals significant disparities with theoretical predictions. We also discuss a new class of polyelectrolytes called poly(ionic liquid)s that exhibit unique physical properties in comparison to ordinary polyelectrolytes. We conclude this review by listing some key research challenges in order to fully understand the conformation and dynamics of polyelectrolytes in solutions.

1 Introduction

The field of polymer science emerged as a distinct scientific discipline in 1920, with the core concept based on the macromolecular hypothesis proposed by Staudinger.[1] Since then, it has been well accepted that polymers are made of molecules covalently bonded to each other. The definition by IUPAC states that polymers are substances composed of macromolecules with a molecular weight exceeding several thousand.[2] During the past century, polymer chemists have made significant advances in creating new polymer species and controlling the polymerisation process, while polymer physicists have focused on understanding the properties of polymers by using theoretical, computational, and experimental approaches. As a result, polymer-based materials are prevalent and extensively used in various industries and daily products.[3]

Despite the significant research progress in the physics of non-ionic polymers, the properties of which (especially in dilute solutions) are relatively well understood, less advancement has been made in charged polymers. Polyelectrolytes, which received their name from Raymond M. Fuoss in 1948,[4] are a class of ion-containing polymers. Historically, polymers with relatively low ion-contents (10–15%) were defined as ionomers, while polymers with very high ion-contents were defined as polyelectrolytes.[5] A better definition was proposed based on the physical properties of ion-containing polymers:[6] polyelectrolytes are polymers whose properties in solution are governed by electrostatic repulsion between dissociated groups along the chain, while ionomers are polymers in which the bulk properties are governed by ionic interactions (*i.e.*, dipole interactions between ion pairs) in discrete regions of the polymer material where attractive forces dominates. In fact, some ion-containing polymers have exhibited transition from ionomer-like to polyelectrolyte-like behaviours, depending on, for example, the temperature.[7] Polyelectrolytes can be further divided into two groups depending on the nature of the ionic groups.[8] Weak polyelectrolytes are conventionally defined as polymers with weakly acidic or basic groups, in contrast to strong polyelectrolytes, which are composed of polymers with definitive strong acid or base groups.[9–12] Note that this differs from strongly charged and weakly charged polyelectrolytes, which refer to systems with high and low densities of ionic monomers along the backbone, respectively. However, there is no universally agreed-upon threshold that defines 'high' *versus* 'low' charge density. Vinylic polyelectrolytes, which carry approximately one charge every 0.2–0.3 nm (*e.g.*, PSS), and polysaccharides that have one charge per monomer unit, equating to roughly one charge every 0.5 nm, are considered as strongly charged.

[a] *Institute of Physical Chemistry, RWTH Aachen University, Aachen, 52056, Germany*
[b] *Department of Applied Chemistry and Biotechnology, Graduate School of Engineering, University of Fukui, 3-9-1 Bunkyo, Fukui City, Fukui 910-8507, Japan. E-mail: atsushi5@u-fukui.ac.jp*
[c] *Micro/Bio/Nanofluidics Unit, Okinawa Institute of Science and Technology Graduate University, 1919-1 Tancha, Onna-son, Okinawa 904-0495, Japan. E-mail: amy.shen@oist.jp*

† Electronic supplementary information (ESI) available. See DOI: https://doi.org/10.1039/d3sm00468f

‡ Present address: Department of Materials Science and Engineering, Penn State University, University Park, Pennsylvania 16802, USA, E-mail: cvg5719@psu.edu

Regardless of the type of polyelectrolytes, their conformation in solution is significantly influenced by the electrostatic interactions. The modelling of charged polymers is rather complicated since ions on the backbone chain are covalently bonded. For example, it is widely accepted that some counterions stay bound (condensed) in the vicinity of the chain backbone due to strong electrostatic attractions between polyions and counterions. This phenomenon is called the counterion condensation.[13] As a result, the effective charge fraction on a polyelectrolyte chain in solution is not always equal to the charge density (*i.e.*, the number of ionic monomers) of the chain. Many theoretical models with different approaches have been reported in the literature, and their predictions could explain some properties of polyelectrolyte solutions.[9,10,14,15] However, many conflicting results between experimental data and theoretical predictions have been reported, even for linear polyelectrolyte chains in solutions.

The number of factors and lengthscales which control the solution properties[14,16,17] is larger for charged polymers than for neutral polymers, making polyelectrolyte theory lag behind that of neutral polymers. These highly complex systems are difficult to study experimentally. For example, if we study the rheology of a neutral polymer in solution, measurements varying the polymer concentration, molar mass, solvent quality and temperature will usually suffice to understand the given system. However, for a polyelectrolyte, additional physical quantities, such as the charge density, the counterion size and its valence, the added salt concentration, and the dielectric constant of the solvent, all become relevant experimental variables. Moreover, it is not possible to define a single solvent quality, and the chemical structure of the polyelectrolyte backbone, side-chain ions and counterions have to be considered separately. In concentrated solutions, the polyelectrolyte systems exhibited fascinating dynamics[18–29] which we are only beginning to understand. Their ability to form complexes with oppositely charged matter made them relevant to many industrial formulations and biological systems and is one of the main aspects of polyelectrolyte research today.[30–34]

We would also like to highlight an emerging category of polyelectrolytes known as poly(ionic liquid)s or polymerized ionic liquids. In this context, poly(ionic liquid)s (PILs) denote polymers in which ionic liquid structures are covalently integrated into the repeating units.[35,36] Here, ionic liquids (ILs) are molten salts consisting of cations or anions which melt below 100 °C.[37] Fig. 1 displays representative chemical structures of a PIL polycation and its counteranions: PIL ions are relatively large, asymmetric, and charge delocalized, making the physical properties of PILs different from those of ordinary ion-containing polymers.[38] For example, PILs have exhibited glass transition at relatively low temperatures even if the charge density is high.[39] This unique glass transition behaviour of PILs has led to active research in manipulating the bulk properties of PILs, *e.g.*, their ionic conductivity and viscoelasticity, which have been extensively investigated over the past decade.[40–53] The research community acquired a basic understanding of the behaviour of PILs, which function similarly to ionomers.

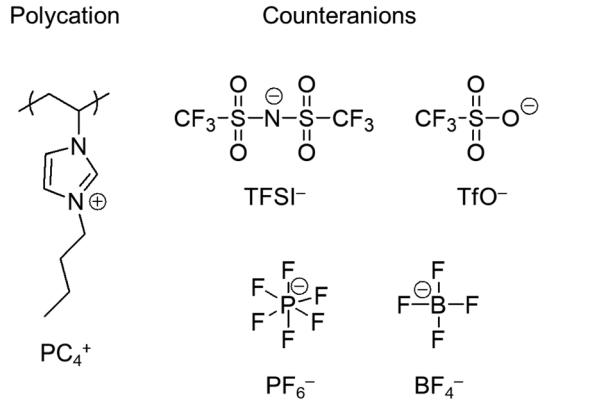

Fig. 1 Representative chemical structures of a PIL polycation and four different types of counteranions. Polycation: PC_4^+; poly(1-butyl-3-vinylimidazolium), counteranions: $TFSI^-$; bis(trifluoromethanesulfonyl)imide, TfO^-; trifluoromethanesulfonate, PF_6^-; hexafluorophosphate, BF_4^-; tetrafluoroborate.

However, the solution properties of PILs, *i.e.*, the behaviour of PILs as polyelectrolytes, have been scarcely investigated.

In solution, PILs can release their counterions into the solvent and possess charges on their chain backbone, showing similar properties to those of ordinary polyelectrolytes, such as poly(sodium styrenesulfonate).[54] In contrast to ordinary polyelectrolytes, PILs can be dissolved in solvents with a wide range of dielectric constants even if the charge density on PIL chains is high.[55] Good solubility of PILs can also be obtained in pure ILs.[55] The unique features of PILs in solutions have raised many interesting questions in the polyelectrolyte research community. For example, how do PILs behave in solvents with low dielectric constants?[56] According to the Manning model for counterion condensation,[13] the number of dissociated counterions is predicted to decrease with decreasing solvent dielectric constant. If so, PILs would behave as neutral polymers or as ionomers in low-dielectric solvents. Investigating the charge screening effects exerted by ionic liquid ions on polymerized ionic liquid chains within pure ionic liquids offers an interesting research avenue, especially considering the distinctive solvent characteristics of ionic liquids.[57]

Our primary aims are (1) to establish scaling laws that elucidate the relationship between the properties of polyelectrolytes and variables such as molar mass, salt concentration, and charge fraction; (2) to test the theoretical models reviewed in Section 2; and (3) to highlight experimental results which expand or challenge the current framework of polyelectrolyte physics. We provide a critical overview of several key questions in polyelectrolyte physics, with an emphasis on the experimental literature where new conclusions can be drawn by compiling and/or re-analysing existing data. We hope this perspective will complement earlier reviews in the field which have focused on the development of theory,[9,15,58–62] simulations,[9,63,64] and particular experimental methods, systems, or properties.[65–81] This article narrows its scope to exploring the intricacies of dilute polyelectrolyte solutions.[82] For experimental reviews dealing with non-dilute solutions and gels, we direct readers to ref. 14, 68 and 83–85.

This review article is structured as follows: Section 2 introduces several theoretical models proposed in the literature to represent the conformation of dilute polyelectrolyte solutions; Section 3 discusses the properties of polyelectrolytes in the dilute regime, dividing our discussion into sixteen subsections along with research questions related to the conformation and dynamics of single chains in solution; Section 4 concludes our review and highlights open questions.

2 Theoretical approaches to the conformation and dynamics of polyelectrolytes in solution

Dilute polymer solutions are defined as those in which the chains do not overlap.[14,86] Considering a chain made up of N chemical monomers with an end-to-end distance R, the overlap concentration (c^*) in units of number of repeating units per volume is:

$$c^* = \frac{N}{R^3}. \tag{1}$$

In this article, we use the symbol c to refer to the concentration, measured as the number of monomers per unit volume. When plotting data or quoting concentration values, it is more convenient to use concentrations in moles of monomers per volume. This is represented by 'M', which denotes moles of monomers per dm^3. Intrinsic viscosities are in units of M^{-1} as opposed to the more common units of dL g^{-1}. We also use N instead of molar masses. The following example illustrates the reason for these choices: suppose we compare the properties of polystyrene sulfonate (PSS) with Na^+ and Cs^+ counterions. Let us assume that the conformation of the chains is not influenced by the choice of counterion. A plot of c^* or $[\eta]$ *vs.* N will overlap for both PSS salts when expressed in units of M and M^{-1}, respectively, thus capturing the essential physics that the chain conformation is unchanged. In contrast, a plot of c^* in g L^{-1} *vs.* M_w results in two separate curves for NaPSS and CsPSS because the Cs^+ ion has a larger mass than the Na^+ ion. A few exceptions, such as in Fig. 6, use the concentration in mass per volume (c_p) as part of a dimensionless product.

2.1 Conformation in dilute salt-free solutions

2.1.1 Scaling approach. The scaling approach to polymer conformation and dynamics was primarily developed by de Gennes *et al.* and Pfeuty and Dobrynin *et al.*[87–90] Consider a polyelectrolyte chain with a bare (non-electrostatic) Kuhn length $l_{K,0}$. Each Kuhn segment is made up of g_K chemical monomers with length b ($l_{K,0} = g_K b$). For chains with characteristic lengthscales smaller than the Kuhn length, they are rigid, and their end-to-end distance R scales as

$$R \simeq bN \quad \text{for } N \leq g_K. \tag{2}$$

For chains with end-to-end distances larger than a Kuhn segment, they adopt random walk statistics up to the thermal blob size ξ_T. Each thermal blob contains g_T monomers; therefore, the end-to-end distance of the chains (between the $l_{K,0}$ and ξ_T) is given by

$$R \simeq l_{K,0}\left(\frac{N}{g_K}\right)^{1/2} \quad \text{for} \quad g_K \leq N \leq g_T. \tag{3}$$

If the end-to-end distance is larger than ξ_T, the polymer conformation depends on the solvent quality exponent ν:

$$R \simeq \xi_T\left(\frac{N}{g_T}\right)^{\nu} \quad \text{for} \quad g_T \leq N \leq g_{el}, \tag{4}$$

where $\nu = \frac{1}{3}$ for poor solvents, $\nu = \frac{1}{2}$ for theta solvents, and $\nu = \frac{3}{5}$ for good solvents. Here, ξ_T is given by eqn (3) with $N = g_T$.

The next relevant lengthscale is the size of the electrostatic blob. This marks the distance at which the electrostatic energy is of the order of the thermal energy k_BT, where k_B is the Boltzmann constant and T is the absolute temperature. The Coulomb energy of an electrostatic blob is

$$U_{el} \simeq (g_{el}f)^2 e^2/(\varepsilon_0\varepsilon_r\xi_{el}), \tag{5}$$

where f is the fraction of monomers bearing a dissociated charge, *i.e.*, the charge fraction, and g_{el} is the number of chemical monomers inside an electrostatic blob. The end-to-end distance of the electrostatic blob is

$$\xi_{el} = \begin{cases} (l_{K,0}b)^{2/3}\left(\dfrac{1}{l_B f^2}\right)^{1/3} & \text{for } T \ll \theta, \\ (l_{K,0}b)^{2/3}\left(\dfrac{1}{l_B f^2}\right)^{1/3} & \text{for } T = \theta, \\ (l_{K,0}b)^{6/7}\xi_T{}^{-2/7}\left(\dfrac{1}{l_B f^2}\right)^{3/7} & \text{for } T > \theta, \end{cases} \tag{6}$$

where l_B is the Bjerrum length and θ is the theta temperature. Eqn (6) was derived by using the equations of $\xi_{el} = \xi_T\left(\frac{g_{el}}{g_T}\right)^{\nu}$ and $\xi_T = \sqrt{l_{K,0}bg_T}$ (ref. 90) under the assumption of $U_{el} = k_BT$ for $T \geq \theta$ and $U_{el} = \gamma\xi_{el}$ for $T \ll \theta$, where γ is the polymer/solvent interfacial tension, given by $\gamma \approx \frac{\tau^2 k_B T}{\xi_T{}^2}$ with $\tau \equiv \frac{\theta - T}{\theta}$ being the reduced temperature.

On distances larger than the electrostatic blob size, the chain is stretched, and its conformation is a pole of electrostatic blobs:

$$R \simeq \xi_{el}\frac{N}{g_{el}} \quad \text{for} \quad N \geq g_{el}, \tag{7}$$

where ξ_{el} is given by eqn (6). The schematic illustration of a dilute polyelectrolyte chain is shown in Fig. 2. In the model reported by Dobyrnin *et al.* in 1995,[89] the shortest lengthscale considered was the monomer size, which was equated to the thermal blob size and the Kuhn length, corresponding to $\xi_T = l_{K,0} = b$ in the above equations. The updated scaling model of Dobrynin and Jacobs[90,91] worked out the solution properties of polyelectrolytes for arbitrary values of ξ_T and ξ_{el}.

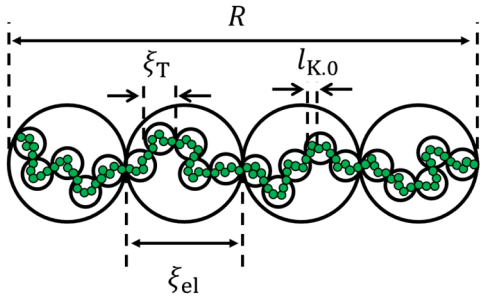

Fig. 2 Dilute polyelectrolyte chain adopts an extended configuration of electrostatic blobs of length ξ_{el} inside which the conformation is a self-avoiding walk of thermal blobs with length ξ_T. A random walk of Kuhn segments with length $l_{K,0}$ forms the thermal blob.

The conformation of polyelectrolytes is often quantified through the 'stretching parameter' (B), which is the ratio of the end-to-end distance of an electrostatic blob (ξ_{el}) to its fully stretched contour length:

$$B = \frac{bg_{el}}{\xi_{el}} = \begin{cases} b^{4/3} l_{K,0}^{-2/3} \left(l_B f^2\right)^{-2/3} & \text{for } T \ll \theta, \\ b^{2/3} l_{K,0}^{-1/3} \left(l_B f^2\right)^{-1/3} & \text{for } T = \theta, \\ b^{4/7} l_{K,0}^{-3/7} \xi_T^{1/7} \left(l_B f^2\right)^{-2/7} & \text{for } T > \theta. \end{cases} \quad (8)$$

The stretching parameter $B \simeq 1$ for semiflexible polyelectrolytes represents a fully stretched state.[23,92–94] For flexible systems, values of $B \simeq 2$–5 are common.[95–97] The end-to-end distance of a polyelectrolyte chain is $R = bN/B$.

If the thermal blob is larger than the electrostatic blob, then eqn (3) is valid for $g_K \leq N \leq g_{el}$. Equivalently, setting $\nu = 1/2$ in eqn (4) gives the same result. If the electrostatic blob is smaller than the Kuhn length, the equations above expect the polyelectrolyte to be in a fully stretched configuration so that $R \simeq bN$. This 'rod-like' configuration assumes no transverse fluctuations. In some cases, it was found that salt-free polyelectrolytes adopted a directed random walk configuration.[98,99] In the next section, we will address the experimental evidence concerning this issue.

Polyelectrolytes having more than one dissociated charge per Kuhn segment ($g_K > f^{-1}$) are sometimes referred to as strongly charged polyelectrolytes. In this case, the above equations predict $\xi_{el} < l_{K,0}$, so that the electrostatic blob concept should not apply. Note that if Manning condensation holds, this is always the case if $l_{K,0} > l_B$ and $\delta > 1/g_K$. Here, δ denotes the fraction of monomers that contain an ionic group. Some experimental evidence[100] suggests that the Coulomb energy inside an electrostatic blob may significantly exceed k_BT, thus adding a pre-factor to eqn (5) and making the size of electrostatic blobs larger than expected by eqn (6). This would mean that the electrostatic blob concept may apply even when there are more than one dissociated charge per bare Kuhn segment, see further discussions in Section 3.10.

2.1.2 Variational approach. Following the work of Muthukumar,[15,101–103] the radius of gyration of a polyelectrolyte in low salt solution was given by

$$R_g \propto \left[\frac{(g_K f)^2 l_B}{l_{K,0}}\right]^{1/3} l_{K,0} N_{K,0}, \quad (9)$$

where $N_{K,0}$ is the number of Kuhn segments per chain. Eqn (9) reproduces the scaling derived by Katchalsky *et al.*[104]

2.2 Conformation in dilute solutions with added salt

2.2.1 Scaling approach. Depending on the polyelectrolyte and added salt concentrations, different screening regimes can apply.[89] Here, we focus on the case when $2c_s + fc > (fN)^{-2}(4\pi l_B)^{-3}$. If this condition is met, the electrostatic screening length scales as:

$$r_{scr} = \left(\frac{B}{cb}\right)^{1/2} \left[1 + \frac{2c_s}{fc}\right]^{-1/2}, \quad (10)$$

where c and c_s are the polymer and added salt concentrations in units of number per unit volume, respectively.

The screening length r_{scr} described by eqn (10) is proportional to the Debye screening length:

$$\kappa^{-1} = \left(\frac{1}{4\pi l_B f c}\right)^{1/2} \left[1 + \frac{2c_s}{fc}\right]^{-1/2}. \quad (11)$$

According to Manning's theory, the number of monomers dissociated between charges is $f^{-1} \simeq l_B/b$. Combining this with the fact that $B \geq 1$, r_{scr} in eqn (10) is always larger than κ^{-1}, see ref. 89 for a more detailed discussion of electrostatic screening in polyelectrolyte solutions.

If the end-to-end distance R of a chain is smaller than the screening length (r_{scr}), the chain conformation is expected to be the same as that in a salt-free solution. For $R > r_{scr}$, sections of the chain with size r_{scr}, containing $g_{scr} = r_{scr} g_{el}/\xi_{el}$ chemical monomers, repel each other with full excluded volume. The end-to-end distance of a chain is $R \simeq r_{scr}(N/g_{scr})^{0.6}$ for $N \geq g_{scr}$. Using the screening length from eqn (10), the dependence of the end-to-end distance on added salt concentration is given by

$$R(c_s) = b^{2/5} c^{-1/5} B^{-2/5} N^{3/5} \left[1 + \frac{2c_s}{fc}\right]^{-1/5}. \quad (12)$$

Eqn (12) holds until the screening length decreases to the size of an electrostatic blob ξ_{el}. At this point, the chain is not stretched by electrostatics but its dimensions are larger than the neutral ones because the electrostatic excluded volume swells the chain on distances larger than $r_{rsc} = \xi_{el}$. The scaling model of Dobrynin *et al.*[89] gave no prediction for $r_{rsc} < \xi_{el}$. For the overlap concentration, the scaling model predicted:

$$c^* \left(1 + \frac{2c_s}{fc^*}\right)^{-3/2} = \left(\frac{B}{b}\right)^3 N^{-2}. \quad (13)$$

2.2.2 The expanded worm-like chain model. A different approach to model the properties of dilute polyelectrolytes in salt solutions has been applied primarily by Norisuye and

co-workers.[105–114] Polyelectrolytes were assumed to behave as expanded worm-like chains (WLC), and their properties were described using four parameters: the chain persistence length (l_p), the excluded volume strength ($\bar{B}$), the mass per unit length ($M_L = M_0/b$), and the cross-sectional chain diameter (d_C).

First, the properties of a polyelectrolyte chain in the absence of excluded volume (*i.e.* an ideal chain) were calculated using the models developed by Yamakawa and co-workers for non-ionic polymers.[115,116] For the end-to-end distance:

$$R_0 = 2l_pL - 2l_p{}^2(1 - e^{-L/l_p}), \quad (14)$$

where the subscript 0 indicates that R corresponds to the ideal chain conformation, and $L = bN$ is the contour length of the chain.

The influence of excluded volume was taken into account using expansion factors (α). The expansion factor $\alpha_R{}^2 = R/R_0$ is:

$$\alpha_R{}^2 = \left[1 + (10\tilde{z} + 70\pi/9)\tilde{z}^2 + 8\pi^{3/2}\tilde{z}^3\right]^{2/15} \times (0.933 + 0.067e^{-0.85\tilde{z}-1.39\tilde{z}^2}), \quad (15)$$

where the functions K and $\tilde{z}$ are:

$$\tilde{z} = \frac{3}{4}K\left(\frac{L}{l_p}\right)z, \quad (16)$$

and

$$K\left(\frac{L}{l_p}\right) = \begin{cases} \frac{4}{3} - 2.711\left(\frac{L}{2l_p}\right)^{-1/2} + \frac{7}{6}\left(\frac{L}{2l_p}\right)^{-1} & \text{if } \frac{L}{l_p} > 12, \\ \left(\frac{L}{l_p}\right)^{-1/2} e^{-6.6112\frac{l_p}{L}+0.9198+0.03516\frac{L}{2l_p}} & \text{if } \frac{L}{l_p} \le 12, \end{cases} \quad (17)$$

and the excluded volume parameter is:

$$z = \left(\frac{3}{2\pi}\right)^{3/2}\frac{\bar{B}}{2l_p}\left(\frac{L}{2l_p}\right)^{1/2}. \quad (18)$$

If chain size measurements covering a sufficiently broad range of N for a fixed salt concentration are available, it is possible to use eqn (14)–(18) to extract l_p, $\bar{B}$ and M_L.[117]

The persistence length and excluded volume strength are separated into intrinsic and electrostatic contributions:

$$l_p = l_{p,0} + l_{p,e}, \quad (19)$$

$$\bar{B} = \overline{B_0} + \overline{B_{el}}, \quad (20)$$

where $l_{p,0}$ and $l_{p,e}$ are the intrinsic and electrostatic persistence lengths, respectively, and $\overline{B_0}$ and $\overline{B_{el}}$ are the intrinsic and electrostatic excluded volume strengths, respectively.

The non-electrostatic excluded volume is calculated as the sum of a hard-core repulsion term and an attractive term:[106,118,119]

$$\overline{B_0} = \frac{\pi}{2}d_C + \overline{B_A}, \quad (21)$$

where d_C is the chain's cross-sectional diameter and $\overline{B_A}$ is the excluded volume strength arising from attractive contributions between Kuhn segments, see ref. 120 and 121.

Approaches to estimate the $\overline{B_A}$ term, which is usually only relevant at very high ionic strengths, can be found in ref. 118. The added salt concentration at which $\overline{B_A} = -(\pi/2)d_C - \overline{B_{el}}$, *i.e.*, $\bar{B} = 0$ is referred to as the θ-salt condition because chains are not perturbed by excluded volume. Note that even at the θ-salt point, the electrostatic effect continues to influence the polymer conformation in comparison to the non-ionic scenario, primarily through the electrostatic contribution to the persistence length.

Experimentally, the electrostatic terms were found to vary as power-laws of the added salt concentration:

$$\overline{B_{el}} = K_B(\kappa^{-1})^{\beta_B}, \quad (22)$$

$$l_{p,el} = K_l(\kappa^{-1})^{\beta_l}. \quad (23)$$

Many theoretical efforts have been devoted to predict prefactors (K_B, K_l) and exponents (β_B, β_l) in eqn (22) and (23). Odijk[122] and independently Skolnick and Fixman[123] predicted $K_l = 4/l_B$ and $\beta_l = 2$, which is known as the OSF limit. While it is apparent that the OSF prediction cannot describe experimental observations over a broad range of c_s,[124–126] no consensus has been reached on whether it should hold over particular conditions. A different prediction was made by Barratt and Joanny,[127] who calculated $\beta_l = -1$ if $bf \gg (l_{p,0}l_B)^{1/2}$.[128] Reviews on this topic can be found in ref. 9, 58 and 129–131.

For the electrostatic excluded volume, Fixman and Skolnick[119] predicted:

$$\overline{B_{el}} = 2\kappa^{-1}R(y), \quad (24)$$

where $y = 2\pi\kappa^{-1}e^{\kappa d_C}/l_B$ and $R(y) \simeq y$ in the $y \to 0$ (or $\kappa \to 0$) limit and $R(y) \simeq \pi/4(0.27 + \ln(y))$ in the $y \to \infty$ (or $\kappa^{-1} \to 0$) limit. Houwart and Odijk[132] worked out a similar prediction but with $R(y)$ taking a constant value, which implies $\overline{B_{el}} \propto \kappa^{-1}$, in agreement also with the scaling model of Dobrynin *et al.*[89]

Note that for weakly charged polyelectrolytes, where $\xi_{el} \gg l_{K,0}$, the scaling model outlined in Section 2.2.1 indicates that the worm-like chain model should not apply because there exist two contributions to the excluded volume (non-ionic and ionic) and these perturb the chain conformation at distinct length-scales: ξ_T for the non-ionic excluded volume and r_{scr} for the ionic excluded volume. This differs from the expanded worm-like chain (WLC), where chains are modelled as having a single cross-over between Gaussian and expanded conformations.

2.2.3 Variational theory. In excess salt, high N limit, the expansion factor for the radius of gyration of a polyelectrolyte ($\alpha_S' = R_g/\sqrt{bNl_{K,0}/6}$) calculated by the variational procedure by Muthukumar matched the theory of Flory:[133]

$$\alpha_S'^5 - \alpha_S'^3 = \frac{134}{105}\left(\frac{3}{2\pi}\right)^{3/2} \times \left[\left(\frac{1}{2} - \chi_0\right) + 4\pi\frac{l_B(g_Kf)^2}{\kappa^2 l_{K,0}{}^3}\right]N_{K,0}{}^{1/2}, \quad (25)$$

where χ_0 is the non-ionic contribution to the solubility parameter (χ) and the last term inside the square brackets accounts

for the electrostatic excluded volume. In the $\alpha_S' \gg 1$ limit, the expression for the radius of gyration becomes:

$$R_g \propto {l_B}^{1/5} f^{2/5} {c_s}^{-1/5} N^{3/5}. \quad (26)$$

Note that in this theory, the unperturbed chain's dimensions $R_{g,0} \simeq (N_{K,0} l_{K,0}/6)^{1/2}$ are c_s independent. This differs from Norisuye *et al.*'s approach, who introduced an ionic strength dependence of R_0 (or $R_{g,0}$) *via* eqn (19), for this reason, we use α_S' for the R_g expansion factor instead of α_S.

The Bjerrum length is included in eqn (26) in two ways: first, the explicit term ${l_B}^{1/5}$ accounts for the fact that as the dielectric constant decreases, the strength of the electrostatic repulsion between two like charges increases. According to Manning's theory, if the distance between ionic groups is smaller than l_B, then $f \simeq b{l_B}^{-1}$, so eqn (26) indicates R_g to be a decreasing function of l_B (as shown in Fig. 24). For weakly charged polyelectrolytes, where f is independent of l_B, R_g is expected to increase with l_B, provided there is no shift to the ionomer regime.

2.3 Comparison of theories

2.3.1 Expanded worm-like chain model. The expanded worm-like chain model can, under certain conditions, be mapped onto the scaling model of Dobrynin *et al.* Specifically, for systems where the electrostatic blob size is on the order of $l_{K,0}$ or smaller, scaling predicts that with excess salt, the chain conformation is rigid up to r_{scr} and then follows excluded volume statistics up to the chain size R. In this case, setting $M_L = M_0 B/b$, $l_p = r_{scr}/2$ and $\tilde{B} \simeq r_{scr}$, the expanded worm-like chain model reproduces the predictions of the scaling model for the configurational properties of polyelectrolyte chains.

Note that the conformation of polyelectrolytes is sometimes modeled as a directed random walk on lengthscales between ξ_{el} and the screening length. Under this assumption, the WLC model would not be applicable. As we will see in our review of the experimental literature, experimental evidence suggests that at least in some cases, fluctuations transverse to the stretching direction are not significant.

2.3.2 Variational theory. The result of the variational theory for the size of polyelectrolyte chains in salt-free solution (eqn (9)) matched the N, f and l_B exponents predicted by Dobrynin *et al.* for the $T = \theta$ case. In excess salt, the c_s and N exponents for the chain size predicted by the variational theory agreed with the scaling calculation (eqn (12)). The f and l_B exponents of the variational theory are $\simeq$ 50% larger than the scaling exponents for $T = \theta$. In terms of the expanded worm-like chain model, the high c_s exponents of variational theory were reproduced using ${l_T} \propto {c_s}^{-1/2}$, $B \propto {c_s}^{-1/2}$ and eqn (25) with $l_p = l_{K,0}/2$, $B \propto {c_s}^{-1}$. The full results from the variational theory for semiflexible chains yielded more complex scaling than would be expected from this simple mapping, see ref. 134 and 135.

2.4 Dynamic properties of polyelectrolyte solutions

2.4.1 Scaling approach. Throughout this section, we use eqn (12) to calculate the size of polyelectrolyte chains in excess salt and eqn (7) and (8) in low-salt solutions. The scaling laws presented here are therefore expected to be valid when $r_{scr} > \xi_{el}$. Polyelectrolytes in dilute solution were expected to be non-draining and described by the Zimm model,[86] which gives the longest relaxation time of:

$$\tau_Z \simeq \frac{\eta_s}{k_B T} R^3 = \begin{cases} \frac{\eta_s}{k_B T}\left(\frac{bN}{B}\right)^3 & \text{for } c_s \ll fc, \\ \frac{\eta_s}{k_B T} N^{9/5}\left(\frac{b}{B}\right)^{6/5}\left(\frac{f}{2c_s}\right)^{3/5} & \text{for } c_s \gg fc, \end{cases} \quad (27)$$

where η_s is the viscosity of the solvent. The diffusion coefficient was estimated as $D \simeq R^2/\tau_Z$:

$$D \simeq \frac{k_B T}{\eta_s R} = \begin{cases} \frac{k_B T}{\eta_s}\frac{B}{Nb} & \text{for } c_s \ll fc, \\ \frac{k_B T}{\eta_s} N^{-3/5}\left(\frac{B}{b}\right)^{2/5}\left(\frac{2c_s}{f}\right)^{1/5} & \text{for } c_s \gg fc. \end{cases} \quad (28)$$

In the low-salt limit ($fc/2c_s \ll 1$), the diffusion coefficient scales as $D \propto N^{-1}$ and for $c_s \gg fc/2$, $D \propto N^{-0.6} {c_s}^{1/5}$. In salt-free solution, D may also be estimated by modelling as cylinders with length R having cross-sectional radius d_C:[136–138]

$$D \simeq \frac{k_B T}{\eta_s R}\left[\ln\left(\frac{R}{d_C}\right) + 0.312 + 0.565\frac{d_C}{R} - 0.100\left(\frac{d_C}{R}\right)^2\right]. \quad (29)$$

Note that the last three terms of eqn (29), which are important for short chains, are not included in many models. Eqn (29) is known to give a quantitative description of the diffusion coefficient of short, rigid DNA segments in excess added salt[139] and is also supported by simulation results for the diffusion coefficient of cylinders of varying aspect ratio.

The intrinsic viscosity $[\eta]$ of a polyelectrolyte can be given by the Flory equation: $[\eta] = \Phi\frac{R^3}{M}$, where Φ is the Flory constant, discussed in detail in Section 3.12.[140] For sufficiently dilute solutions, the reduced viscosity (η_{red}) follows the Huggins equation:

$$\eta_{red} \equiv \eta_{sp}/c = [\eta] + k_H[\eta]^2 c, \quad (30)$$

where $\eta_{sp} \equiv (\eta - \eta_s)/\eta_s$ is the specific viscosity and k_H is the Huggins constant, which is discussed in detail in Section S5 (ESI†). For other equations proposed to describe the dilute solution behaviour of polyelectrolytes in excess salt, see ref. 141 and references therein. In salt-free solutions, eqn (30) holds only at extreme dilution, as discussed in the next section. The scaling prediction for the intrinsic viscosity in the high-salt limit shows:

$$[\eta] \simeq \left(\frac{b}{B}\right)^{6/5} N^{4/5}\left(\frac{f}{2c_s}\right)^{3/5}. \quad (31)$$

Extensions of the above models to account for the influence of dipolar interactions or charge induced correlations, which become more significant as the dielectric constant of the

solvent is decreased, can be found in ref. 142–147 and are not discussed here due to the lack of experimental data to test these theories.

2.4.2 Worm-like chain (WLC) model. The WLC model can also be used to calculate the dynamic properties of polyelectrolyte solutions using the same procedure outlined in the previous section for the end-to-end distance. Equations for the diffusion coefficient (D_0) and intrinsic viscosity ($[\eta]_0$) of ideal worm-like chains are given in ref. 148 and 149. Note that two of the coefficients listed in ref. 148 contain an error, as noted in ref. 150. The corresponding expansion factors ($\alpha_D = D/D_0$, $\alpha_\eta = ([\eta]/[\eta]_0)^{1/3}$, where the subscript 0 refers to the quantity in the absence of excluded volume effects) can be found, for example, in ref. 105 and 115. The equations for z, $\tilde{z}$ and K apply equally regardless of the property being calculated.

2.5 Counterion condensation

Throughout Section 2, we have seen that the charge fraction f is a key factor governing the conformation and dynamics of polyelectrolytes in solution. Polyelectrolytes can be regarded as salt molecules covalently bound to each other. Therefore, one may assume that all ion pairs of a polyelectrolyte chain dissociate completely into cations and anions. However, many experimental parameters,[151] such as electrophoretic mobility,[152] osmotic pressure,[73,153] and shear viscosity[97] measurements, suggest that this scenario is valid only when the charge density δ is lower than a certain critical value which depends on the systems investigated. Instead, it is well-recognized that some of the charges on the polyelectrolyte chain are neutralised by their counterions, so that the charge fraction becomes smaller than the charge density (*i.e.*, $f < \delta$). This phenomenon is called the counterion condensation, paramount for discussing almost every aspect of polyelectrolytes in solution.

The idea of the condensation of counterions was first introduced by Oosawa[154] to explain the osmotic and activity coefficient data of polyelectrolyte solutions. Subsequently, the well-known classical counterion condensation model was proposed by Onsager and formulated by Manning.[13] In the Manning model (see eqn (4) and (5) in ref. 13), we consider a single and infinitely long line charge bearing a point charge of $+Z_p e$ with a uniform distance b_c between two neighboring charges, and place a free counterion of $-Z_c e$ at a certain distance from the line charge. Here, Z_p and Z_c denote the valence of the point charge and the free counterion, respectively. With this charge configuration, the model calculates the Helmholtz free energy in order to discuss whether or not the counterion keeps dissociated from or is bound onto the line charge. Manning found that the system considered became unstable when the product of $Z_c Z_p u_M$ is greater than unity, leading to the conclusion that a sufficient number of counterions will condense onto the line charge, effectively reducing the product of $Z_c Z_p u_M$ to a value less than one, thereby stabilizing the system. Here, u_M ($= l_B/b_c$) is the so-called Manning parameter. Consequently, the Manning model predicted that counterion condensation occurs when $Z_c Z_p u_M \geq 1$. For instance, for polyelectrolytes composed of monovalent monomers ($Z_p = 1$) and counterions ($Z_c = 1$), condensation is predicted to occur when the charge distance b_c becomes smaller than the Bjerrum length l_B, *i.e.*, $u_M = 1$. Once the counterion condensation comes into play, the Manning model predicted the charge fraction f to be:

$$f = \frac{1}{u_M} = \frac{b_c}{l_B}. \tag{32}$$

The Manning model predicted that the charge fraction was solely dependent on three material parameters; the charge density, the solvent dielectric constant, and solution temperature.

Manning's two-state model has been elaborated over the past half century by accounting for conditions ignored in the original model.[143,144,146,147,155–166] For example, Nyquist *et al.*[155] incorporated the chain connectivity effects on the electrostatic interaction into the two-state model, showing that the transition from the complete dissociation to the condensation regimes was broad instead of a sharp transition at $u_M = 1$ predicted by the Manning model. The charge fraction was also found to decrease with increasing polymer concentration due to the chain contraction. Deserno *et al.*[164] studied the effect of the salt concentration on the counterion condensation and found that the charge fraction was not largely affected by the addition of salts, and therefore, the salt effect on the counterion condensation was negligible at low c_s. By considering the dielectric mismatch between the bulk solution and the local region around polyelectrolyte chains, Muthukumar[144] found stronger condensation at low ε_r but weaker condensation at high ε_r than predicted by the Manning model. As a result, the Muthukumar model predicted that the dependence of f on ε_r was stronger than that of the Manning model. The solvent quality also made the condensation process more complex, in particular in the case of poor solvents. We refer the readers to ref. 146, 147 and 166 for more details. Reviews on this topic have also been provided by Dobrynin and Rubinstein.[9,10]

3 Review of experimental data

This section is structured as follows: Section 3.1 discusses the solubility of polyelectrolytes in various types of solvent media and the phase behaviour of these polyelectrolyte solutions. Sections 3.3–3.8 focus primarily on the behaviour of polyelectrolytes in salt-free solutions. Sections 3.9–3.12 examine the behaviour of polyelectrolytes in excess added salt. Special attention is paid to polystyrene sulfonate, the most widely studied polyelectrolyte system. Section 3.13 discusses the static and dynamic scattering of polyelectrolyte solutions. Section 3.14 discusses the transition between salt-free solutions, where polyelectrolytes are highly stretched, and excess salt solutions, where they behave as neutral polymers in good solvents. We conclude by discussing the ion-specific effects and underscreening in Sections 3.15 and 3.16. Sections, 3.1, 3.2 and 3.12–3.16 can be read independently from one another. For coherence, it is recommended that Sections 3.3–3.8 and 3.9–3.11 be read sequentially.

3.1 Phase behaviour

3.1.1 Salt-free solutions. The large entropic gain arising from counterions being released into solution ($\simeq k_BT$ per counterion) is usually assumed to be the leading factor promoting polyelectrolyte solubility in salt-free media. The counterion entropy does not depend on N; hence, the solubility of polyelectrolytes in salt-free solution is predicted to be almost independent of their molar mass,[167] in contrast to neutral polymers.[86] Here, we recall Manning's prediction that the larger the solvent dielectric constant, the larger the charge fraction.[13] Since the number of dissociated counterions determines the entropic gain upon polyelectrolyte dissolution, high solvent permittivities should promote polyelectrolyte solubility. In fact, many polyelectrolytes can dissolve in high dielectric solvents, such as water at $\varepsilon_r \sim 80$. Dissolution of polyelectrolytes in low dielectric solvents can be impeded by the attractive dipole–dipole interactions between condensed counterions.[142,168,169] This can be overcome by reducing the charge density of a polyelectrolyte chain, *e.g.*, by replacing some of the charged monomers with non-ionic monomers[170–172] or by using hydrophobic counterions.[173]

In contrast, poly(ionic liquid)s exhibited excellent solubility in low dielectric solvents even if the charge density is high. Jousset *et al.*[174] investigated the solubility of poly([[(2-methacryloyloxy)-ethyl]trimethylammonium 1,1,2,3,3-pentacyanopropenide) (P(M-PCP)). The P(M-PCP) did not dissolve in water but exhibited an excellent solubility in various organic solvents with a broad range of dielectric constants ε_r, including *N*-methylformamide (NMF; ε_r = 182), propylene carbonate (PC; ε_r = 65), dimethylformamide (DMF; ε_r = 37), acetone (AC; ε_r = 21), cyclohexanone (CH; ε_r = 16), and triethyl phosphate (TEP; ε_r = 11).

Marcilla *et al.*[55] investigated the effect of the chemical structure of PILs on their solubility in five organic solvents, including an ionic liquid, 1-vinyl-3-ethylimidazolium bis(trifluoromethanesulfonyl)imide (ViEtIm-TFSI). As can be seen in Table 1, the difference in the alkyl chain length and the structure of counteranions influenced the solubility of PILs, implying the presence of ion-specific effects on the conformation and dynamics of PILs in solution. For example, acetone did not dissolve PC_2-BF_4 with ethyl groups but dissolved PC_4-BF_4 with butyl groups. Even for PILs with the same cation, methanol dissolved PC_2-TfO but not PC_2-BF_4. Furthermore, they showed that PILs were soluble in pure ionic liquids without non-ionic solvents.

The results in Table 1 show that the dielectric constant of the solvent cannot be used to predict the solubility of poly(ionic liquid)s. This agrees with the findings of Horne *et al.*,[175] who showed that the capacity of solvents to swell a cross-linked network of poly(1-[(4-ethenylphenyl)methyl]-3-methylimidazolium bistriflimide) did not correlate with their dielectric constant. Instead, Horne *et al.* demonstrated that solvent's dipole moment (μ) showed a strong correlation with a swelling degree of polyelectrolyte gels. The data in Table 1 make it clear that the dipole moment of the solvent does not predict solubility for the systems considered. Several systems are soluble in solvents with high μ and insoluble in solvents with low μ while others show the opposite trend.

Table 1 The solubility of poly(1-ethyl-3-methylimidazolium)-based, PC_2-X, and poly(1-butyl-3-methylimidazolium)-based, PC_4-X, poly(ionic liquid)s with various counteranions X^- (= BF_4^-: tetrafluoroborate; PF_6^-: hexafluorophosphate; TfO^-: trifluoromethanesulfonate; $TFSI^-$: bis(trifluoromethanesulfonyl)imide; $PFSI^-$: bis(pentafluoroethanesulfonyl)imide) against five organic solvents including an ionic liquid, 1-ethyl-3-vinylimidazolium bis(trifluoromethanesulfonyl)imide (ViEtIm-TFSI). The data are taken from Table 1 of ref. 55. The dielectric constant (ε_r) and dipole moment (μ) of the solvents are listed in brackets. All the PILs are insoluble in water (ε_r = 80, μ = 1.9 D)

		Methanol (ε_r = 32, μ = 2.6 D)	Acetone (ε_r = 22, μ = 2.7 D)	Tetrahydrofuran (ε_r = 8, μ = 1.7 D)	Ethyl acetate (ε_r = 6, μ = 1.9 D)	ViEtIm-TFSI
PC_2^+	BF_4^-	−	−	−	−	−
	PF_6^-	−	+	−	−	−
	TfO^-	+	+	−	−	+
	$TFSI^-$	−	+	+	−	+
	$PFSI^-$	+	+	+	+	+
PC_4^+	BF_4^-	−	+	−	−	
	PF_6^-	−	+	+	+	
	TfO^-	+	+	+	+	
	$TFSI^-$	−	+	+	+	
	$PFSI^-$	−	−	+	+	

(+): soluble; (−): insoluble.

Given the limited experimental data available for ionic polymers in salt-free media,[56,174,176,177] it is unlikely that solid conclusions can be drawn with regards to which parameters determine the polyelectrolyte solubility. The use of solubility parameters[178–180] might help establish a framework to understand monomer and counterion solvation, but these approaches require extensive solubility datasets. Insightful work on the solubility/swelling of charged polymers can be found in the literature on ionomers and polyelectrolyte gels.[176,181–191] Table 1 shows that the solubility of polyelectrolytes in ionic liquids depends on the chemical nature of the ionic groups. Since ionic liquids can act as salt ions to regulate the electrostatic interaction, understanding the influence of charge screening on the solubility of these systems can be an interesting research subject.

3.1.2 Solutions containing salts. Polyelectrolytes can be precipitated (and sometimes re-dissolved) by the addition of low molar mass salts. Experiments have been performed to resolve the influence of temperature,[192–195] added salt concentration,[192,194,196,197] molar mass,[192] and salt type,[196–200] see the review of Volk *et al.*[201] and the subsequent work.[202–204]

The phase behaviour of polyelectrolytes in excess added salt can be separated into two classes: H-type behaviour, where a large concentration of the added salt is needed to cause precipitation of the polymer (salting out); and L-type behaviour, where a small concentration of added salt induces phase separation.

3.1.2.1 H-Type phase behaviour. Results by Eisenberg and co-workers,[194,205,206] plotted in Fig. 3, illustrate the main phenomena observed for H-type phase behaviour. Fig. 3(a) and (b) show the influence of counterion and co-ion on the phase separation temperature (T_p) of polyvinyl sulfate in aqueous media. At high

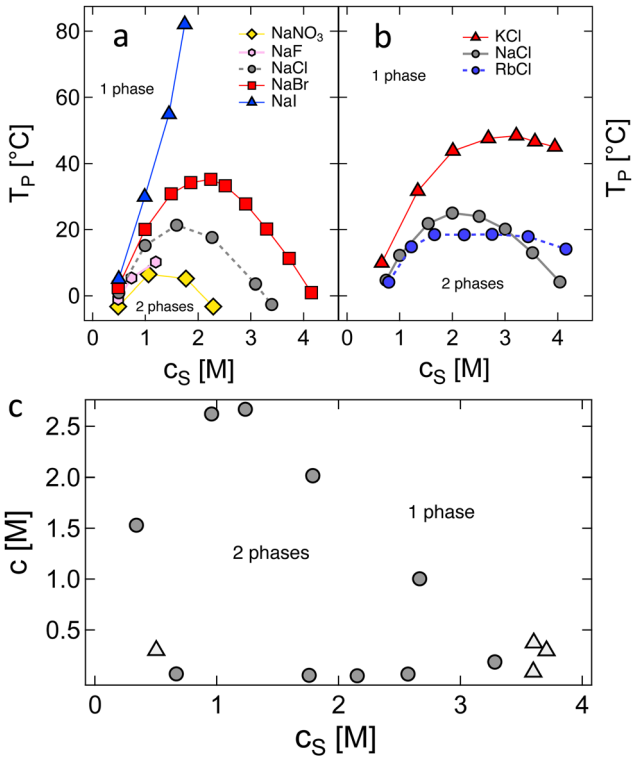

Fig. 3 Phase behaviour of polyvinyl sulfate. (a) and (b): Phase separation temperature as a function of added salt concentration for sodium salts (a) and chloride salts (b). (c) Solubility diagram for NaPVS/NaCl/H_2O system at T = 0 °C, see text for the meaning of symbols. Data are from ref. 194, 205 and 206.

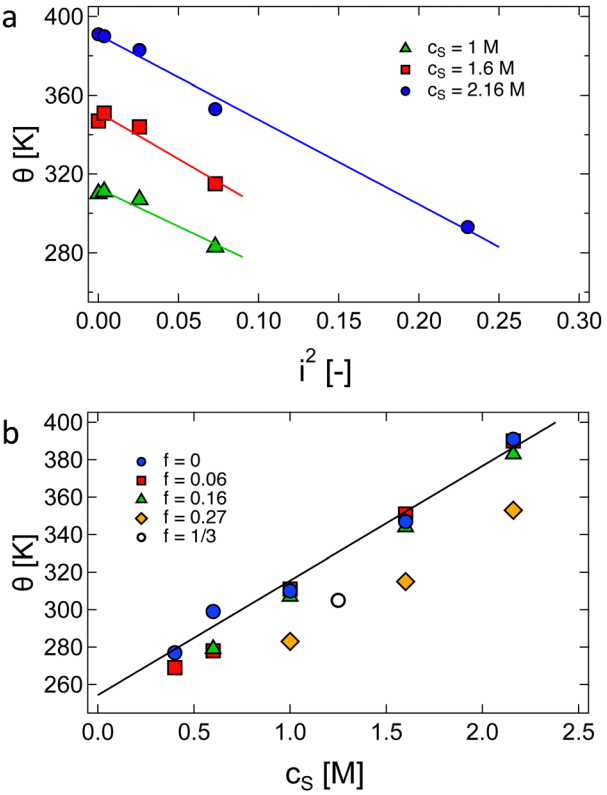

Fig. 4 Dependence of θ temperature of polyacrylic acid in aqueous NaCl solutions as a function of (a) the degree of ionisation (i^2) squared and (b) the concentration of added salt c_s. Data are from ref. 192, except for the hollow circle which is from Flory and Osterheld.[195]

c_s, the selection of the cation or anion has a profound influence on the phase behaviour of the system, in contrast to the expectation from simple treatments relying solely on electrostatic screening. The full c_s–c diagram at T = 0 °C shows closed-loop behaviour, as plotted in Fig. 3(c). Data were obtained using two methods: (1) solutions were cooled below T_p and allowed to phase separate into polymer-rich and polymer-poor phases and the compositions of the two phases were evaluated. These data are plotted in circles. (2) The triangles correspond to data obtained by preparing solutions at fixed c and c_s and decreasing the temperature until the solution phase separates at T_p. Plots of T_p *vs.* c_s at fixed c were then constructed and values of c_s at T_p = 0 °C obtained by interpolation. The discrepancy between the two methods arises from the polydispersity of the polymer, which leads to fractionation during phase separation in the first method. As depicted in Fig. S1 (ESI†), the inverse of the critical temperature ($1/T_c$), deduced from the peaks in the T_p *vs.* c graphs, displays a linear dependence on $N^{-1/2}$. This behaviour mirrors what is observed in neutral polymer solutions, and the intercept at $N^{-1/2}$ = 0 can be identified with θ^{-1}.[86,207]

Buscall *et al.*[192] studied the phase behaviour of polyacrylic acid as a function of temperature, degree of ionisation and polymer and added salt concentrations. We plot their values for the θ temperature of polyacrylic acid in Fig. 4, which illustrates the linear dependence on c_s and the fraction of neutralised monomers squared (i^2). The linear c_s dependence was observed for other systems, see Fig. S2 (ESI†).

H-type behaviour[192,195,197,208] can be described in terms of a Flory–Huggins theory using a χ parameter consisting of an intrinsic and an electrostatic term.[9,133,201] An open question is to understand the variation of the excluded volume strength as a function of c_s: increasing the ionic strength of the solvent leads to a reduction in the electrostatic term of the excluded volume (see Section 3.11), thus increasing χ_{elec}, and decreasing the solubility. The mean field approaches[9] usually expect $\chi_{elec} \propto f^2/c_s$, in agreement with Muthukumar's result, but the experimental data favour a weaker scaling of $\chi_{elec} \sim 1/\sqrt{c_s}$, see ref. 209 and Section 3.11. The phase behaviour discussed above shows that addition of salt can also modify the non-ionic term of the solubility parameter (χ_0). If χ_0 decreases with increasing c_s, "salting in", a phenomenon where polyelectrolytes exhibit a re-entrant phase and/or chain expansion at high added salt, can be observed.[103,201,210,211] This type of behaviour is usually found to be strongly dependent on the ion type,[103,201,210–212] suggesting that solvent-mediated ion-binding to the polymer backbone plays a role, as observed earlier for polyethylene oxide,[213,214] cellulose ethers[215] and other systems.[216] Addition of salt can also lead to a reduction of the non-ionic contribution to solubility, *i.e.* an increase in χ_0.[121]

The interaction of added salts with non-ionic polymers has been studied in detail for polyethyelene oxide. In aqueous solutions, addition of electrolytes usually leads to a decrease in the solvent quality.[217–219] In contrast, in polar organic

solvents such as methanol, the opposite behaviour is observed.[220] The mechanism underpinning these phenomena remains controversial. Generally, it is accepted that ion-binding to the backbone[221–224] as well as changes in the solvent properties by the added electrolyte modify the solvent quality for the PEO chain. However, a detailed understanding of how and why their relative importance depends on solvent type remains an open question. While such effects are often not discussed when modelling the properties of polyelectrolytes, they should generally not be expected to be absent.

3.1.2.2 L-Type phase behaviour. The phase behaviour of polyelectrolytes in the presence of di-, tri- and tetra-valent ions is considered in Fig. 5. We discuss these in turn. L-Type precipitation, while usually associated with divalent and higher-valent ions,[201,225] is also observed for monovalent ions with high coordination numbers notably Ag^+.[226,227]

The critical added alkaline earth concentration (c_s^{**}) to precipitate 90% neutralised polymethacrylic acid (PMA) is plotted in Fig. 5(a). In the absence of added NaCl, the concentration of M^{2+} (= Mg^{2+}, Ca^{2+} and Ba^{2+}) is nearly proportional to the polymer concentration. Similar behaviour is observed for sodium polyacrylate (NaPA) with added $CaCl_2$ for $c \gtrsim 3$ mM, see Fig. S3(a) (ESI†). The data of Sabbagh and Delsanti[230] also show that for sufficiently low c, c_s^{**} scales as $\sim c^{-0.6}$. Other polyelectrolyte systems displayed this feature or a plateau in c_s^{**} in the low c region.[93,198,233,234] The phase boundary shown in Fig. 5(a) is seen to be identical for $MgCl_2$, $CaCl_2$, and $BaCl_2$. If NaCl was added, c_s^{**} increased, a feature also observed for NaPA[200,201] (see Fig. S3(b) and (c), ESI†) presumably due to the competitive binding of Na^+ and M^{2+} to the ionic side groups. For lower degrees of neutralisation, Ikegami and Imai[197] showed that Ba^{2+} and Ca^{2+} precipitate NaPA at much lower c_s^{**} than Mg^{2+}.[235] The phase behaviour of PSS/$BaCl_2$[233,234,236,237] is discussed in Section S1 of the ESI,† where it is shown that θ depends linearly on c_s, as for H-type systems.

The phase diagrams of polyelectrolytes in the presence of trivalent ions are shown in Fig. 5(b). Phase separation occurs for $c_s^{**} \simeq c/5$, indicated by the solid line. This precipitation boundary was found to be N-independent for NaPSS/$LaCl_3$.[199] The data presented in Fig. 5(b) also show that c_s^{**} is largely insensitive to the ionic group, with acrylate, sulfonate and sulfate groups all falling onto the same curve, except for NaPA/$LaCl_3$. This suggests that electrostatics and not ion-specific interactions are the primary driving force at play. Dubois and Boue[238] found $c_s^{**}/c \simeq 0.24$ for NaPSS/$LaCl_3$. Jan and Breedveld[229] reported $c_s^{**}/c \simeq 0.2$ for NaPSS with added $LaCl_3$ and $CeCl_3$ and a higher ratio of 0.3 for $AlCl_3$ and $GaCl_3$; $InCl_3$ precipitated NaPSS with $N \simeq 5000$ at $c_s^{**}/c \simeq 0.32$. For NaPSS with $N \simeq 2500$ and 600, $InCl_3$ did not lead to precipitation. As the added salt concentration was further increased, re-dissolution of the polyelectrolytes was observed at $c_s = c_s^D$. The re-entrant boundary is nearly c-independent and increases with N.[199] c_s^D was found to depend on the trivalent cation type. For NaPSS, c_s^D varies on the order $La^{3+} \simeq Ce^{3+} > Ga^{3+} \gtrsim Al^{3+} > In^{3+}$. In the presence of a monovalent salt, c_s^{**} increases and c_s^D decreases, narrowing the two-phase region of the phase diagram.[199] In some cases, re-dissolution does not occur, leading to the formation of a gel phase instead. This phenomenon is observed, for instance, when sodium carboxymethyl cellulose (NaCMC) or alginate are exposed to (Al^{3+} or Fe^{3+} ions[239–243]).

The phase diagrams of systems in the presence of tetravalent cations are plotted in Fig. 5(c). The behaviour is similar to that of the trivalent systems with $c_s^{**} \simeq 0.2c$ and a nearly

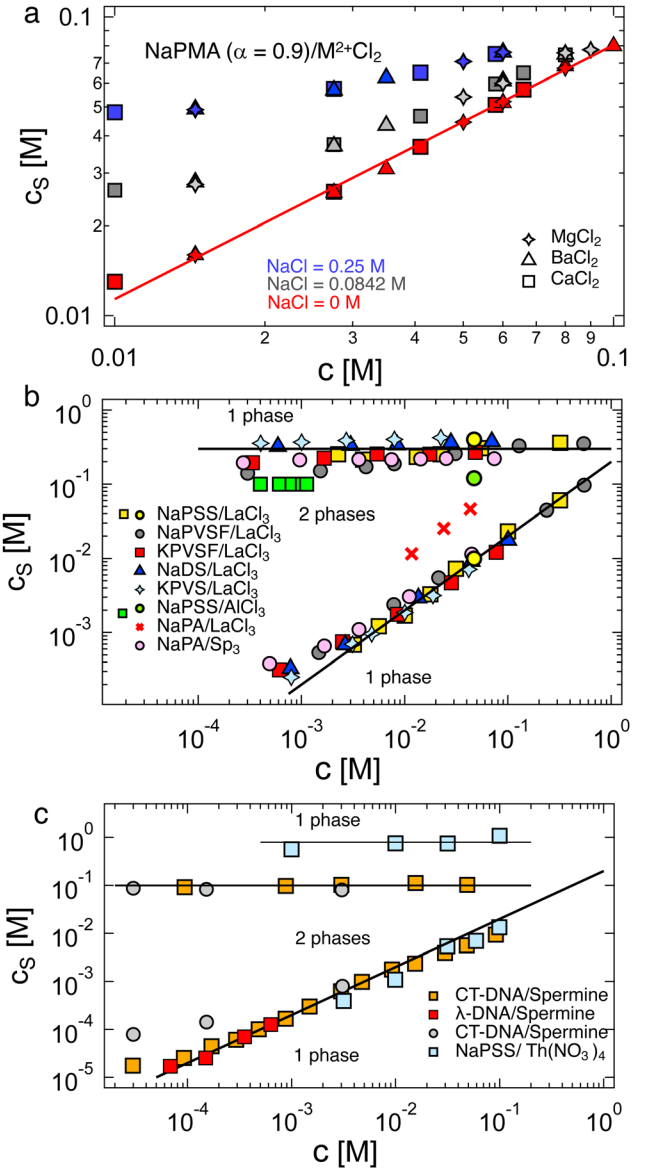

Fig. 5 (a) Added salt concentration as a function of polymer concentration for polymethacrylic acid (i = 0.9) in DI water and aqueous NaCl solutions. Line is $c_s = 0.57c^{0.85}$. Data are from ref. 228. (b) Added salt concentration for precipitation (c_s^{**}) and re-dissolution(c_s^D) for polyelectrolytes with added trivalent salts. NaPSS/$LaCl_3$ data are from ref. 199 (yellow squares) and ref. 229 (yellow circles), NaPSS/$AlCl_3$ from ref. 202 (green squares) and ref. 229 (green circle) and NaPSS/$LaCl_3$ (red crosses) from ref. 197. Sp stands for trivalent cation spermidine. All others are from ref. 230. Top line is c_s = 0.3 M, bottom line is $c_s = 0.2c$. (c) Precipitation and re-dissolution c_s for DNA and PSS in the presence of tetravalent ions. NaPSS data are from ref. 199 DNA data are from ref. 231 (squares) and ref. 232 (circles). Bottom line is $c_s = 0.2c$.

c-independent re-entrant phase boundary. In the re-entrant region for both tri-valent and tetra-valent ions, increasing c_s leads to chain expansion,[229,238,244–248] presumably linked to charge-inversion, a phenomenon by which the binding of multivalent ions to the polymer backbone leads to a reversal of the net charge of the polymer backbone, see ref. 249–253 for explanations of the underlying physics and its role in biological phenomena.

Understanding how the strength of binding of ions to the polyelectrolyte influences their phase behaviour remains a challenge. Experimental approaches to quantifying ion specificity are usually based on measuring relative binding constants by potentiometry (or less commonly by spectrophotometric methods[254] or equilibrium dialysis[255,256]), and have been applied comprehensively to polyacrylic acid,[257–260] see ref. 66 and 261 for overviews. The available phase data do not allow for a meaningful correlation to be established between phase behaviour and ion binding strength. Thermodynamic data on ion binding can also be obtained by isothermal titration calorimetry,[202,204,262,263] which has been correlated with trends in polyelectrolyte conformational changes.[264] Ion-binding and bridging[265,266] mechanisms, which are important for divalent and higher-valent ions, are poorly understood. The influence of divalent salts on the conformation of polyelectrolytes has been studied extensively for sodium polyacrylate by Huber and co-workers[74,264,267–273] but these datasets have not yet been comprehensively accounted for in any theoretical framework.

3.2 Viscoelasticity

The scaling assumption for calculating the dynamic properties of dilute polyelectrolytes is that chains are non-draining and can therefore be described by the Zimm model. Measuring the viscoelasticity of dilute solutions is experimentally challenging, and relatively little data exists.[275] Rosser *et al.*[274] made use of Birnboim–Schrag resonators to probe the dynamics of NaPSS in water and water/glycerol media. Fig. 6 shows the storage and loss modulus for NaPSS in an excess of 0.001 M salt solutions. The prediction of the Zimm model, following ref. 86 with a scaling exponent of $\nu = 0.59$, shows good agreement with experimental data, thus supporting the non-draining nature of dilute polyelectrolyte coils. Note that the black lines shown in Fig. 6 do not contain any fit parameters. The validity of the Zimm model for dilute polyelectrolytes is also supported by the scaling of the diffusion coefficient and the intrinsic viscosity with the molar mass, see Section 3.9.

3.3 Dilute solution viscosity

Fuoss and co-workers[4,276–284] observed that the reduced viscosity ($\eta_{red} = \eta_{sp}/c$) of dilute polyelectrolyte solutions in low ionic strength media increased upon dilution. Addition of a low molecular weight salt suppressed the 'polyelectrolyte effect' and resulted in a linear η_{red} *vs.* c trend, characteristic of non-ionic systems. The studies also showed that due to the strong non-Newtonian effect of polyelectrolyte solutions in salt-free solutions, measurements with capillary viscometers did not always capture the zero shear rate viscosity value.[278,279,281,283] This important point has been

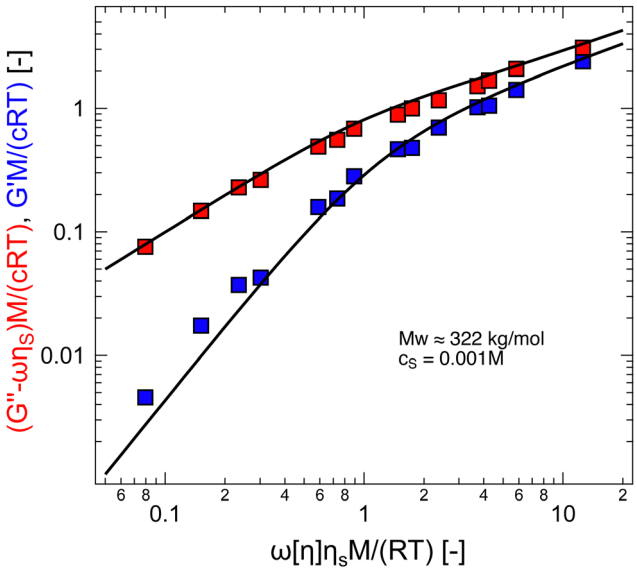

Fig. 6 Storage and loss modulus for sodium polystyrene sulfonate in 0.001 M NaCl salt solutions. Measurements at T = 5, 15, and 25 °C were plotted into a single master-curve. Lines are the Zimm model using eqn (8.67) and (8.68) from ref. 86 with $\nu = 0.59$. Data are from ref. 274.

neglected in a large part of the literature, see ref. 285, 286 and Section 3.4 for further discussion. It is important to note that while for sufficiently dilute solutions the shear viscosity becomes largely insensitive to the applied shear rate, the polymer contribution to the shear viscosity ($\eta - \eta_s$), which is the relevant quantity to determine conformational properties at infinite dilution, remains significant.[287,288] An empirical function was proposed by Fuoss and co-workers to fit polyelectrolyte shear viscosity data in low ionic strength media:

$$\frac{\eta_{sp}}{c} = \frac{J}{1 + Wc^{1/2}}, \tag{33}$$

where W is a constant that correlates with the polyelectrolyte charge and J can be identified with the intrinsic viscosity. Addition of a constant term to the right hand side of eqn (33), or other modifications[289–292] were sometimes found to be necessary to describe data accurately. Following eqn (33), the intrinsic viscosity of polyelectrolytes was estimated by plotting $1/\eta_{red}$ *vs.* $c^{1/2}$.[293] Inagaki *et al.*[294] later showed that for sufficiently low polymer concentrations, η_{red} exhibited a maximum at $c = c_{max}$ below which an approximately linear decrease of η_{red} in polymer concentration was observed.[295] This feature has been observed for many systems.[285,296–298] A clear example is shown in Fig. 7(a), which plots the reduced viscosity of NaPVS in aqueous media with varying amounts of added salt. Data for dilute solutions, *i.e.* those with $\eta_{sp} < 1$ are plotted as full symbols. Semidilute data ($\eta_{sp} > 1$) are plotted as hollow symbols. The data from Nishida *et al.*[299] were not extrapolated to the zero-shear limit and we expect the lowest concentrations in DI water to be slightly affected by shear thinning and therefore to represent lower bound estimates for η_{red}.[300] The Fuoss power-law of $\eta_{red} \propto c^{-1/2}$ is shown as a black line. Note that in DI water, the Fuoss law holds below the overlap concentration, in agreement with the observation of Han *et al.*[301]

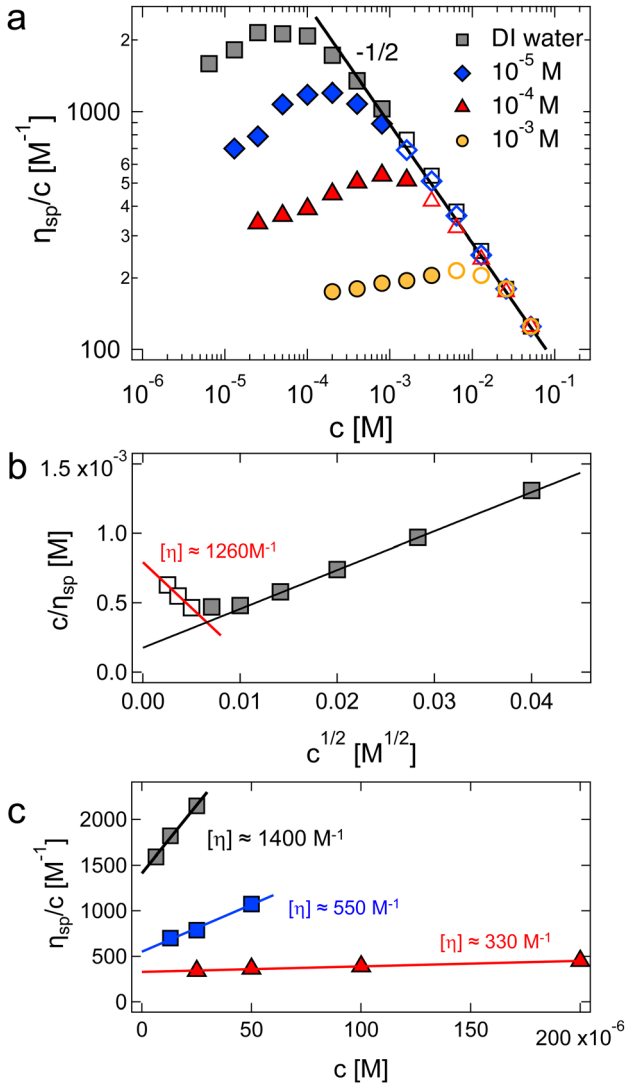

Fig. 7 (a) Specific viscosity of NaPVS with 31% charged groups as a function of polymer concentration for different concentrations of added NaCl. Data are measured in a nitrogen atmosphere. Solid symbols represent results for dilute solutions ($\eta_{sp} < 1$) and hollow symbols for semidilute solutions ($\eta_{sp} < 1$). The solid line represents the Fuoss power-law ($\eta_{red} \propto c^{-1/2}$). (b) Inverse of reduced viscosity as a function of $c^{1/2}$ for salt-free data. The black line gives an apparent intrinsic viscosity of $\simeq$5200 M^{-1}, see eqn (33). The red-line estimates [η] from the low-c region, corresponding to data below the viscosity maximum in plot (a). (c) Huggins plot for low concentration regime. Colours are the same as in plot (a). Data are from ref. 299.

The existence of the maximum in η_{red} means that the extrapolation methods by Fuoss and co-workers overestimate the intrinsic viscosity of polyelectrolytes in low ionic strength media. For example, the black line shown in Fig. 7(b) (Fuoss' method) gives $[\eta] \simeq 5200\ M^{-1}$. A more reasonable estimate based on data for concentrations below the η_{red} maximum gave 1260 M^{-1}, shown by the red line, which matched the estimate from the Huggins plot shown in Fig. 7(c). This value is considerably larger than $[\eta] \simeq 440\ M^{-1}$ calculated by Nishida *et al.* on the basis of their model to account for inter-chain contributions to the reduced viscosity. Note also that using Nishida's method, the intrinsic viscosity was almost identical for DI water and $c_s = 10^{-4}$ M, in contrast to the strong c_s dependence observed using the Huggins equation shown in Fig. 7(c). Other empirical methods,[289–292,302,303] including an equation developed by Wolf (eqn (S3), ESI†),[304–312] have been widely employed to estimate the intrinsic viscosity of polyelectrolytes in recent years.[313,314] These suffer from similar problems as the Fuoss method (eqn (33)) because the fits do not produce maxima in the η_{red} *vs.* c profiles, see the ESI† (Section S5.5).

3.3.1 Correlation between c_{max} and c_s. Cohen *et al.*[297] observed that for NaPSS, the maximum in η_{red} occurs at $c_{max} \simeq 4c_s$. This corresponds to $fc \simeq c_s$. In their case, $c_s \simeq 5 \times 10^{-6}$ M in DI water was assumed to arise from carbon dioxide dissolved in the air. In a later study,[315] discussed in the ESI† (Section S3), Cohen *et al.* found that c_{max} depends on the temperature and molar mass, suggesting that the ratio of c_{max} and c_s is not a constant.

The polymer concentration at the maximum in η_{red} as a function of the total salt concentration in the solvent from different literature reports on NaPSS and data reported by Kato *et al.*[316] for HPSS is plotted in Fig. 8(a). Points for which $c_{max} > c^*$ are shown as hollow symbols and those for which $c_{max} < c^*$ are shown as full symbols. For samples measured in a nitrogen atmosphere, we estimated $c_s \simeq 10^{-7}$ M from the self-dissociation constant of water. The value of c_{max} is usually found to be independent of shear rate or weakly dependent of shear rate,[317] with the exception of Vink's measurements,[318,319] where c_{max} varied strongly with $\dot{\gamma}$. We therefore include data measured in both the Newtonian regime and the shear-thinning regime. The latter include Cohen's[297] high molar mass samples, Batzill's[320] highest molar mass sample, and the two highest molar masses from Vink.[321] The data from the various reports display a high degree of scatter and it is therefore not possible to establish if a fixed c_{max}/c_s ratio exists. The data reported by Yamanaka *et al.* are particularly interesting: despite the very low level of residual salt due to the measurements being carried out in a nitrogen atmosphere,[322,323] c_{max} takes a higher value than for Cohen's samples. The low residual salt content of Yamanaka *et al.*'s samples is confirmed by their c^* values, see Fig. 11. Other strong departures from the trend are observed by Boris and Colby,[285] Ganter *et al.*[298] and Gulati *et al.*[100] in DI water. A common feature of these datasets is the high molar mass of the polymers, all of which have $N > 5000$. However, Batzill's samples with high N do not deviate from the overall trend. The origin of these discrepancies remains unclear.

The plot of c_{max} *vs.* c_s for other flexible polyelectrolytes is shown in Fig. 8(b). A correlation is observed, except for Eisenberg's[324] samples in DI water. The same plot is also shown in Fig. 8(c) for ionic polysaccharides, where the scatter is considerably smaller than for NaPSS, despite the fact that many different polymer systems are considered.[325] The combined data in Fig. 8(c) suggest that c_{max} may follow a sublinear relationship with c_s. The $c_s/c_{max} \simeq 10$ and $c_s/c_{max} \simeq 4$ obtained for flexible polyelectrolytes and polysaccharides, respectively, are qualitatively consistent with $fc_{max} \simeq c_s$ since polysaccharides have typically one dissociated charge per two monomers

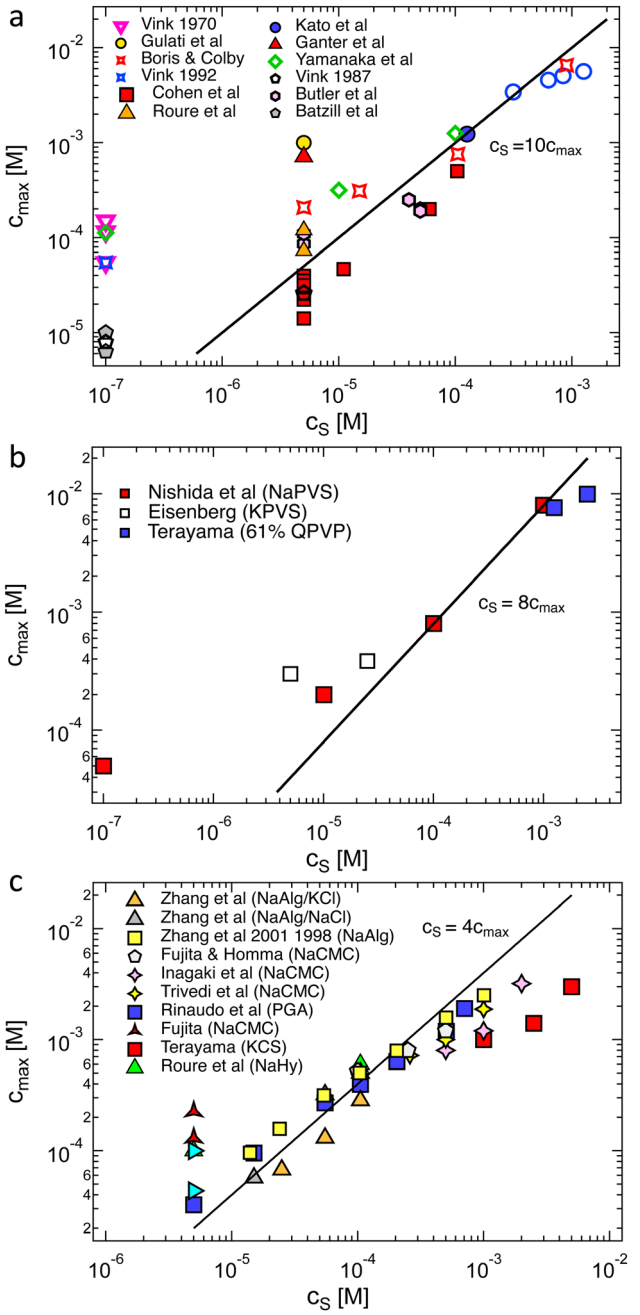

Fig. 8 Polymer concentration at maximum in the reduced viscosity as a function of monovalent added salt content for: (a) polystyrene sulfonate. Filled symbols are when $c_{peak} < c^*$ and hollow symbols for $c_{peak} > c^*$. Data are from ref. 285, 297, 298, 316–320, 331 and 332 (b) polyvinyl sulfate and quaternised polyvinyl pyridine (degree of quaternisation = 61%). Data from ref. 299, 324 and 333 (c) carboxymethyl cellulose, sodium hyaluronate, poly(galacturonic acid), sodium alginate and potassium cellulose sulfate. Data are from ref. 290, 294, 296, 321 and 334–339. Lines are power-laws with a slope of unity, illustrating a fixed ratio between the polymer and added salt concentration.

($\simeq$1 nm along the backbone)[326–330] while PSS has one dissociated charge per five monomers.[68]

All data for which c_s is assumed to arise solely from the self-dissociation of water clearly deviated from the trend observed for other samples, suggesting that the actual residual salt is an order of magnitude larger than our estimate. Most measurements are carried out in capillary viscometers made of glass, which likely results in contamination of the solution from ion leaching, as reported by Butler *et al.*[331] Unfortunately, most attempts to quantify the residual salt content in polyelectrolyte solutions (usually by electrical conductivity measurements) have been performed for samples prior to their rheological measurements. This assumes that the measurement itself does not lead to contamination, which may not necessarily be the case.[301]

The T- and N-dependence of c_{max} reported by Cohen *et al.*[340] is incompatible with $2c_s \simeq fc_{max}$ as neither parameter influences f or c_s significantly. In contrast, other studies[341,342] have reported a much weaker temperature dependence of η_{sp} for NaPSS as discussed in Section S3 (ESI†). Therefore, the current experimental evidence is inconclusive and does not clearly support (nor disprove) that $c_{max} \simeq 2c_s/f$.

The behaviour of η_{red} in dilute solution has been assigned to single chain effects[58,343] (*i.e.* chain expansion for $c < c^*$ leads to an increase in η_{red}). Alternatively, several theories explain that the viscosity maximum arises primarily from intermolecular effects (the secondary electroviscous effect) and not due to chain expansion upon dilution, see ref. 344–347. Antonietti *et al.*[344] found that many of the features observed for linear polyelectrolytes were reproduced for ionic microgels. Their results could be described by a modified Hess–Klein model.[348] The authors noted that since "*charge density inside the* [*microgel*] *particles is always rather high, thus suppressing pronounced Coulomb-effects*", they expected no significant electrostatic swelling and the increase of $[\eta]$ upon decreasing c_s was attributed to effects other than changes in particle size. They concluded that these results provided proof of the intermolecular nature of the polyelectrolyte effect. In our view, the size invariance assumption should be revised in light of recent experimental evidence.[349–355] The work of Schurtenberger and co-workers[349] showed that polyelectrolyte microgels display a "porcupine" morphology in low ionic strength solvents due to highly extended dangling chains on their outer surface. A discussion of mode-mode coupling approaches to polyelectrolyte solution viscosity can be found in ref. 297, 340, 347 and 356 these generally fail to capture several experimentally observed phenomena such as the molar mass dependence of c_{max}.

3.4 Shear rate dependence of intrinsic viscosity

The non-Newtonian characteristics of dilute polyelectrolyte solutions have been reported by many authors,[321,324,335,357–361] but only a few systematic experimental studies on the subject have been published.[287,288,317,362–364]

Fixman[365] developed a theory for the non-Newtonian intrinsic viscosity of flexible polymers. The shear rate dependence on the intrinsic viscosity is expressed as:

$$[\eta(\dot{\gamma})] = [\eta]G(K_\eta\dot{\gamma}), \quad (34)$$

where $[\eta]$ refers to the intrinsic viscosity measured in the Newtonian region and G is a function tabulated in ref. 365,

which depends primarily on the excluded volume parameter z (eqn (18)) and $K_\eta\dot{\gamma}$ is a reduced shear rate with:

$$K_\eta = \frac{1.71\eta_s[\eta]M_w}{\bar{R}T}, \quad (35)$$

where $\bar{R}$ is the gas constant. This is the same as the longest relaxation time predicted by the Zimm model (see eqn (8.34) of ref. 86), except for the pre-factor of 1.71.

In agreement with Fixman's theory, experiments show that polymers in theta solvent exhibit shear thinning and that $[\eta](\dot{\gamma})/[\eta]$ for a constant K_η decreases as the excluded volume parameter z increases.[366–368] A quantitative description of the shear rate dependence of $[\eta]$ is still considered an open question in the rheology of dilute polymer solutions.[369]

Fig. 9(a) and (b) show plots of the shear rate dependence of the relative decrease in $[\eta]$ for a NaCMC polymer in aqueous solvents of varying added NaCl concentration (part a) and for a polymethacrylic acid in 0.003 M NaCl solutions of varying degrees of neutralisation (part b). In both cases, the data for different c_s or i are seen to collapse onto a single mastercurve. This result is at odds with Fixman's theory as the excluded volume parameter z is expected to be an increasing function of c_s and the degree of ionisation i for these systems (see Section 3.11). An analysis of data reported by Yanaki *et al.* for NaHy,[288] provided in the ESI† (Fig. S5) shows that Fixman's theory does not quantitatively predict the dependence of $[\eta](\dot{\gamma})$ on z. The power-law exponent for the NaCMC data is $\simeq -1/3$. This exponent appears to work also for PMA, but since data are only available up to $K_\eta\dot{\gamma} < 5$, the $-1/3$ slope may not correspond to the limiting $K_\eta\dot{\gamma} \gg 1$ value.

In salt-free solution, the data reported by Yamanaka *et al.*[317] for NaPSS, plotted in Fig. 9(c) display a stronger power-law of $-2/3$ at high shear rates, which exceeds the predictions[370–372] and experimental observations[373] of $[\eta(\dot{\gamma})] \sim \dot{\gamma}^{-1/2}$ for rod-like neutral polymers, but agrees with a simulation of rigid dumbbells.[374]

Simulation studies have quantified the degree of chain stretching[374–378] and alignment[377,379] of polyelectrolytes under shear flow. Ref. 374 and 376 indicate that for different ionic strengths, the plot shown in Fig. 9(a) should not collapse onto a single curve. The $[\eta]$ *vs.* $\dot{\gamma}$ curves are expected by Shogin and Amundsen[374] to gradually transition to a power-law behaviour with a universal exponent of $-2/3$ at high $\dot{\gamma}$. Other studies give weaker exponents.[376] Simulation studies have revealed that the dynamics of polyelectrolytes under shear display several features which are not encountered for neutral polymers: for example, Jarasree *et al.*[378] showed that the dynamics of condensed counterions can have an influence on the tumbling of polyelectrolyte chains. Two studies noted that shear flow can promote counterion dissociation from the backbone,[377,379] in agreement with the experimental results of Zhao and co-workers.[380] Simulation work in elongational flows, under which a different set of transitions are expected,[381] is more sparse.[382]

For the three systems considered, $[\eta](\dot{\gamma})/[\eta] \simeq 0.8$–$0.9$ for $K_\eta\dot{\gamma} = 1$ is found, which suggests that measurements with $K_\eta\dot{\gamma} \lesssim 1$ should reasonably approximate the zero-shear rate value of the intrinsic viscosity. For the most common

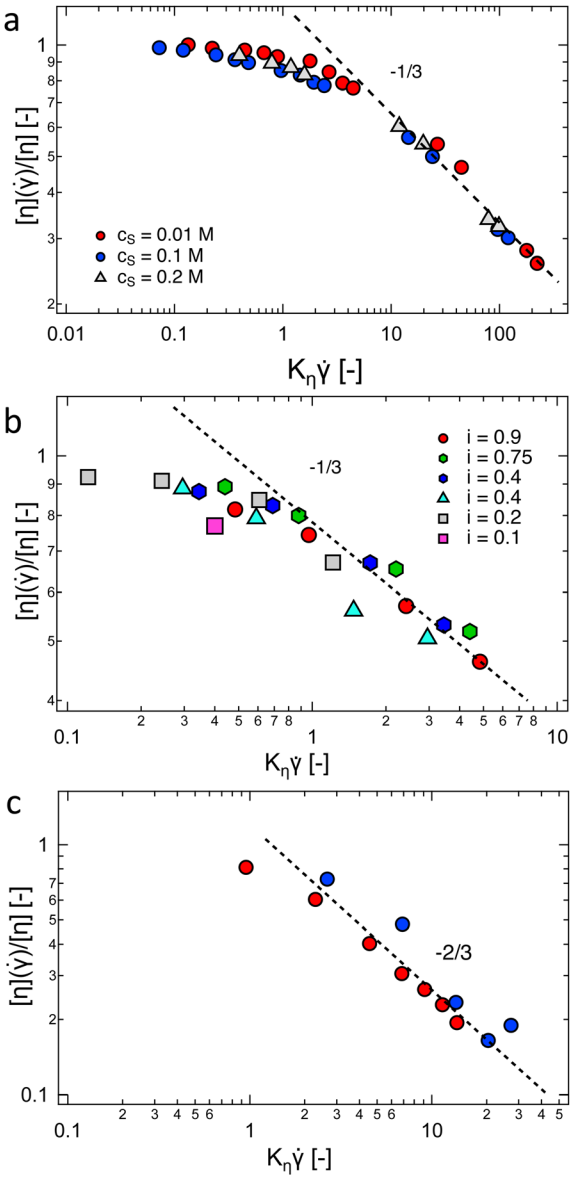

Fig. 9 Intrinsic viscosity normalised by its zero-shear value as a function of the reduced shear rate $K_\eta\dot{\gamma}$, see eqn (35). (a) NaCMC in aqueous NaCl solutions, c_s indicated on the legend. Data are from ref. 287. (b) Polymethacrylic acid in 0.003 M NaCl, neutralised with NaOH to different degrees, as indicated in the legend. Data are from ref. 362. (c) NaPSS in DI water (measurements in a nitrogen atmosphere). Data from ref. 317. Lines are power-laws with exponents indicated in the graphs.

experimental conditions of aqueous solutions at T = 298 K, $K_\eta \simeq 6 \times 10^{-7}[\eta]NM_0\dot{\gamma}$, which gives a critical shear rate for the onset of shear thinning of:

$$\dot{\gamma}_C \simeq \frac{1.6 \times 10^9}{N[\eta]}, \quad (36)$$

if $[\eta]$ is expressed in M^{-1} and $\dot{\gamma}$ in s^{-1}.[300]

3.5 Conformation in salt-free solution at infinite dilution

The hydrodynamic radius of NaPSS in water without added salt[383] as a function of the degree of polymerisation at infinite

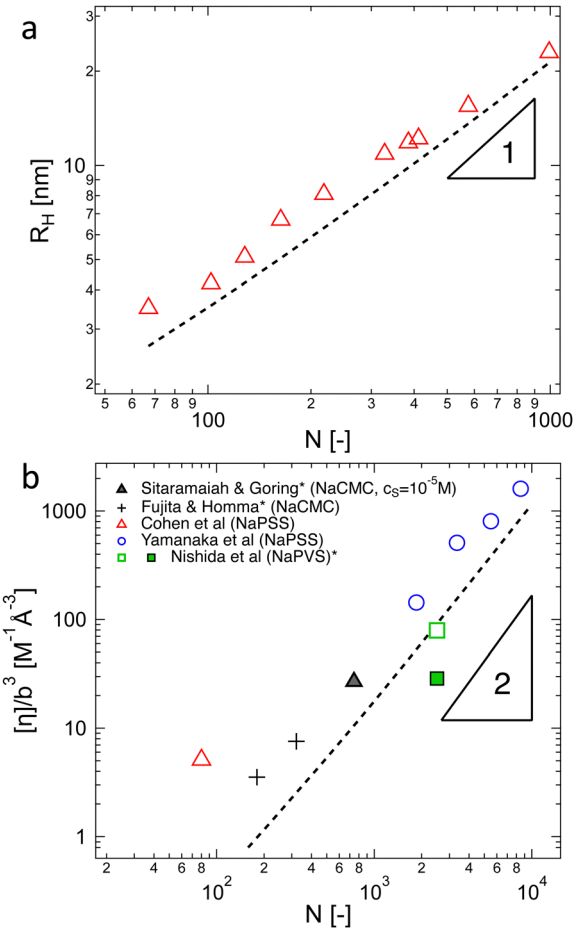

Fig. 10 Properties of polyelectrolytes in the infinite dilution limit in DI water. (a) Hydrodynamic radius of NaPSS as a function of the degree of polymerisation, data from ref. 383. Line is the calculated hydrodynamic radius of a cylinder (eqn (37) using eqn (29) to calculate D). (b) Intrinsic viscosity for various polyelectrolytes normalised by monomer length cubed as a function of the degree of polymerisation. Data are from ref. 297, 299, 322, 323, 335 and 385. Line is the intrinsic viscosity of a cylinder calculated using Yamakawa's theory (eqn (38) with d_C = 1 nm), see text for details. Points marked with an asterisk are likely affected by shear thinning. The datum by Sitaramaiah and Goring[385] is for c_s = 10^{-5} M and can be considered a lower-bound estimate for $[\eta]$. The data for NaPVS are obtained from the fit shown in Fig. 7(c) (hollow symbol) or by Nishida's method (full symbol).

dilution is plotted in Fig. 10(a). The hydrodynamic radius is related to the diffusion coefficient of a chain *via* the Stokes–Einstein equation:

$$R_H = \frac{k_B T}{6\pi\eta_s D}. \quad (37)$$

The dashed line is the theoretical calculation for cylinders (eqn (29) and (37)) assuming a fully stretched chain size, *i.e.*, B = 1, which is expected if $\xi_{el} < l_{K,0}$ and chains adopt a rod-like conformation on distances larger than the electrostatic blob. The model under-predicted experimental results by around ≃20%. If less stretched conformations ($B > 1$) are assumed, the disagreement becomes larger.

The intrinsic viscosity of rod-like objects of length L and cross-sectional diameter d_C was calculated by Yamakawa and Yoshizaki as:

$$[\eta]_{rod} = \frac{\pi N_A}{24}\frac{L^3}{M}F_\eta(L/d_C), \quad (38)$$

where $[\eta]_{rod}$ is expressed in units of volume per mass and $F_\eta(L/d_C)$ is a function given in ref. 384, which tends to $1/\ln(L/d_C)$ in the large L/d_C limit.

Following eqn (38), the intrinsic viscosity of NaPSS in deionised water is plotted as a function of N in Fig. 10(b). In order to allow comparison with other systems, we expressed $[\eta]$ in units of M^{-1} and normalised it by b^3 (b = 2.5 Å and b = 5 Å for vinyl and cellulose polymers, respectively). Note that in the $c \to 0$ limit, polyelectrolytes are in the excess salt regime ($fc < 2c_s$) due to the residual salt content of water. The estimation method of the residual salt concentration can be found in ref. 100, 285 and 301. In Fig. 10(b), we selected data in a sufficiently dilute solution to reach the linear η_{red} *vs.* c region and discarded intrinsic viscosity data obtained by use of fitting functions that do not yield a peak in η_{red} *vs.* c dependence. Data by Cohen *et al.*[297,315] for high molar masses are not included as these are likely far from the zero-shear limit. Their results from ref. 315, discussed in Section S3 of ESI,† are also not included. Results reported by Yamanaka *et al.* for higher molar masses were measured over a wide range of shear rates and extrapolated to $\dot{\gamma} \to 0$.[322,323] For comparison, we included Fujita and Homma's two lowest M_w samples[335] and data reported by Sitaramaiah and Goring[385] for sodium carboxymethyl cellulose (NaCMC) in 10^{-5} M NaCl. We expect Sitaramaiah and Goring's sample to correspond to the shear thinning region. Fujita and Homma's samples are expected to be weakly influenced by shear thinning (see Fig. 10 of ref. 336). Therefore, the NaCMC data should be viewed as lower bound estimates for $[\eta]$. The intrinsic viscosity of NaPVS, estimated from the Huggins plot in Fig. 7(c) and from Nishida *et al.*'s method, is also included for comparison. The theoretical calculation for the intrinsic viscosity for chains in their fully extended conformation (eqn (38) with $L = Nb$), shown as a dashed line, under-predicted all experimental results.

The data of Zhao and co-workers[386] showed that the diffusion coefficients of NaPSS at extreme dilution in DI water and in 10^{-4} M aqueous NaCl were nearly identical, see also Fig. 31. The intrinsic viscosity of NaPVS, when estimated by Nishida's method, similarly showed no significant change for $c_s < 10^{-4}$ M.[299] In contrast, data reported by Cohen *et al.*[315] indicated that $[\eta]$ for NaPSS ($N \simeq 1600$) in 10^{-4} M NaCl was ≃3× lower than those in DI water.[387] The origin of this discrepancy is not clear to us, but it may point to an error in the estimates of $[\eta]$. The fact that Cohen's $[\eta]$ value exceeded the maximum theoretical value by over an order of magnitude at low N supports this. The intrinsic viscosities shown in Fig. 10(b) for $N > 100$ are ≃×2 higher than the theoretical prediction. Since $[\eta] \simeq R_H^3/N$, this is consistent with Zhao and co-worker's data, which exceeds the theoretical prediction for R_H by ≃20%. The hydrodynamic drag generated by counterions, known as the primary electroviscous effect,[388,389] seems like the most likely cause for R_H and $[\eta]$ exceeding the theoretical values of a fully

stretched rod. Experiments analogous to those presented in Fig. 10 probing the influence of the counterion size could provide confirmation of this.

The available data in the infinite dilution limit therefore suggest that NaPSS adopts a fully stretched chain conformation ($B = 1$) with no fluctuations perpendicular to the end-to-end vector of the chain. In contrast, measurements of the correlation length of NaPSS in dilute and semidilute solutions for 0.005 M $< c <$ 1 M give a larger stretching parameter of $B \simeq 1.8$.[234,390,391] An analysis of the correlation length data over a very broad concentration range[234,392–395] suggests that the stretching parameter displays a weak increase with increasing concentration, which could explain this discrepancy.[396] Conclusions drawn from intrinsic viscosity and/or diffusion data should be taken with caution until a more comprehensive grasp of the primary electroviscous effect is obtained. To enhance our understanding, experimental measurements similar to those depicted in Fig. 10, but conducted on polyelectrolytes with varying counterions, would be particularly valuable.

3.6 Overlap concentration in salt-free solutions

3.6.1 Influence of molar mass and charge density. For neutral polymers, the overlap concentration can be estimated as $c^* = [\eta]^{-1}$, $c^* \simeq 4M\pi/3R_g{}^3$, $c^* \simeq M/R^3$ or a similar method based on the static or hydrodynamic size of the chains.[400–402] For polyelectrolytes in salt-free solutions, the aforementioned difficulties in determining $[\eta]$ or the single chain dimensions mean that these methods are not widely used. Instead, c^* can be estimated as the point at which the solution viscosity is twice that of the solvent or $\eta_{sp} = 1$.[14,285,301,403,404] This method yielded results which are largely consistent[301,397,405] with the more rigorous estimates based on the cross-over in the scaling of the correlation length between $\xi \sim (N/c)^{1/3}$ (dilute) to $\xi \sim c^{-1/2}N^0$ (semidilute). Two other methods to estimate c^* based on dielectric spectroscopy data were developed by Colby and co-workers also agreed with the viscosity method, see Fig. 12 of ref. 68.

The overlap concentration of NaPSS in salt-free solution obtained by viscosity and scattering methods is compared in Fig. 11. The two estimates agreed well and showed $c^* \propto N^{-2}$ in the high-N region, as expected from scaling theory. This scaling has also been reported for other systems.[286,406] For $N \gtrsim 3000$, the data from Gulati *et al.*,[100] Han *et al.*,[301] Boris and Colby,[285] and Ganter *et al.*[298] deviated to a power-law of $N^{-0.78}$, as expected in eqn (1) in the $2c_s \gg fc$ region. These datasets follow eqn (1) with $c_s \simeq 10^{-5}$ M, shown by the dashed line. This is

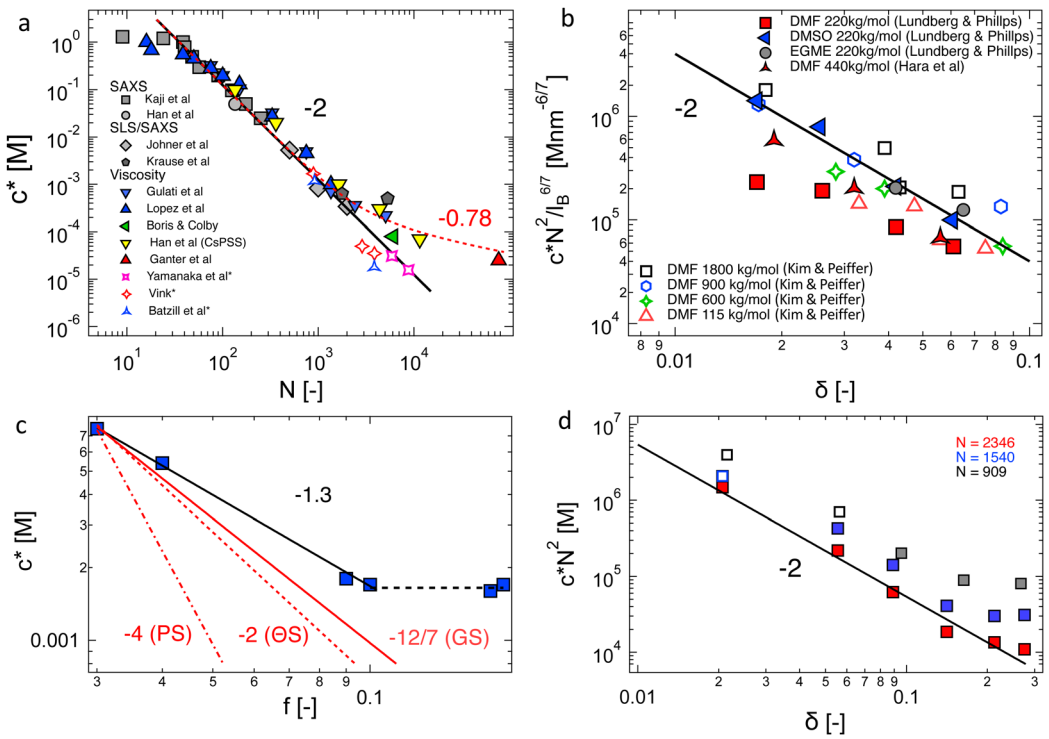

Fig. 11 (a) Overlap concentration of NaPSS in DI water determined by scattering methods (grey symbols, data from ref. 390 as compiled in ref. 285 and 14, see also ref. 397) and using the $\eta_{sp}(c^*) = 1$ criterion (coloured symbols from ref. 96, 100, 285, 298, 301, 318, 320 and 322). Refs marked with an asterisk are for measurements carried in a nitrogen atmosphere, which minimises carbonic acid content. Full and dashed lines are the fits at $c_s = 0$ M, $B = 2.5$ and $c_s = 10^{-5}$ M, $B = 2.5$, see eqn (1). (b) Overlap concentration of lightly sulfonated polystyrene, normalised by $N^{-2}l_B{}^{6/7}$, as expected by eqn (6c) as a function of the fraction of monomers bearing a charge, δ. Given the low degrees of sulfonation (<9%), no counterion condensation is expected and δ is expected to coincide with f. Data are from ref. 185 and 398. (c) Overlap concentration of quaternized P2VP in ethylene glycol as a function of the fraction of groups bearing a dissociated counterion, f, which was measured by conductivity. Data are from ref. 97. Red lines are scaling predictions for good solvent, theta solvent and poor solvent. (d) Overlap concentration of aminoacetalized polyvinyl acetate as a function of charged group fraction, degree of polymerisation indicated in the legend. See the text for an explanation of the hollow symbols. Data are from ref. 399.

consistent with estimates for the residual salt in NaPSS solutions, which arise due to carbonic acid dissolved from the air, of $\sim 10^{-5}$–10^{-4} M, see ref. 100, 285, 297 and 301. Vink,[318] Yamanaka *et al.*[322,323] and Batzill *et al.*[320] measured the viscosities of NaPSS in a nitrogen atmosphere to avoid contamination from carbonic acid. Their data displayed lower c^* values in the high-N region with no apparent crossover to the high salt scaling. Fitting eqn (1) and (7) to the data in the $c^* \propto N^{-2}$ region gave $B \simeq 2.5$, which indicates that chains are significantly less extended at the overlap point than at infinite dilution. The estimate of B from c^* data is close to those obtained from correlation length data in the semidilute regime.[96] For $N \lesssim 20$–30, corresponding to chains with fewer than 2–3 Kuhn segments,[391] the c^* data systematically deviated to lower values relative to the high-N power-law. This may be interpreted as a cross-over to the $R < \xi_{el}$ regime, where chains are not electrostatically stretched and adopt neutral polymer conformation which is consistent with the weak variation of c^* with added salt in this N range.[397] Such interpretation gives $\xi_{el} \simeq 3$ nm. This is not entirely consistent with eqn (6), which indicates $\xi \simeq l_B \simeq 0.71$ nm for PSS in water.[407,408] Further, the $\xi_{el} \simeq 3$ nm value does not agree with scattering data for the chain dimensions in the semidilute regime[19,391] or with the cross-sectional diameter of chains measured by the zero-average contrast method.[125] The $c^* - N$ exponent has been observed to take apparent values as low as -2.5 in a recent simulation,[409] which are not seen in Fig. 11(a).

Chain shrinkage from the infinite dilution limit to the overlap concentration is consistent with the simulation work of Stevens and Kremer.[98] Oostwal *et al.*'s data showed that the diffusion coefficient of NaPSS decreased upon dilution below c^*, which also suggests chain expansion upon dilution.[410] The charge fraction is known to increase with dilution below c^*,[80,411] and may be in part related to the differences in chain dimensions at infinite dilution and at the overlap point.[412]

The influence of charge fraction and solvent's Bjerrum length on the overlap concentration of lightly sulfonated ionomers in polar solvents is considered in Fig. 11(b). All estimates of c^* are viscosimetric. The datasets of Kim and Peiffer[398] for four degrees of polymerisation and varying charge densities (δ) in dimethylformamide (DMF) solution and that of Hara *et al.*[172] for a single molar mass reasonably collapsed onto a single curve with a slope of -2, supporting the validity of eqn (7). Lundberg and Phillips' data[185] for a single molar mass in three solvents dimethylformamide (DMF, $\varepsilon_r = 37$), dimethyl sulfoxide (DMSO, $\varepsilon_r = 49$) and ethylene glycol monomethylether (EGME, $\varepsilon_r = 17$) also collapsed broadly and agreed with the observed trend, but the $c^*N^2/{l_B}^{6/7}$ values in DMF were clearly lower than in the other two solvents. Differences in solvent quality for the backbone may help explain these discrepancies because DMF is a good solvent for the PS backbone[413,414] while DMSO or EGME are non-solvents for polystyrene. However, if DMSO and EGME data correspond to the $T \ll \theta$ condition, it is not clear why poor solvent scaling ($c^* \propto f^{-4}$), calculated from eqn (1) and (8) does not apply. This suggests that there are factors influencing polyelectrolyte conformation not captured in eqn (6). Further evidence for this can be seen from the fact that in cyclohexanone ($\varepsilon_r = 18$), the viscosity of NaPSS displayed ionomer behaviour while in EGME, which has a lower dielectric constant, a polyelectrolyte behaviour is apparent.

Eqn (6) was also be tested using the data of Dou and Colby[97] for the intrinsic viscosity of P2VP quaternized to different degrees in ethylene glycol (EG) solutions, as shown in Fig. 11(c). The authors estimated the fraction of monomers bearing a dissociated charge from conductivity measurements. Comparing the intrinsic viscosity for P2VP in EG with the values for a theta solvent,[415] we estimated that the thermal blob of the uncharged polymer contain $\simeq 59$ chemical monomers. The number of monomers in an electrostatic blob is estimated as follows:

$$g_{el} = \frac{N}{g_K}\left(\frac{[\eta]}{[\eta_0]}\right)^{-5/6}, \tag{39}$$

where $[\eta]$ and $[\eta_0]$ are the intrinsic viscosities of the polyelectrolyte and non-ionic polymers, respectively, in units of vol/mol. For all charge fractions, we find $g_{el} > g_T$ and therefore expect eqn (6c) to apply, which predicts $c^* \propto f^{-12/7}$, shown by the full red line. The experimental data displayed a weaker dependence of $f^{-1.3}$ for $f < 0.1$ and $c^* \sim f^0$ at higher f. The scaling predictions for theta and poor solvents are also shown as dashed lines and display a greater deviation from the experimental results.

Matsumoto and Eguchi[399] reported diluted viscosity data for aminoacetalyzed polyvinyl alcohol with different fractions of charged groups in salt-free water. As 0.1 M K_2SO_4 is a near theta solvent for the uncharged polymer,[416] we expect water to be a marginally good solvent for the backbone and $\xi_T \gg \xi_{el}$. The c^* values normalised by N^2 are plotted as a function of the fraction of charged groups in Fig. 11(d) and are consistent with the $c^* \propto f^{-2}$ scaling prediction, assuming no significant counterion condensation ($\delta \simeq f$), see the ESI,† Section S4, for the calculation of δ. The hollow points are c^* obtained by extrapolating the data significantly beyond the measurement range.

Lastly, it is worth noting that plots of c^* as a function of the reduced contour length Nb/B, where B is determined using scattering techniques, do not exhibit the universal behavior as predicted by the scaling model.[286]

3.6.2 Influence of solvent permittivity for highly charged polyelectrolytes. We next consider the influence of the solvent dielectric constant on the overlap concentration of highly charged polyelectrolytes. Unlike the polystyrene ionomers considered in Fig. 11(b), the spacing between charged groups is smaller than the Bjerrum length and counterion condensation takes place.

We analyzed the literature data reported by Jousset *et al.*[174] for poly([(2-methacryloyloxy)ethyl]trimethylammonium 1,1,2,3,3-pentacyanopropenide) (P(M-PCP)) and Matsumoto *et al.*[56] for poly(1-butyl-3-vinylimidazolium bis(trifluoromethanesulfonyl)imide) (PC_4-TFSI) in solvents having a broad range of dielectric constants ε_r ranging from 7.9 to 182. The solution viscosities of PC_4-TFSI were measured as a function of shear-rate ($\dot{\gamma}$) and the $\dot{\gamma} = 0$ limit was taken to calculate η_{sp}. For P(M-PCP), capillary viscometers were used, and thus, it is possible that some of the

data at low c and high ε_r may be influenced by shear thinning. The overlap molar concentration of monomers, c^*, was determined using the viscosimetric criterion outlined earlier ($\eta_{sp}(c^*) = 1$) and plotted as a function of the solvent's Bjerrum length l_B in Fig. 12. Here, when the η_{sp} dataset did not contain the data points crossing at $\eta_{sp} = 1$ over the measured c range, we extrapolated the power-law fit towards $\eta_{sp} = 1$.

For PC_4-TFSI solutions, the value of c^* initially decreased slightly with increasing l_B for $l_B < 1$ nm, beyond which it increased as $c^* \propto {l_B}^{2.1}$. It appears that the obtained exponent agrees with the scaling law of c^* in poor solvents, *i.e.*, $c^* \sim {l_B}^{2.0}$. Additional experimental evidence (for example from phase behaviour or A_2 data in excess salt) is needed to establish if the various solvents considered correspond to the $T \ll \theta$ condition.[417] The observed non-monotonic dependence of c^* for PC_4-TFSI could be attributed to the high content of residual salts in the solvent NMF (*N*-methylformamide).[418] Matsumoto *et al.* reported a residual salt concentration of 3.6 mM in NMF, which is higher than the measured $c^* \simeq 1$ mM. Assuming $f = 1$ in eqn (13), we estimated the overlap monomer concentration in salt-free NMF to be $c^* \simeq 4.3 \times 10^{-5}$ M. This estimate is included as a filled circle shown in Fig. 12 and agrees well with the trend observed for other solvents. The reduction of ε_r in NMF may be an alternative cause for the observed non-monotonic behaviour of c^*. Dou and Colby[418] have pointed out that a high dielectric constant of NMF stems from the Kirkwood correlations involving effective alignment of NMF molecules, and therefore solutes, *e.g.*, PC_4-TFSI, can randomize such a molecular alignment, leading to the reduction of ε_r in NMF containing polyelectrolytes. Adopting $\varepsilon_r = 55$ proposed for NMF with no alignment correlations,[418] we also observed a good agreement with the trend line shown in Fig. 12 (see an open triangle at $l_B = 1.0$ nm). However, further experimental work is required to confirm this hypothesis, for example, through dielectric relaxation spectroscopy.[419]

For P(M-PCP) solutions, we observed a discontinuous change in c^*, as shown in Fig. 12. The value of c^* increased with increasing l_B for $l_B < 0.6$ nm, exhibited a significant reduction of c^* at $l_B \sim 0.6$ nm, increased again as l_B was increased further while displaying a power-law behaviour with exponent similar to that for PC_4-TFSI. Two data points at $l_B = 0.52$ nm and $l_B = 0.31$ nm correspond, respectively, to the c^* data for P(M-PCP) in formamide (F) and in NMF having higher ε_r than the other solvents for $l_B > 0.6$ nm. According to the Manning model (eqn (32)), we anticipate a more stretched configuration in F and NMF and thus a monotonic decrease of c^* with respect to the decreasing l_B. However, the experimental result showed a drastic change in the size of the P(M-PCP) chain when crossing $l_B \sim 0.6$ nm. The observed increase in c^* might be explained again by considering either the presence of residual salts in NMF or the reduction of the solvent dielectric constant, as we discussed above. Note that the origin of the high ε_r in F is the same as that in NMF.[420] Although Jousset *et al.* did not report the residual concentration in their NMF, the residual salt of commercial NMF grades has been reported to be as high as 0.02 M.[421,422] Therefore, assuming $f = 1$ and $c_s = 0.02$ M, we estimated c^* in salt-free NMF, which yielded $c^* \simeq 6 \times 10^{-3}$ M. As seen as a filled square and an inverted triangle in Fig. 12, both scenarios appear insufficient to fully account for the drastic change of c^* in magnitude. We will provide a further discussion on this point in Section 3.8.1.

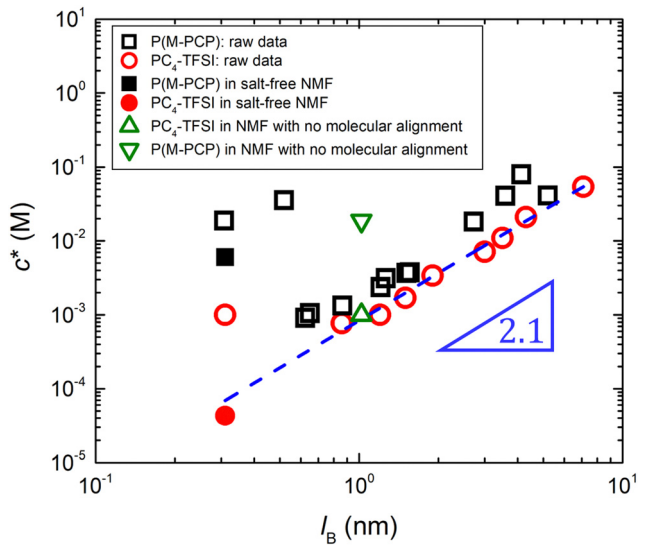

Fig. 12 The dependence of the overlap monomer concentration c^* on the Bjerrum length l_B for PC_4-TFSI (red circles) and P(M-PCP) (black squares) solutions without added salt. Dashed blue line is the best-fit power-law to PC_4-TFSI data for $l_B > 0.7$ nm. The full red and black points are the estimate of c^* in salt-free NMF, while the hollow green points are the estimate of c^* in NMF with no alignment correlations at $\varepsilon_r = 55$. Data are from ref. 56 and 174.

3.7 Counterion condensation

The estimation of the charge fraction f is not trivial because how many of the counterions on a polyelectrolyte chain are detected as dissociated counterions depends on how we measure it. As a result, the measured value of f can vary within a factor of order unity even if the same test sample is used, depending on the measurement technique applied.[419] From literature reports, experimental methods using osmotic pressure,[89,423–426] light scattering,[423,427–429] potentiometry,[80,328,430–436] ionic conductivity,[326,330,437,438] and complex permittivity[419] have been used to evaluate the charge fraction on a polyelectrolyte chain more accurately. Many of these data are in the semidilute regime and we do not review them here (see ref. 68 and 80, for more details). In this review, we estimated the charge fraction f based on the scaling law of c^* given by eqn (13). In estimating f, we assume B for theta solvents, *i.e.*, eqn (8b) and assume $l_{K,0} = \xi_T = 2$ nm for flexible polymers in the athermal solvent due to the lack of experimental data of $l_{K,0}$ and ξ_T for the tested polyelectrolytes. Because of these assumptions, the estimated f contains uncertainties in magnitude. b was set at $b = 0.25$ nm for vinyl polymers.

3.7.1 Influence of the molar mass. We analyzed the c^* data for NaPSS in a salt-free solution, as shown in Fig. 11. According to eqn (13), the scaling law of c^* at $c_s = 0$ M (*i.e.*, salt-free) is given by

$$c^* \approx N^{-2} l_B^{-1} b^{16/7} l_{K,0}^{-30/7} f^{-2}. \quad (40)$$

Therefore, the charge fraction f can be estimated as

$$f \approx [c^* N^2 l_B b^{-16/7} l_{K,0}^{30/7}]^{-1/2}. \quad (41)$$

Fig. 13(a) shows the dependence of f on the degree of polymerisation N for NaPSS in salt-free aqueous solutions.

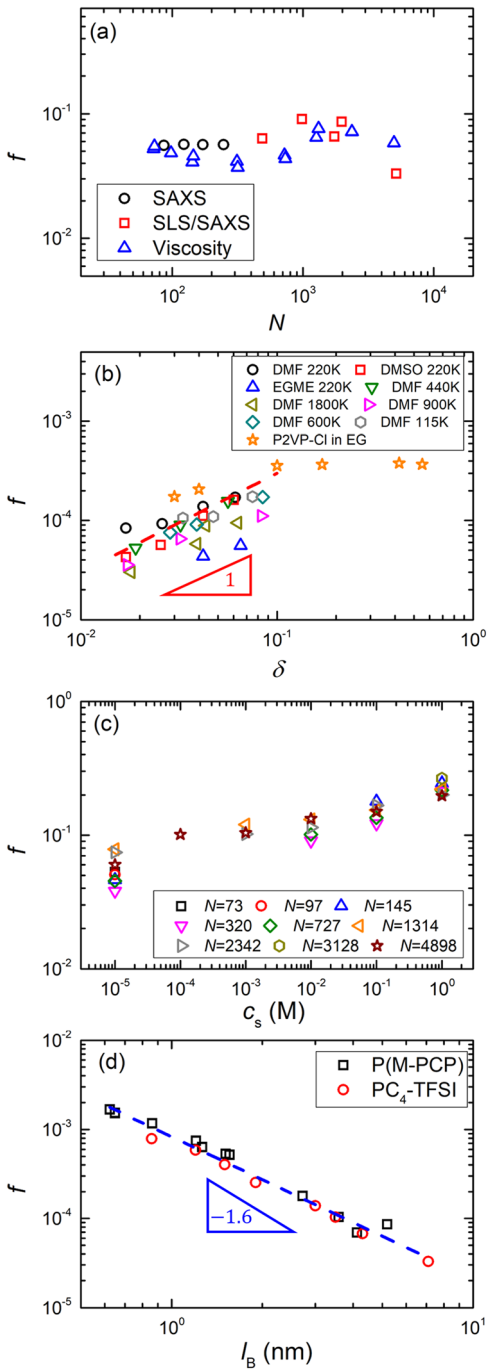

Fig. 13 The dependence of the charge fraction f on (a) the degree of polymerisation N for NaPSS, (b) the fraction of ionic monomers δ, (c) the molar concentration of salts c_s, and (d) the Bjerrum length l_B. c^* data used to calculate f for plots (a)–(c) are from Fig. 11. Plot (d) uses c^* data from Fig. 12.

Here, we did not consider data points at $N < 60$ from our f analysis since eqn (13) does not apply. In Fig. 13(a), we observed that the value of f was independent of N for $N < 2 \times 10^3$, in good agreement with the trend predicted by the Manning counterion condensation model, *i.e.*, $f \propto N^0$. It appears that f starts to decrease with increasing N for $N > 2 \times 10^3$. This is probably because the overlap concentration in a salt-free solution becomes comparable to the level of the concentration of residual salts in water. The effect of residual salts in water on the measured c^* is also observed in Fig. 11(a). While the N^{-2} power-law depicted in Fig. 11(a) shows the overlap concentration of the order of 10^{-5} M for NaPSS at $N > 3 \times 10^3$, experimental results display overlap concentrations greater than 10^{-4} M. Therefore, the observed apparent decrease of f might be explained by taking the contamination of residual salts into account. In fact, when setting the overlap concentration larger than measured, the estimated f value using eqn (41) becomes larger than plotted in Fig. 13(a).

The estimated value of f in the plateau regime was much smaller than the value of $f \sim 0.2$ obtained using conductivity[330] and osmotic pressure[89] measurements. This indicates that the charge fraction f values from eqn (41) are approximately 100 times smaller than expected. Nevertheless, the trends illustrated in Fig. 13 remain noteworthy.

3.7.2 Influence of the charge density. In order to evaluate the dependence of f on the charge density δ of polyelectrolytes, we analyzed the c^* data provided in Fig. 11(b) for NaPSS ionomers and Fig. 11(c) for P2VP in ethylene glycol (EG). The obtained f was plotted as a function of δ, as shown in Fig. 13(b). We observed that for NaPSS ionomers, although the difference in the strength of the excluded volume interaction among the tested solvents may result in the difference in magnitude of f, the value of f was found to increase linearly with increasing δ. A similar linear dependence of f on δ was observed for the P2VP in EG at $\delta < 0.1$. Moreover, for $\delta \geq 0.1$, the value of f became independent of δ, indicating an occurrence of the counterion condensation at $f \sim 0.1$. Remarkably, the observed critical point at $f \sim 0.1$ showed fair agreement with Manning's model prediction that the condensation occurs at $\delta \sim 0.16$ for vinyl polymers in EG since $u_M = 6.1$. However, note that our estimate of f from c^* differs from that obtained by Dou and Colby using the conductivity measurements.

3.7.3 Influence of the salt addition. For this purpose, we leveraged the c^* data for NaPSS in aqueous NaCl solutions, shown in Fig. 16. Fig. 13(c) shows the dependence of f on the molar concentration of NaCl, c_s, at five different concentrations. The value of f was estimated by solving eqn (13) with respect to f. Specifically, we computed the value of f as the x value of the intersection point between the following two functions:

$$y = 1 + \frac{O}{x}, \quad (42)$$

$$y = Hx^{4/3}, \quad (43)$$

where O and H are constants, given by $O = \frac{2c_s}{c^*}$ and $H = (c^*)^{2/3} N^{4/3} b^{2/3} l_{K,0}^{2/3} l_B^{2/3}$. In the calculation, the variation of the solvent

dielectric constant ε_r with respect to the increasing c_s was also included.[439]

Fig. 13(c) shows that the value of f increases with increasing c_s. This result suggests that the number of dissociated counterions increases with increasing c_s. However, theoretical[144] and simulation[164] results predict a decrease in the charge fraction with the increasing c_s. The apparent increase observed in Fig. 13(c) at high salt concentrations can be understood by noting that eqn (40) only applies when the screening length is larger than the electrostatic blob size, which breaks down at high c_s. Beyond this limit, polyelectrolyte chains will exhibit an asymptotic decrease in chain size with respect to the increasing c_s, approaching a constant end-to-end distance at high c_s determined by the intrinsic (non-electrostatic) chain stiffness. Applying eqn (13) in this regime could lead to an over-prediction of f. For comparison, transference experiments for NaPA in aqueous NaCl solution showed that f is independent of c_s for $c_s < 0.1$ M.[151,440,441]

3.7.4 Influence of the solvent permittivity. We finally discuss the effect of the solvent dielectric constant ε_r on f while using the c^* data provided in Fig. 12. The obtained values of f are plotted as a function of l_B in Fig. 13(d). Here, we removed the data of PC_4-TFSI in NMF and of P(M-PCP) in F and NMF. The degree of polymerisation N was set at $N = 1504$ for P(M-PCP) and at $N = 2474$ for PC_4-TFSI based on the molecular weight data available in the literature.[174,442] Strikingly, the f estimates for both PIL systems were collapsed onto the same trend line. These results suggest that the charge fraction of PILs is solely dependent on the dielectric constant of solvents, regardless of the chemical structure of PIL repeating units. The value of f decreased monotonically with increasing l_B, showing a scaling relationship of $f \propto l_B^{-1.6}$. Here, we recall the scaling relationship between f and l_B predicted by Manning's counterion condensation model, *i.e.*, $f \propto l_B^{-1}$. Our findings reveal a more pronounced exponent than the Manning model forecasts, which may be attributed to the solvent's dielectric constant influencing the local conformation of flexible polyelectrolytes. It is also important to consider that the polymer's presence could alter the dielectric properties of the solvent, particularly in the case of hydrogen-bonding solvents. Therefore, it is crucial to directly measure the dielectric constant of the solutions rather than relying solely on the permittivity values of the solvent, as we discussed in Section 3.6.2.

The procedure to estimate the $f \propto l_B^{-1.6}$ relation relied on three assumptions: (1) chains adopt a rod-like conformation on distances larger than the electrostatic blob (eqn (7)); (2) the electrostatic blob size for a polyelectrolyte in theta solvent scales with the charge fraction as $\xi_{el} \propto f^{2/3}$ (eqn (6b)); (3) ξ_T and $l_{K,0}$ do not depend on ε_r. The first assumption is validated by the $c^* \propto N^{-2}$ scaling observed for various systems,[95,285,286,404,406] as discussed in the preceding sections. The second assumption is supported by the data shown in Fig. 11(d), but has not been tested extensively. The third assumption, while difficult to test rigorously, is supported by the fact that the two PILs showed the same scaling despite their very different chemical structures. Deviations from the Manning model for ionenes in solution were reported by Popov and Hoagland on the basis of measurements of electrophoretic mobility[152] and by Rodivc *et al.*[443] from electrical conductivity and transport numbers data. In both studies, ion-solvent interactions appeared to influence the degree of counterion binding.

The Muthukumar model[144] might capture the observed trend of f against l_B, *i.e.*, by considering the dielectric mismatch between the bulk and the local region around polyelectrolyte chains. However, the use of the Muthukumar model requires *a priori* knowledge of several material parameters, such as the dipole length of ion-pairs, the local dielectric constant, and the excluded volume parameters, which are not available in literature reports. The observed discrepancy between the experimental data and the theoretical prediction warrants more in-depth studies in the future.

3.8 Influence of solvent type on the solution viscosity

3.8.1 Poly(ionic liquid)s. Jousset *et al.*[174] first reported a systematic analysis on the shear viscosity of a PIL, P(M-PCP), in various solvents with a wide range of ε_r: from $\varepsilon_r = 182$ for *N*-methylformamide (NMF) to $\varepsilon_r = 11$ for triethyl phosphate (TEP). Fig. 14 shows the dependence of the specific viscosity η_{sp} on the molar concentration of monomers c. Five viscosity trends can be identified from the plot:

(I) For P(M-PCP) in CPY, EC–PC, PC, DMSO, DMF, and ACN solutions, η_{sp} followed the scalings of $\eta_{sp} \propto c^{0.5}$ and $\eta_{sp} \propto c^{1.0}$ at high and low c. The transition occurred at $\eta_{sp} \sim 1$ and the exponents matched Dobrynin *et al.*'s predictions for the semi-dilute unentangled and dilute regimes. The value of η_{sp} for a given c increased with increasing ε_r, indicating that the number

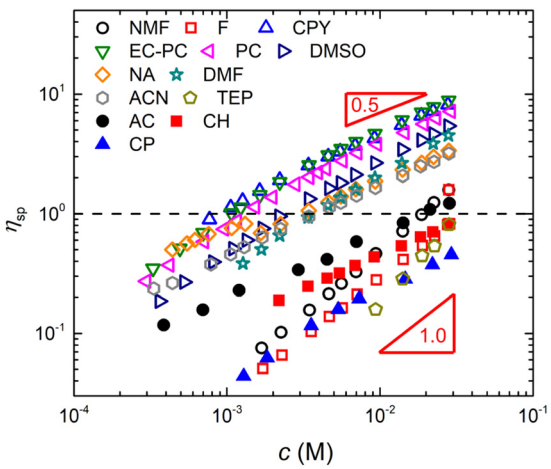

Fig. 14 Dependence of the specific viscosity η_{sp} on the monomer concentration c of P(M-PCP) in various solvents with different dielectric constants ε_r. The solvents are triethyl phosphate (TEP: open pentagons, $\varepsilon_r = 11$), cyclopentanone (CP: filled triangles, $\varepsilon_r = 14$), cyclohexanone (CH: filled squares, $\varepsilon_r = 16$), acetone (AC: filled circles, $\varepsilon_r = 21$), acetonitrile (ACN: open hexagons, $\varepsilon_r = 36$), dimethylformamide (DMF: open stars, $\varepsilon_r = 37$), 2-nitroanisole (NA: open diamonds, $\varepsilon_r = 44$), dimethyl sulfoxide (DMSO: open right-pointing triangles, $\varepsilon_r = 46$), propylene carbonate (PC: open left-pointing triangles, $\varepsilon_r = 65$), ethylene carbonate–propylene carbonate mixture (EC–PC: open inverted triangles, $\varepsilon_r = 86$), 2-cyanopyridine (CPY: open triangles, $\varepsilon_r = 90$), formamide (F: open squares, $\varepsilon_r = 108$), and *N*-methylformamide (NMF: open circles, $\varepsilon_r = 182$). The values of η_{sp} are estimated from Fig. 2 of ref. 174.

of dissociated counterions increased with increasing ε_r, as discussed in Section 3.6.2.

(II) For NA, AC, and CH solutions, η_{sp} displayed a single power-law dependence with respect to c over the measured c range. The power-law fit to the measured η_{sp} yielded the scaling of $\eta_{sp} \propto c^{0.55}$. Interestingly, the estimated power-law exponent was smaller than unity, although the tested solutions fell under the dilute concentration regime. These results suggest that the conformation of the P(M-PCP) chains depends on the concentration,[56,146,444] or the influence of interchain repulsion[345,346] on the solution viscosity.

(III) In the CP solutions, the measured η_{sp} exhibited two different power-law trends in the dilute regime. For $c < 7 \times 10^{-3}$ M, $\eta_{sp} \propto c^1$, consistent with the prediction for dilute solutions. However, at higher c, the power-law exponent became smaller. The observed trend of η_{sp} against c might be explained by considering the conformation change of polyelectrolytes in the dilute regime.[146] Alternatively, the presence of a small amount of residual salt in the solvent could account for the decrease in the exponent at higher polymer concentrations.

(IV) In TEP solutions with the lowest ε_r, the value of η_{sp} decreased linearly with the decreasing c, showing a similar trend of η_{sp} for neutral polymer solutions.

(V) In F and NMF solutions with the highest ε_r, the value of η_{sp} decreased linearly with the decreasing c, suggesting that the P(M-PCP) chain behaves as a neutral polymer in F and NMF even though ε_r was higher than those in the other solvents. Waigh *et al.*[444] confirmed the observed neutral polymer-like behaviour of the P(M-PCP) in NMF from its SAXS profile where no peak was detected.

For group (IV) and group (V) solvents, the value of η_{sp} increased linearly with increasing c, consistent with the behaviour for dilute polymer solutions. Indeed, most of the reported η_{sp} were smaller than one, proving that the solutions fall under the dilute regime. For TEP which has the lowest ε_r of the solvents studied, the measured values of η_{sp} were significantly smaller than those in group (I) solvents and suggest a strong counterion condensation. On the other hand, the observed neutral polymer-like behaviour of P(M-PCP) in the F and NMF is rather counter intuitive since the amount of dissociated counterions is predicted to be large in the high ε_r, *i.e.*, a more stretched polyelectrolyte-like configuration of P(M-PCP) chains is expected in the F and NMF solvent.[13] The apparent strong condensation in F and NMF can be recovered when the solvent contains salt impurities or alters its dielectric constant by the polymer addition. However, we showed in Section 3.6.2 that both effects could not explain the observed degree of chain shrinkage in NMF.

Jousset *et al.*[174] reported a large increase in the specific viscosity of P(M-PCP) in NMF with increasing temperature, shown in Fig. 15. Their experiment produced two striking features: First, the overlap concentration, estimated as the point at which $\eta_{sp} \simeq 1$, increases by roughly an order of magnitude as the temperature increases from 40 °C to 50 °C, corresponding to a doubling of the end-to-end distance of the chains. This large change contrasts with the weak variation of the viscosity in the T = 25–40 °C and T = 50–60 °C intervals, suggesting a sharp transition. The observed transition can be

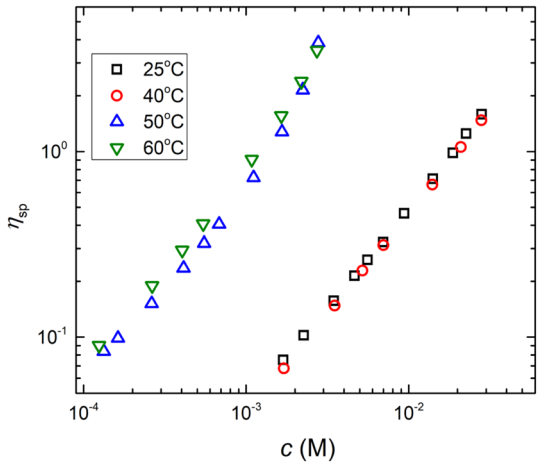

Fig. 15 Temperature induced transition for P(M-PCP) in NMF solution. Specific viscosity η_{sp} is plotted as a function of monomer concentration c for P(M-PCP) in NMF at different temperatures, as indicated in the legends. Data are from ref. 174.

explained by considering an increase in the charge fraction on the P(M-PCP) chain. However, several researchers[445,446] reported a significant reduction of the dielectric constant ε_r of NMF with the increasing temperature, indicating an increase in the Bjerrum length of NMF. This should lower the charge density of the polyelectrolyte, which clearly did not occur in Fig. 15.

As electrostatics alone does not seem to explain the drastic viscosity change in Fig. 15, it seems plausible that the transition may be driven by the change in solvent quality. In fact, poly(methyl methacrylate), whose chemical structure of the main chain is similar to that of P(M-PCP), is insoluble in F.[174] Note that this is different from the solvent quality collapse observed for hydrophobic polyelectrolytes,[147,447] as these systems display polyelectrolyte behaviour (*e.g.*, a sub-linear exponent of η_{sp} with concentration and a peak in their scattering function) even in the poor solvent regime.[341,448,449] It therefore appears that stronger excluded volume effects enable higher counterion dissociation and the emergence of polyelectrolyte behaviour. While it is known that solvation can influence the conformation of polyelectrolyte chains and the counterion distribution around them,[450–454] the exact mechanism that leads to this sharp transition remains unclear and deserves further investigation.

3.8.2 Ionomers. The shear viscosity of dilute polymer solutions has been widely used to probe the influence of electrostatics on the behaviour of charged polymers.[455] An increase of the reduced viscosity upon dilution (see Fig. 7(a)) is referred to as 'polyelectrolyte behaviour' and is recognized to arise primarily from electrostatic repulsion between chains.[346] This regime is associated with electrostatic repulsion dominating over other interactions, which leads to highly extended chain configurations. Solution viscosities in this regime tend to be either an increasing function of the fraction of charged monomers or independent of it. The opposite case, known as the ionomer regime, is characterised by a decrease in η_{red} upon dilution,[172] which is similar to the neutral polymer behaviour. In this regime, the dipolar attraction between condensed counterions is the

dominant form of electrostatic interaction.[456–458] As a result, the viscosity decreases as the fraction of charged monomers increases.[172,459,460]

The transition between polyelectrolyte behaviour and ionomer behaviour[455] can be induced by varying the solvent, counterions, or charge density. It seems clear that the solvent permittivity as well as solvation of counterions,[181,183,459,461] polymer backbone[462] and ionic side groups[184] play a role in the transition. Generally, it is observed that high solvent permittivity and good solvation of the counterions and ionic groups promote polyelectrolyte behaviour.[170,459] For example, Ono *et al.*[170] showed that an ionic polymer with large organic counterions behaved as a polyelectrolyte in non-polar media with low permittivity (ε_r = 5–9). A theoretical framework for the balance of dipolar attractions and electrostatic repulsion has been developed,[7,463] but understanding the influence of solvation remains a challenge. For example, it has been suggested that poor solvation of ions suppresses counterion dissociation,[183,461] but models to quantify these effects have not been developed. The available datasets appear to be insufficient to test simple models to quantify solvation interactions such as the use of Hansen solubility parameters. Some highly charged polyelectrolytes in low permittivity solvents (*e.g.* PC_4-TSFI in THF[56] or PAA in dioxane[195,464,465]) display neutral polymer behaviour, indicating that despite the large density of condensed counterions, the dipolar attraction is not significant, the reason for this is not clear to us. Analogous transitions to this polyelectrolyte-to-ionomer crossover are observed in polymer gels, for which more systematic studies on the influence of solvent parameters have been published.[466–477] Finally, we note that for highly charged polyelectrolytes in intermediate or low dielectric constant solvents, an ionomer-like regime, where chains are collapsed due to dipolar or charged induced attraction have been predicted,[142–147] but relatively little experimental data to test those predictions exist.[421]

3.9 Behaviour in excess salt solutions: scaling with c_s and N

Gulati *et al.*[100] reported the solution viscosity of NaPSS in aqueous solutions as a function of polymer concentration, molar mass and added NaCl concentration. The semidilute viscosity data showed a cross-over between the high salt exponent $\eta_{sp} \propto c^{5/4}$ and $\eta_{sp} \propto c^{1/2}$ at $c \simeq 10^{-3}$ M, which suggests a residual salt concentration in DI water of $c_s \simeq 7.4 \times 10^{-5}$ M, similar to the conductometric estimate of Han *et al.* (2×10^{-4} M).[301] Using the $c_s \simeq 7.4 \times 10^{-5}$ M value for the residual salt, we test eqn (13) in Fig. 16 by plotting $c^*[1 + fc^*/(2c_s)]^{-1.5}$ as a function of N, where c_s includes the added NaCl and the residual salt concentration. The value of f is set to 0.2.[68,91,96] This plot is seen to collapse data for different added salt concentrations except for the highest one (c_s = 1 M) into a single curve following a power-law of N^{-2}, in agreement with eqn (13). For c_s = 1 M, the experimental values of c^* strongly deviate downwards from the other datasets, indicating that chains are more extended than expected by eqn (13). At these high salt concentrations, where the intrinsic (non-electrostatic) contributions to chain stiffness are significant and $\kappa^{-1} < \xi_T \simeq l_B$, eqn (10) and (12) overpredict the c_s dependence of R, and hence of c^*.

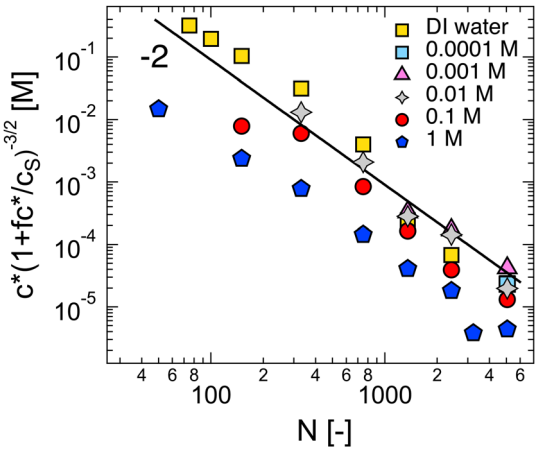

Fig. 16 Overlap concentration of NaPSS in aqueous NaCl solutions, normalised according to eqn (13). Line is power-law of −2. c^* are calculated using $\eta_{sp}(c^*) = 1$ criterion using data from ref. 100. A residual salt content of $c_s = 7.4 \times 10^{-5}$ M was assumed.[100]

Fig. 17(a)–(c) show the radius of gyration, the diffusion coefficient and the intrinsic viscosity of dilute PSS as a function of molar mass in 0.5 M salt solutions. The various studies considered indicated that the PSS polymer used had a low polydispersity ($M_w/M_n \lesssim 1.05$–1.2, see Table 2). However, due to the limited data presented in these reports, the accuracy of the polydispersity estimates could not be consistently verified.

For experiments that use static light scattering for the determination of R_g, M_w or A_2, only studies using refractive index increment measured at constant chemical potential are included.[480,481] The scaling exponents observed are close to those of neutral polymers in good solvent, in agreement with the scaling theory predictions for any polyelectrolyte regardless of solvent quality.[9,88,89] The R_g data display considerably more scatter than either D or $[\eta]$, perhaps in part due to the larger influence of polydispersity on R_g values. The N-exponent for $[\eta]$ (γ_η) is theoretically related to those for R_g (γ_R) and D (γ_D) as:[86]

$$\gamma_\eta = 2\gamma_R - \gamma_D - 1. \quad (44)$$

Considering the experimental values of $\gamma_\eta \simeq 0.71$, $\gamma_R \simeq 0.6$ and $\gamma_D \simeq -0.59$, this relationship is satisfied within ≃10%.

Data for the second virial coefficient are shown in Fig. 17(d). The results are from static light scattering measurements except for Hirose *et al.*'s dataset, where A_2 values are measured from sedimentation equilibrium.[105] The data are highly scattered, and it is therefore not easy to draw quantitative conclusions from them. For reference, we plot the theoretical polymer in a good solvent scaling prediction ($A_2 \sim N^{-0.23}$), which is approximately obeyed for an order of magnitude in N. For $N \lesssim 100$, a crossover to $A_2 \propto N^{-0.8}$ is observed for the dataset of Hirose *et al.* Datasets for NaPSS by other groups in this range are not available to check whether this cross-over is the result of experimental error. For comparison, polystyrene in toluene follows a power-law of $A_2 \sim N^{-0.27}$ for $N \gtrsim 20$. Deviations from a stronger power-law were observed only for oligomers ($N \simeq$ 5–10), as shown in Fig. S19 (ESI†). This phenomenon has

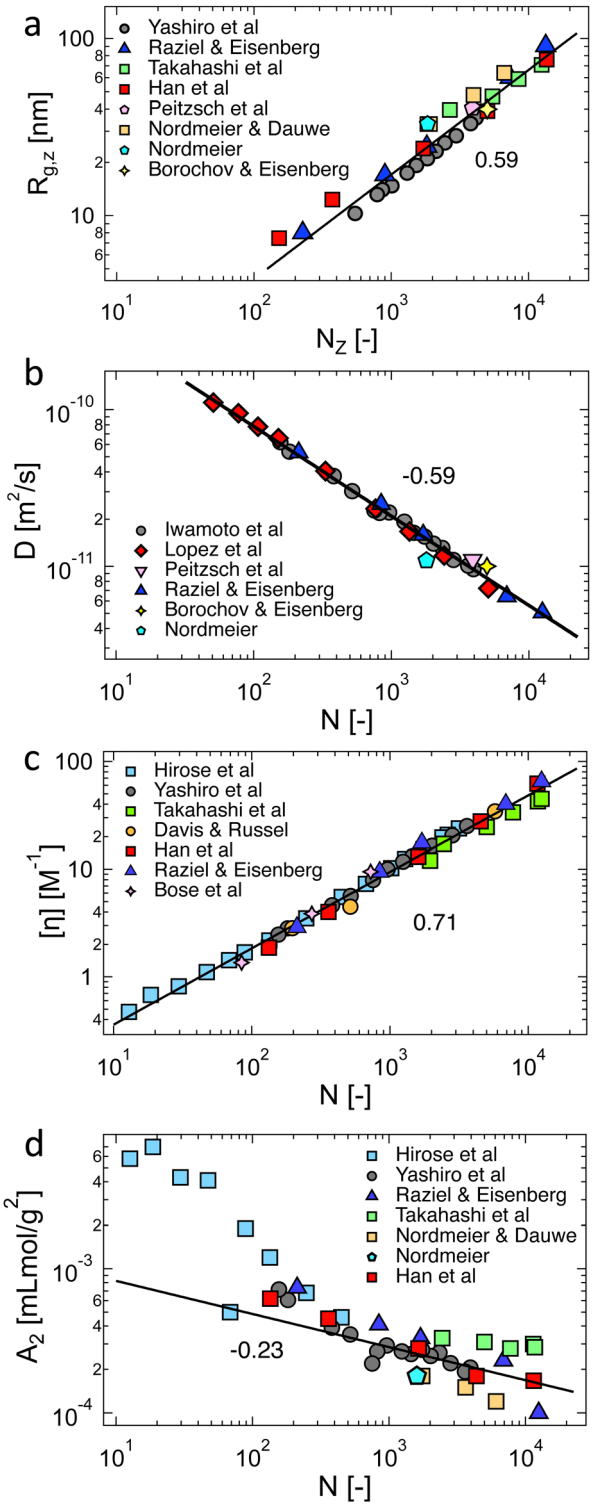

Fig. 17 N-Dependence of (a) the radius of gyration, (b) the diffusion coefficient, (c) the intrinsic viscosity, and (d) the second virial coefficient of PSS in 0.5 M salt solution. Data are from ref. 19, 105–107, 193, 301 and 472–479, see ref. 19 for a discussion of D and $[\eta]$ data. Davis and Rusell's[479] values are interpolated to c_s = 0.5 M. Lines for plots (a)–(c) are best-fit power laws ($R_g = 0.3N_z^{0.59}$ [nm], $D = 1.1 \times 10^{-9}N^{-0.59}$ [m^2 s^{-1}], $[\eta] = 0.07N^{0.71}$ [M^{-1}]). The line for A_2 is the scaling prediction for neutral polymers in good solvents. Analogous plots for polystyrene in toluene and cyclohexane are given in the ESI† (Section S7).

Table 2 Polydispersity of samples considered in Fig. 17

Authors	M_w/M_n	Ref.
Bose *et al.*	<1.1	478
Borochov and Eisenberg	—	476
Davis *et al.*	1.05–1.05	479
Han *et al.*	1.04–1.19	301
Hirose *et al.*	1.01–1.1[a]	105
Iwamoto *et al.*	1.01–1.1[a]	105 and 106
Lopez *et al.*	1.04–1.09	19 and 100
Nordmeier	≃1.2	472
Nordmeier and Daue	≃1.2	473
Peitz < 1.1	<1.1	477
Raziel and Eisenberg	—	475
Takahashi *et al.*	—	193
Yashiro *et al.*	1.01–1.1[a]	105 and 107

[a] M_z/M_w, where M_z is the z-averaged molar mass. For samples where no polydispersity is given, we assume M_z/M_w = 1.05, corresponding to sharp molar mass distribution. For samples where M_w/M_n is reported, we estimate M_z by assuming a Schulz distribution.

been assigned to the influence of chain ends.[482] Data for short poly(2-acrylamido-2-methylpropanesulfonate) (NaPAMS) chains by Norisuye and co-workers[109,112] reported a similar behaviour to that for the short NaPSS chains in Fig. 17(d). On the other hand, sodium hyaluronate[110,483] and xanthan[484,485] with a small number of Kuhn segments per chain did not display such large exponents. This implies that the presence of chain ends, rather than a transition to rod-like conformations, is the likely cause of the upturn at low N. To gain more clarity on these unusual observations, additional experimental investigations into the second virial coefficient of short flexible chains are needed. Exponents for the N-dependence of A_2 in excess salt solution are found to be consistently larger than the scaling prediction (−0.23) for flexible and semiflexible polyelectrolytes. Data for NaPAMS, sodium poly(3-methacyloyloxypropane-1sulfonate) (NaPOMS), xanthan and DNA are listed in Table 3.

3.9.1 Effects of incomplete sulfonation on NaPSS conformation. The results shown in Fig. 17 include data for fully sulfonated polystyrene, obtained by polymerisation of sodium styrene sulfonate (NaSS), and for PSS obtained by sulfonation of PS, which typically results in a degree of sulfonation of 80–100%.[490–493] No appreciable discrepancy is apparent between the two types of polymers, see ref. 19 for more details. At very high c_s, differences have been observed: NaPSS obtained by polymerisation of NaSS in aqueous NaCl solutions displays a theta point at c_s = 4.17 M and T = 17.8 °C. In contrast, the theta point of NaPSS obtained by sulfonation of polystyrene has been

Table 3 A_2 *vs.* N exponents for different systems

System	Exponent	Ref.
Xanthan/0.1 M NaCl	−0.19	484 and 485
NaHy/0.2 M NaCl	−0.27	110 and 483
NaPAMS/0.1 M NaCl	−0.39	109 and 112
NaPAMS/0.5 M NaCl[a]	−0.31	109 and 112
NaPOMS/0.01–5 M NaCl	−(0.27 to 0.3)	486
PS/toluene	−0.26	487–489[a]

[a] Data in the high N limit, see more details in Section S7 of the ESI.

reported by Takahashi *et al.*[193] at c_s = 4.17 M and T = 25 °C. The difference likely arises from the hydrophobicity of the unsulfonated monomers. Assuming 90–95% sulfonation for Takahashi *et al.*'s samples, an increase of θ by ~1 °C per percentage point of unsulfonated monomers can be estimated. A comparison of Nordmeier's data with ref. 105 and 193 gives the decrease in c_s at a fixed temperature that is required to compensate for a lower degree of sulfonation as ≃0.1 M per percentage point in the degree of sulfonation.[494,495] These effects likely contribute to the large scatter of experimental data observed for NaPSS at high c_s.[103]

3.9.2 The theta solvent dimensions of PSS. The reduced dimensions of NaPSS in theta solvents reported in different literature studies are presented in Fig. 18(a). The polydispersities assumed to calculate N_z are listed in Table 2. The $R_g^2/N_z \simeq 6$ Å^2 values of Hirose *et al.*[105] and Takahashi *et al.*[193] at 4.17 M NaCl and 3.1 M KCl, respectively, agree well. Raziel and Eisenberg reported a somewhat larger value of ≃11 Å^2. In contrast, Nordmeier[472] gave much larger chain dimensions of $R_g^2/N_z \simeq 34$ Å^2 in the 2.25 M < c_s < 3.74 M range, independent of c_s. This

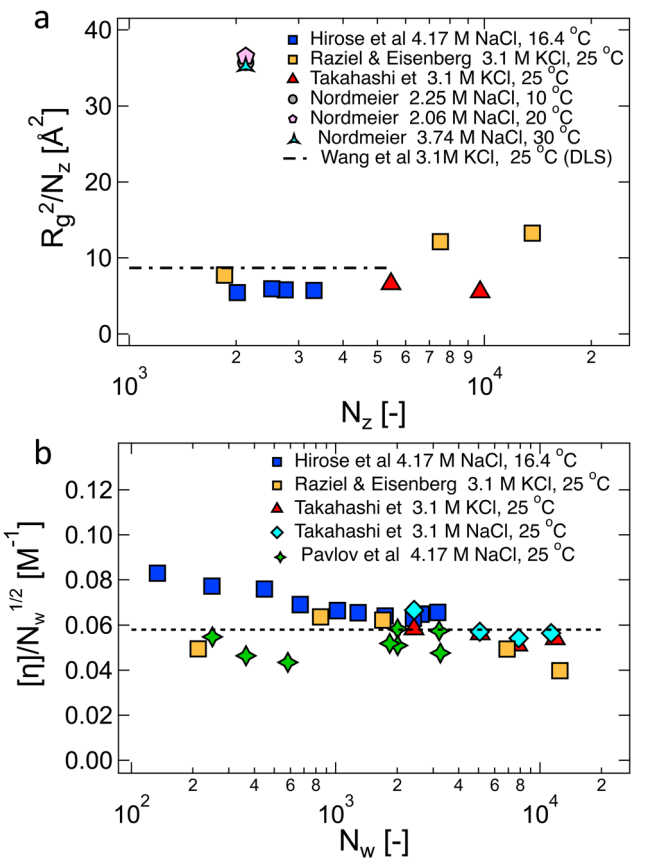

Fig. 18 Dimensions of PSS chain under different theta conditions. (a) Square of radius of gyration measured by light scattering divided by z-averaged molar mass, see Table 2 for polydispersities. Data are from ref. 105, 193, 472 and 475. The dashed line is calculated from Wang and Yu's[496] R_H data for NaPSS with 127 < N < 5300 in 3.1 M KCl solution assuming R_g/R_H = 1.32. (b) Intrinsic viscosity at the theta point divided by the square root of a weight-averaged degree of polymerisation. Data are from ref. 105, 193, 475 and 497. For Pavlov's data, N was estimated from the intrinsic viscosities in 0.2 M NaCl using an MHS relation from ref. 19.

c_s-independence is surprising because the persistence length of the polymer varies with ionic strength. The R_g and D values for Nordmeier's polymer deviated from the trend observed for samples from other studies as shown in Fig. 17(a) and (b). An error of ×1.7 in Nordmeier's estimate of the molar mass would account for these discrepancies, but is insufficient to explain the deviation shown in Fig. 18. The data of Wang and Xu[496] in 3.1 M KCl solution gave R_H^2/N = 5.0 ± 0.5 Å^2, which corresponds to $R_g^2/N \simeq 8.7 \pm 0.9$ Å^2 using R_g/R_H = 1.32 found for polystyrene in cyclohexane for $N \gtrsim 250$, see Sections S7 and S8 (ESI†) for details.

In Fig. 18(b), the intrinsic viscosity at the theta point is plotted. The $[\eta]/N^{1/2}$ ratio is seen to be approximately independent of N for $N \gtrsim 200$. The intrinsic viscosity depends on the polydispersity more weakly than the R_g data considered in part a, and therefore may offer a more reliable estimate of the theta dimensions of the PSS chains. Data were obtained from ref. 105, 193, 475 and 497. For Pavlov *et al.*'s samples, the degree of polymerisation was calculated from the intrinsic viscosity in 0.2 M NaCl, using an Mark-Houwink-Sakurada (MHS) equation from ref. 19. These values agree well with Pavlov *et al.*'s estimates from sedimentation-diffusion using the Svedberg relationship. The data shown in Fig. 18(b) display reasonable consistency around a value of $[\eta]/N^{1/2} \simeq 0.058$ M^{-1}, indicated by the dashed line. Using a value for the Flory viscosity factor of Φ = 6, see Section 3.12, the intrinsic viscosities correspond to $R_g^2/N \simeq 6.4 \pm 0.3$ Å^2, in reasonable agreement with the R_g and R_H data considered in part a. Based on the R_g, R_H and $[\eta]$ data, we judge the $R_g^2/N \simeq$ 6–10 Å^2 estimate to be correct and consider Nordmeier's data as an outlier. The theta dimensions of PSS are important for the discussion on the excluded volume screening in semidilute solutions.[209,391] The data of ref. 192, 195, 472 and 498 show that θ of polyelectrolytes depends linearly on the concentration of added salt, see Fig. S4 (ESI†).

3.9.3 Scaling of R_g and A_2 with added salt concentration. Fig. 19(a) shows the added salt dependence of R_g and R_H for a long ($N \simeq 3 \times 10^4$) and fully neutralised sodium polyacrylate chain.[499] The scaling exponents are close to the scaling prediction (−1/5), eqn (12) for both quantities. Similar[103] and weaker[475,476,500] exponents have been observed for polystyrene sulfonate. The ratio $\rho = R_g/R_H$, which is discussed in Section 3.12, decreases with increasing c_s, as expected when the polymer crosses over from the good solvent regime to the theta solvent regime. For c_s < 0.1 M, $\rho \simeq$ 1.8–2 is observed, which is larger than the values observed for monodisperse, flexible neutral polymers in good solvent (see Table 5). The discrepancy likely arises, at least in part, due to the modest polydispersity of the NaPA polymer.

The application of the variational theory to the R_g data in Fig. 21(a) was discussed in ref. 499. Eqn (25) requires three fit parameters: $l_{K,0}$, f, and χ_0. The Kuhn length is easily obtained as $l_{K,0} = R_g^2/N_z$ at the theta point. Leaving f and χ_0 as free parameters, a reasonable agreement (≲30% deviation from the experimental results) was found using f = 0.24 and $\chi_0 \simeq 0.59$. The fitted values appear quite plausible: f = 0.24 is nearly identical to an estimate using ion-selective electrodes[501] and the value of $\chi_0 > 1/2$ is expected due to the hydrophobic nature of the backbone. Fitting the variational theory to NaPSS

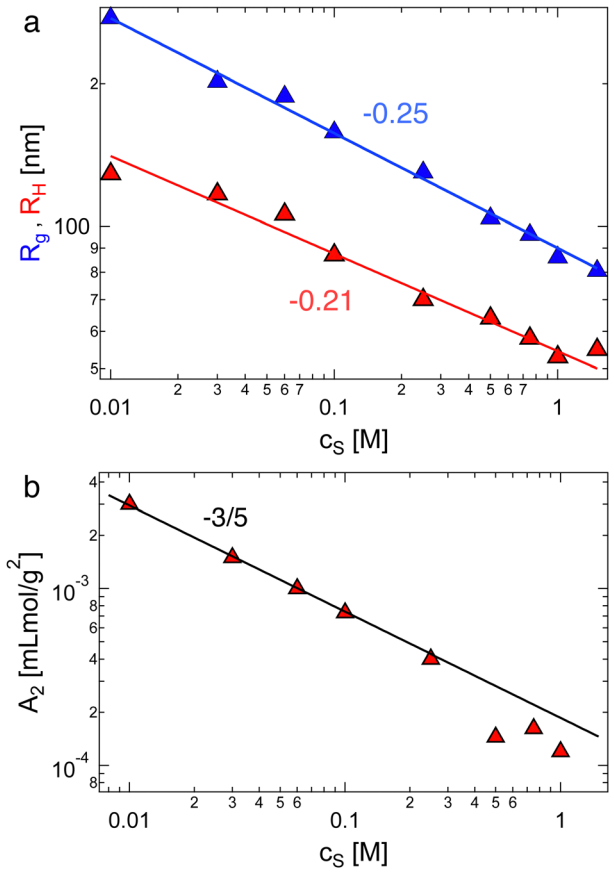

Fig. 19 (a) Radius of gyration and hydrodynamic radius of sodium polyacrylate ($N_w \simeq 35\,000$, $N_w/N_n \simeq 1.2$) as a function of added NaCl concentration. Lines are the best-fit power-law lines: $R_g \propto c_s^{-0.25}$ and $R_H \propto c_s^{-0.21}$. Eqn (12) indicates $R \propto c_s^{-1/5}$. (b) Second virial coefficient for the same polymer. c_s = 1.5 M corresponds to the theta condition, where A_2 = 0. Data are from ref. 499.

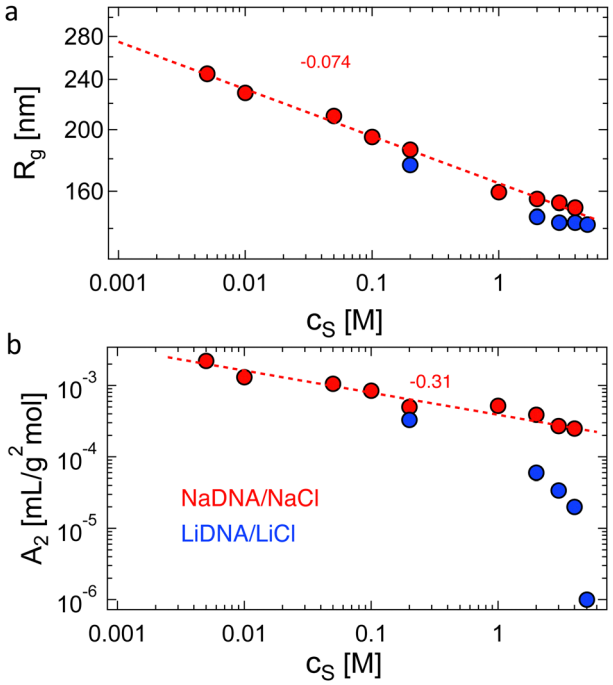

Fig. 20 (a) Radius of gyration for the same systems as a function of added salt. The line is the best-fit power-law with the exponent indicated in the figure. Note that the weak exponent of R_g with c_s arises due to the high rigidity of double-stranded DNA. (b) Second virial coefficient of NaDNA in aqueous NaCl solutions and LiDNA in aqueous LiCl solutions as a function of the added salt concentration. Line is the best-fit power-law to sodium data, with the exponent indicated in the figure. Data are from ref. 502 and 503.

data[103] yielded values of f that were consistent with independent estimates from conductivity,[68] but values of $\chi_0 < 1/2$, which are incompatible with the hydrophobic nature of the PSS backbone.[105,193]

The second virial coefficient of NaPA, plotted in Fig. 19(b), followed a power-law of $A_2 \sim c_s^{-3/5}$, which agreed with the scaling prediction in the high excluded volume limit ($A_2 \sim R_g^3/M^2$) until $c_s \simeq 0.2$ M. For higher salt concentrations, as the polymer approached the theta salt conditions, a steeper decrease of A_2 with c_s was observed. Near the theta salt condition, a different scaling applies, and A_2 does not vary as R_g^3/M^2. A clear example of this can be seen in Fig. 20, which compares the radius of gyration and second virial coefficients of the Li and Na salts of DNA in excess LiCl and NaCl. The LiDNA/LiCl system approaches the theta point ($A_2 = 0$) at $c_s \simeq 5$ M, while the NaDNA/NaCl system remains in the good solvent regime ($A_2 > 0$) over the entire c_S range considered. While R_g of the two polymers is nearly identical, the Li system shows a sharp drop in A_2 as the theta point is approached. A review of second virial coefficient data for flexible,[486,504–509] semiflexible,[109,296,359,360,476,510–516] and rigid polyelectrolytes[120,517] revealed that A_2 does not follow a universal power-law with c_s. Exponents both larger and smaller than −0.6 are observed in the low c_s region (*i.e.* well below the theta salt concentration).

The ideal behaviour of PAA at c_s = 1.5 M is illustrated in Fig. 21, which shows the ratios R_g^2/N_z and R_H^2/N_w are independent of the degree of polymerisation, as expected for Gaussian chains. In 0.1 M NaCl solution, the chains adopt expanded coil conformations and $R_g^2/N \sim R_H^2/N \propto N^{0.2}$, indicated by the dashed lines. We note that the ratio $\rho = R_g/R_H$ is known to increase with excluded volume, which could explain the higher exponent observed for the R_g data compared to R_H. However, the scatter in the results does not allow for a meaningful conclusion on this aspect. The data suggest that excluded volume influences R_g for shorter chain lengths more than it does R_H. Weaker exponents for the R_g and R_H dependence on c_s are observed for published literature on polystyrene sulfonate[193,472,475–477,500] and other systems including carboxymethyl cellulose,[359,360,510] NaPAMS,[518] and NaPOMS.[486]

3.9.4 Scaling of k_D and k_H. The molar mass and added salt concentration of the diffusion virial coefficient (k_D, see eqn (S2), ESI†), which describes the concentration dependence of the apparent diffusion coefficient in dilute solution are considered in the ESI† (Section S6). An analysis of the literature data[106–109,112,477,499,500,519–526] revealed $k_D \sim N^{0.78} c_s^{-1}$, although the specific exponents varied depending on the system considered. For several systems, the ratio $k_D/(A_2 M_w)$ was independent

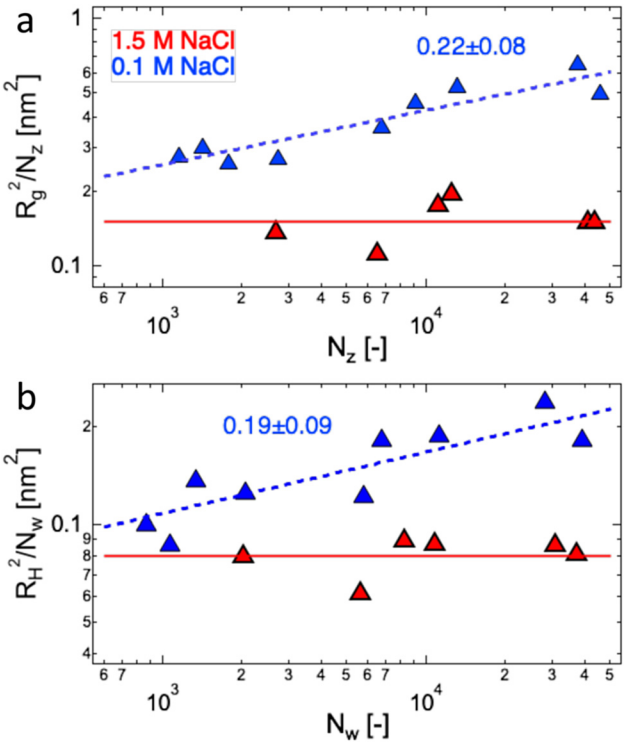

Fig. 21 Square of (a) radius of gyration and (b) hydrodynamic radius normalised by degree of polymerisation for sodium polyacrylate at the theta salt condition (1.5 M NaCl) and below the theta salt condition (0.1 M), corresponding to the 'good solvent' universality class (expected exponent of 0.18). Errors in exponents are two standard deviations. Data are from ref. 499.

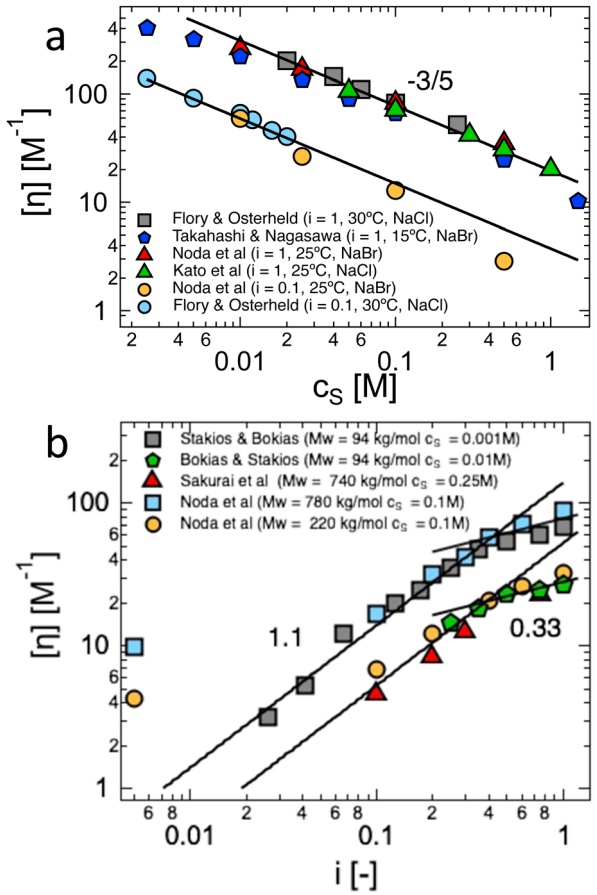

Fig. 22 (a) Dependence of intrinsic viscosity of polyacrylic acid on added salt concentration for $N \simeq 8170$ (see text) for 10% ionisation (i = 0.1) and full ionisation (i = 1). Power-law of −3/5 is the scaling prediction. (b) Intrinsic viscosity *vs.* degree of neutralisation i. Exponents are best fit values. Data are from ref. 195, 537 and 540–543. Results reported by Bokias and Stakios[542] were obtained by isoionic dilution.

or weakly dependent on c_s and M_w. The scaling of the sedimentation coefficient with molar mass and added salt was not considered here, readers are referred to ref. 19, 491, 497, 498 and 527–530.

The Huggins and Kraemers coefficients of polyelectrolytes are discussed in the ESI† (Section S5). Briefly, an analysis of literature data[111,141,210,299,416,531–536] revealed that: (1) increasing the charge fraction leads to a large increase in k_H in salt-free solutions and a modest decrease in k_H for solutions in excess salt; (2) the Huggins coefficient shows a non-monotonic dependence on the added salt concentration; (3) k_H decreases with increasing N until it reaches a constant value, which appeared to be similar to that of neutral polymers; (4) introducing hydrophobic groups leads to a large increase in k_H if the added salt concentration is sufficiently high.

3.10 Behaviour in excess salt solutions: scaling with the charge density

The c_s-dependence of the intrinsic viscosity of NaPA at 10% (i = 0.1) and full (i = 1) neutralisation is shown in Fig. 22(a). We plot Flory and Osterheld's data[195] for NaPA with $N \simeq 8170$ and combine it with interpolated values based on Noda *et al.*'s[537] and Kato *et al.*'s[538] results. Values extrapolated from Takahashi *et al.*'s data,[193] which cover the $160 < N < 5300$ range, are also included. These results are taken at slightly different conditions (temperature and co-ion), as shown in the legend of Fig. 22(a). For both degrees of neutralisation, the experimental data agree well with the theoretical prediction in the high c_s limit of the scaling and variational theories (eqn (31) and (26), $[\eta] \propto c_s^{-3/5}$). The data at the highest c_s for both degrees of neutralisation deviate downwards from the trend as the samples approach the theta points.[192,539]

The dependence of the intrinsic viscosity on the degree of ionisation (i) of polyacrylic acid is plotted in Fig. 22(b). The results show two clear power-laws. For $0.02 < i < 0.3$, $[\eta]$ increases as $i^{1.1}$. In this regime, the degree of ionisation is proportional to the fraction of monomers bearing a dissociated counterion (f). For higher degrees of ionisation, where counterion condensation sets in,[11] a weaker exponent is observed. Considering $f \propto i^{0.3}$ for $i > 0.3$,[544] the intrinsic viscosity data for $i > 0.02$ are consistent with a single power-law $[\eta] \propto f^{1.1}$ for $0.02 < i < 1$. Data for different degrees of polymerisation and added salt concentrations show the same scaling exponent, which indicates that the exponent is independent of the number of electrostatic blobs in a chain. Matsumoto and Eguchi's[416] intrinsic viscosity data, discussed in the ESI† (Section S4), display a weaker scaling of $[\eta] \propto f^{0.7}$.

At very low degrees of ionisation, the $[\eta] \propto f^{1.1}$ scaling breaks down as the polymer chains approach their neutral polymer dimensions. The cross-over between $[\eta] \sim f^{0}$ to $[\eta] \sim f^{1.1}$ can in principle be used to obtain an estimate of the molar mass of the electrostatic blob, but we have been unable to get consistent values from this. Similar behaviour can be observed in the data of Matsumoto and Eguchi for polyvinyl sulfate,[416] as shown in Fig. S8 (ESI†). These results suggest a deficiency in the electrostatic blob model.

The $[\eta] \propto f^{1.1}$ scaling implies $R \sim f^{0.36}$. This exponent differs from the scaling theory exponents for good solvents (0.46), θ solvent (0.47) and poor solvent (0.73). Since NaPA has a θ point in 1.5 M NaBr, we infer water to be a poor solvent for its backbone. However, without an estimate for the size of the thermal blob, it remains ambiguous whether the behavior aligns more closely with that of a poor solvent or a θ solvent. The variational theory prediction of $R \propto f^{0.4}$ (eqn (25)) is in closer agreement with the experimental results. Note that for PAA with $l_{K,0} \simeq 4$ nm, there is more than one dissociated charge per bare Kuhn segment if $i > 0.06$ (assuming $f \simeq i/2$).[11] Under these conditions, the scaling theory indicates that the electrostatic blob concept should not apply. Interestingly, no change in the exponent is observed across $i = 0.12$. Thus, it is possible that the electrostatic blobs are significantly larger than expected by the scaling theory, see ref. 100.

Reed *et al.* reported the dependence of the radius of gyration of sodium polyacrylate-*co*-acrylamide random co-polymers as a function of the charged group fraction (δ).[545,546] In ref. 545, the refractive index increment is reported to be independent of the added salt content, in contrast to other reports for NaPA. As we only consider R_g data, which are not affected by the choice of dn/dc, we do not discuss this further. The polymer with the highest sodium acrylate content contained a fraction of $\delta = 0.27$ charged monomers. In this regime, $f \simeq \delta/2$ is expected.[11] The radius of gyration of the co-polymers is plotted as a function of the fraction of ionisable units in Fig. 23. The exponents observed ($R_g \sim \delta^{0.3} \sim f^{0.3}$) are relatively close to the relationship deduced from the intrinsic viscosity data shown in Fig. 22(b). For both added salt concentrations considered, the best fit exponent is lower than the variational theory prediction by $\simeq 0.1$. The scaling theory indicates the exponent to be $\simeq 50\%$ larger than the experimentally observed exponent.

The variation of the radius of gyration on dielectric constant for quaternized PVP polyelectrolytes in different salt solutions is considered in Fig. 24, based on the results of Beer *et al.*[103] The solvents considered differ in the quality of the solvent backbone, which may explain the scatter in the data.[415,547–550] Data for the various added salt concentrations collapse well onto a single curve when normalised by $c_s^{1/5}$, as expected by the variational (eqn (25)) and the scaling theories (eqn (6) and (12)). Assuming Manning condensation holds ($f \propto \varepsilon$), the variational theory (eqn (26)) indicates $R_g c_s^{1/5} \propto \varepsilon^{0.2}$, which is weaker than the experimentally observed exponent. The scaling theory indicates $R_g c_s^{1/5} \propto \varepsilon^{0.32}$ under good solvent conditions and $R_g c_s^{1/5} \propto \varepsilon^{0.47}$ under poor solvent conditions. The poor solvent exponent matches the experimental value. The variational theory could describe the c_s and ε dependence of R_g for these results, but the fitted f dependent on the solvent permittivity in an unusual way ($f \sim 0.02(\varepsilon - 16)^{1/2}$).[103]

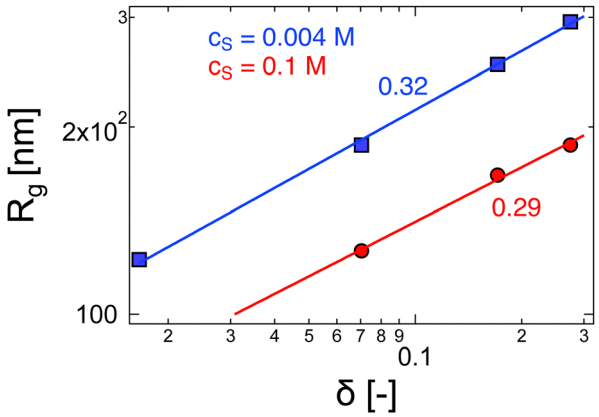

Fig. 23 Dependence of the radius of gyration on fraction of ionic groups (δ) for polyacrylate-*co*-acrylamide co-polymers for two concentrations of added NaCl. Lines are best-fit power-laws, with the exponents indicated by the numbers. Data are from ref. 545 and 546.

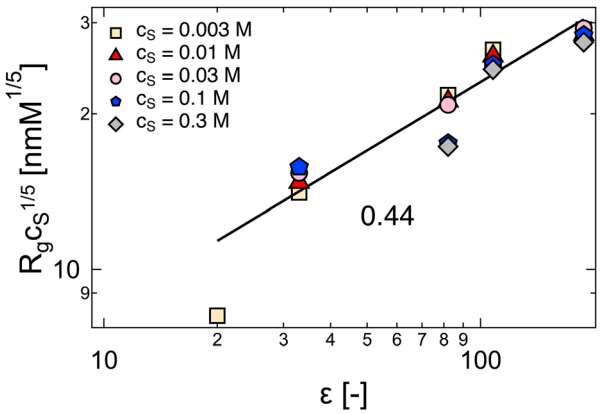

Fig. 24 Dependence of radius of gyration multiplied by $c_s^{1/5}$ on the solvent dielectric constant. Data are from ref. 103. The line is the scaling prediction for good solvent.

The scaling of other parameters with the charge fraction, particularly A_2, is of interest to understand the nature of the electrostatic excluded volume, but the available data[551–554] do not allow for any systematic conclusions to be drawn, particularly in the low charge fraction limit. The Huggins coefficient of a PVA polyelectrolyte in excess added salt was shown to be a decreasing function of charge fraction,[416] see Fig. S8 (ESI†). This contrasts with the behaviour at low c_s, where charged polymers display much higher k_H values than neutral ones.

3.11 The expanded worm-like chain model

The expanded worm-like chain model has been used to explain the conformational and transport properties of polyelectrolytes in dilute solution in a large number of studies.[105–112,118,121,477,479,483,545,555–557] Reliable fitting of the model to experimental data is made difficult by the fact that both the persistence length and the excluded volume are a function of solvent's ionic strength. Robust methods for

obtaining the ideal conformation, analogous to, for example, the Stockmayer–Fixman[558] plot for flexible polymers or the Bohdanecky–Bushin[559,560] plot for polysaccharides, do not exist for flexible polyelectrolytes. This means that datasets covering degrees of polymerisation from a few Kuhn segments to several hundreds are usually necessary for reliable extraction of l_p and $\bar{B}$, the excluded volume strength. Approaches which estimate $\bar{B}$ from A_2 are in our view not reliable, because the interpenetration function is not a unique function of the excluded volume, see ref. 482 and 561.

Norisuye and co-workers carried out extensive experimental light scattering and viscosimetric investigations of the conformational and hydrodynamic properties of three polyelectrolytes: NaPSS, NaPAMS and NaHy[110,111,483,557] as a function of molar mass and added salt concentration. These experimental reports, in our opinion, constitute the 'gold standard' against which theories of dilute polyelectrolytes can be tested.[562] Here, we focused on experimental work based on measurements of R_g, D and $[\eta]$ instead of l_P data obtained from force-extension curves, as the latter method was shown to underestimate the persistence length of neutral flexible polymers.[563] The authors were able to extract the excluded volume strength and persistence length for their systems without making assumptions about the ionic strength dependence of either parameter.

An example of Norisuye's and co-workers procedure is shown in Fig. 25, which plots the intrinsic viscosity of sodium hyaluronate in 0.2 M NaCl solution as a function of degree of polymerisation, where we define the 'monomer' as having a molar mass of 201.5 g mol^{-1}, corresponding to a length of $\simeq$0.5 nm.[569] The data display $[\eta] \propto N$ for short chains and $[\eta] \propto N^{0.78}$ at high N after a broad cross-over. The intrinsic viscosity of a worm-like chain without excluded volume, shown by the dashed line, is calculated using the procedure from ref. 384 for low molar masses and ref. 148 for higher ones. The values of l_p = 4.2 nm, d = 1 nm and M_L = 400 g mol^{-1} nm^{-1} are taken from ref. 483. This model 9provides an accurate fit to the data for $N \lesssim 80$, but underpredicts the data for higher molar masses. As electrostatics are short-ranged, the chain conformation can be understood in terms of a 'thermal blob' incorporating the influence of electrostatic excluded volume.[100] For NaHy in 0.2 M, $n_T \simeq 100$, $\xi_{T,el} \simeq 20$ nm. Here, $\xi_{T,el}$ refers to a thermal blob incorporating both the effects of ionic and non-ionic excluded volume, and the former is presumed to be sufficiently short-ranged. The full line shows the calculation of $[\eta]$ including the excluded volume effects using $\bar{B}$ = 4.0 nm, as detailed in ref. 483.

The fitted values of l_p and the excluded volume strength for the three aforementioned systems are plotted as functions of the Debye screening length in Fig. 26. The excluded volume strength $\bar{B}$ shows a linear dependence on κ^{-1}, with a c_s-independent term $\overline{B_0} \simeq 2$ nm, which is close to the expected

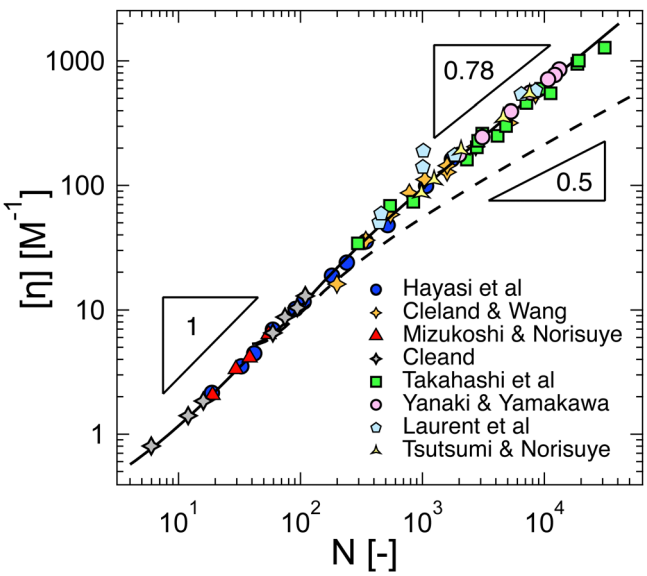

Fig. 25 Intrinsic viscosity of NaHy in 0.2 M NaCl. Full line is the fit to the WLC model with d = 1 nm, M_L = 400 g mol^{-1} nm^{-1} and l_p = 4.2 nm $\bar{B}$ = 4.0 nm, following ref. 483. The dashed line is the WLC model with the same parameters as the full line but $\bar{B}$ = 0. Data are from ref. 111, 288, 483 and 564–568. The points by Mizukoshi and Norisuye are extrapolated to c_s = 0.2 M from their data in 0.02 and 0.1 M NaCl. Data from Foussiac *et al.* were interpolated to c_s = 0.2 M.

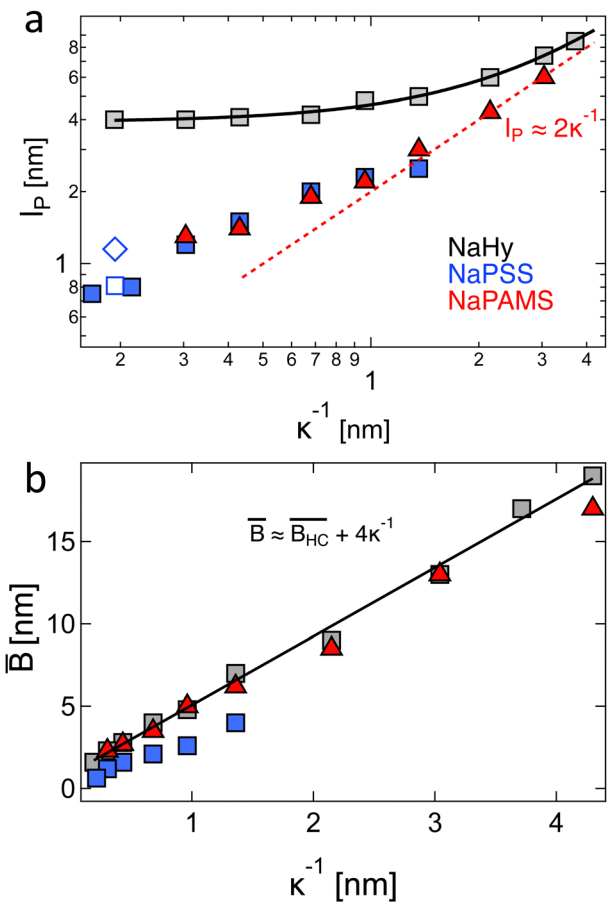

Fig. 26 (a) Persistence length for NaPSS, NaPAMS and NaHy as a function of the solvent Debye screening length. The red dashed line shows $l_p \simeq l_{p,el} \simeq 2\kappa^{-1}$ in the low-salt limit for the two flexible systems. Full black line is $l_p = 4 + 0.7(\kappa^{-1})^{1.44}$ for NaHy. Hollow diamond and hollow square are calculated from R_g^2/N values from Wang and Yu's[496] and Takahashi *et al.*'s[540] data in 3.1 M KCl, respectively. (b) Total excluded volume strength for the same three polyelectrolyte systems. Black line is fit to a linear function, where the intercept $\overline{B_{HC}} \simeq 1$ nm can be identified with the hard-core repulsion term in $\bar{B}$. Data are from ref. 105–112 and 483.

value of $\overline{B_{HC}}$ for NaHy and NaPAMS. The electrostatic part of the excluded volume is $\overline{B_{el}} \simeq 4\kappa^{-1}$, corresponding to $R(y) = 2$ in eqn (24). This does not agree with the theories of Fixman and Skolnik[119] and matches the estimates of Odijk[132] and Dobrynin *et al.*[89] for $\overline{B_{el}}$ up to a pre-factor.

The persistence length follows a non-monotonic dependence with κ^{-1} and appears to approach a linear relationship in the high κ^{-1} limit, as expected by various theories,[89] but in disagreement with the OSF model.[122,123,570] Note that the scaling theory predicts $l_p = r_{scr}/2 \simeq 2\kappa^{-1}$ for NaPSS, where we have assumed $f = 0.2$, in good agreement with the observed results. For NaHy, a semiflexible polylelectrolyte, there exists a region for high c_s (low κ^{-1}), where the persistence length is virtually independent of the added salt concentration because the non-electrostatic term dominates in eqn (20). In this regime, changes in chain dimensions with added salt arise from the decrease in excluded volume with increasing c_s. For sufficiently rigid polyelectrolytes, such as xanthan gum, $l_{p,0}$ is of the order of or larger than the contour length, and the chain dimensions are independent of c_s.[484,485,571]

In the high-N limit, eqn (14)–(18) for the chain size of a polyelectrolyte reduce to:

$$R \propto N^{0.59} l_p^{1/5} \bar{B}^{1/5}. \quad (45)$$

If the dependences $\bar{B} \propto \kappa^{-1}$ and $l_p \propto \kappa^{-1}$ are introduced into eqn (45), Dobrynin *et al.*'s prediction of $R \propto c_s^{-1/5}$ (eqn (12) for $2c_s \gg fc_p$) is recovered. A second regime is expected where $l_p \simeq l_{p,0}$ and $\bar{B} \simeq \overline{B_{el}}$. Here, the c_s dependence of the chain size is expected to approach $R \propto c_s^{-1/10}$, which is consistent with the weak power-laws observed for the intrinsic viscosity of polysaccharides in the high c_s regime.[111,404,406] In terms of the scaling theory, this regime is analogous to $r_{scr} < \xi_{el}$, where no electrostatic stiffening of the chain is expected, but electrostatic excluded volume results in chain expansion relative to the non-ionic dimensions. At sufficiently high c_s, we anticipate a regime characterized by $R \propto c_s^0$, where electrostatics does not perturb chain conformation under certain conditions, as discussed below.

For strongly charged polyelectrolytes, it is possible to combine the effects of electrostatic and non-electrostatic excluded volume into a single parameter (*i.e.* $\bar{B} = \overline{B_0} + \overline{B_{el}}$). This approximation has been found to agree with experiments under certain conditions. It is then possible to define an effective thermal blob size:

$$\xi_{T,el} \simeq \frac{l_K^2}{\bar{B}}. \quad (46)$$

$\xi_{T,el}$ differs from ξ_T introduced in Section 2, which considers only non-ionic interactions.

For sodium hyaluronate, a semiflexible polyelectrolyte, the parameters plotted in Fig. 26, setting $l_K = 2l_p$, give $\xi_{T,el} \simeq 16/\kappa^{-1}$ for $c_s \gtrsim 0.2$ M. For $c_s = 0.2$ M, this corresponds to an effective blob size containing $\simeq 8$ Kuhn segments, each with a molar mass of $\simeq 3.2$ kg mol^{-1}. For NaHy, the WLC model therefore indicates $R \sim c_s^0$ when $M_w \lesssim 26$ kg mol^{-1} and $c_s \gtrsim 0.2$ M, which is qualitatively consistent with the intrinsic viscosity data from Hayashi *et al.*[111] However, without more detailed conformational data, it is not possible to clearly test this result. For flexible polyelectrolytes, l_p contains a non-negligible electrostatic contribution over the entire c_s range studied and it is therefore not clear if the $R \propto c_s^0$ applies at any added salt concentration. Most literature data for the static and hydrodynamic sizes of polyelectrolyte chains display exponents which do not clearly fall into the three regimes discussed above ($R \propto c_s^{-0.2}$, $R \propto c_s^{-0.1}$ and $R \propto c_s^0$), probably because the cross-over between these are quite broad.

The expanded worm-like model conceptualizes polyelectrolytes as neutral polymers with persistence length and thermal blob size dependent on salt concentration (c_s). This implies that there is a single lengthscale beyond which excluded volume perturbs the chain conformation. However, for weakly charged polyelectrolytes with large electrostatic blob sizes, two distinct length scales emerge for the onset of excluded volume effects: ξ_T for the intrinsic (non-electrostatic) excluded volume and r_{scr} for the electrostatic excluded volume. For these systems, the expanded WLC model is not expected to apply.

Simulation studies on polyelectrolytes in excess salt have noted that the bond-bond orientational correlation function $s(l)$, where l is the distance along the chain contour, follows non-exponential behaviour.[28,572–574] Gubarev *et al.*[572] found that $s(l)$ followed a monomodal exponential decay if $\kappa^{-1} < 6b$ (for the NaPSS/NaCl/H_2O system, this would translate to $c_s \gtrsim 0.025$ M) and a bimodal decay otherwise, where the short-ranged decay scaled linearly with κ^{-1} for high c_s and the lengthscale for the second decay varied as κ^{-2}. Non-exponential decays in $s(l)$ were also observed for neutral polymers in good solvents.[116,575,576] Several formulae have been proposed to fit the simulated results for $s(l)$, which are sometimes interpreted as resulting from a length-scale dependent persistence length, see ref. 577 for a discussion. Quantifying the persistence length is complicated because different measurements which are equivalent for the ideal Kratky–Porod worm-like chain become different from each other when $s(l)$ does not follow a single exponential decay.

For the EWLC model discussed above, the meaning of l_p is straight-forward: it is the persistence length of the worm-like chain for a polyelectrolyte in the absence of excluded volume interactions. Yamakawa *et al.*'s simulation work[126] showed that for non-ionic polymers with excluded volume, where $s(l)$ follows non-exponential behaviour, the initial decay ($d \ln[s(l)]/dl$) gave the persistence length of the system. Based on a comparison of simulation data for WLCs with Debye–Huckle interactions and experimental data for NaPSS and NaHy, it was concluded that the initial decay rate in $s(l)$ also serves as a measure of the persistence length for polyelectrolytes in excess salt.

In summary, it is not clear over what conditions the expanded WLC approach is valid for polyelectrolytes. Because $s(l)$ cannot be measured experimentally, testing the theoretical simulation work discussed above is difficult. A theoretical derivation of form factors for such systems may allow a more rigorous comparison of experimental and simulation results.

3.12 Universal ratios

The dilute solution properties of polymers in good solvents can be characterised by a number of "universal ratios", which, in the long N limit, are expected to take constant values independent of the chemical nature of the system. For flexible neutral polymers, these ratios have been studied and their values have been compared to theoretical predictions of renormalisation group and two-parameter theories.[116,578–588] Extensive datasets are available for polystyrene and several other flexible polymers in good and theta solvents, see for example, the review of Fetters *et al.*[589] and subsequent experimental work.[487–489,531] Significantly, less attention has been paid to ionic polymers. In our view, polyelectrolytes are interesting systems to study these ratios because the range of excluded volume strengths attainable ($\sim\kappa^{-1}$) far exceeds that of neutral polymers ($\sim d_C$). Usually, five ratios are computed:[579,588]

$$U_{A\eta} = \frac{[\eta]}{A_2 M}, \tag{47}$$

$$U_{\eta S} = \frac{[\eta]M}{N_A R_g^3}, \tag{48}$$

$$U_{AS} = 4\pi^{3/2}\Psi = \frac{A_2 M^2}{N_A R_g^3}, \tag{49}$$

$$U_{\eta F} = \frac{1}{6\pi}\left(\frac{[\eta]M}{N_A R_H^3}\right)^{1/3}, \tag{50}$$

$$\rho = \frac{R_g}{R_H}. \tag{51}$$

The second of these is related to the Fox–Flory viscosity parameter ($\Phi = [\eta]M/N_A R^3 \simeq U_{\eta S}/6^{3/2}$), and U_{AS} is related to the well-known interpenetration function ψ ($= (4\pi^{3/2})^{-1}U_{AS}$).[116,591] An additional ratio, analogous to the interpenetration function but using R_H^3 instead of R_g^3 as the reference volume has been proposed[592–594] and evaluated for polystyrene in toluene:[592]

$$X = \left(\frac{3A_2 M^2}{16\pi N_A R_H^3}\right)^{1/3}. \tag{52}$$

$U_{\eta F}$ and $U_{\eta S}$ are plotted as a function of polymer molar mass for polystyrene in cyclohexane at T = 34.5 °C (theta solvent), polystyrene in toluene T = 20–25 °C (good solvent) and NaPSS in salt solutions in Fig. 27. The data for $U_{\eta F}$ for all three systems studied (PS/Tol, PS/CH and NaPSS/H_2O/NaCl) display a constant value of $U_{\eta F} \simeq 0.12$, see also Table 4. The exception is the data of Pavlov for NaPSS at c_s = 4.17 M, which appear to be an outlier. The ratio $U_{\eta F}$ is seen to be insensitive to the strength-excluded volume interactions.The values of $U_{\eta F}$ for polystyrene and NaPSS in various solvents as well as two semiflexible systems: polyelectrolyte sodium hyaluronate and non-ionic poly(hexyl isocyanate) are compiled in Table 4.[595] Data reported by Fetters and co-workers for polystyrene stars[596,597] in good and theta solvents also give $U_{\eta F} \simeq 0.12$. All systems display almost identical values, suggesting $U_{\eta F} \approx 0.120 \pm 0.005$ applies

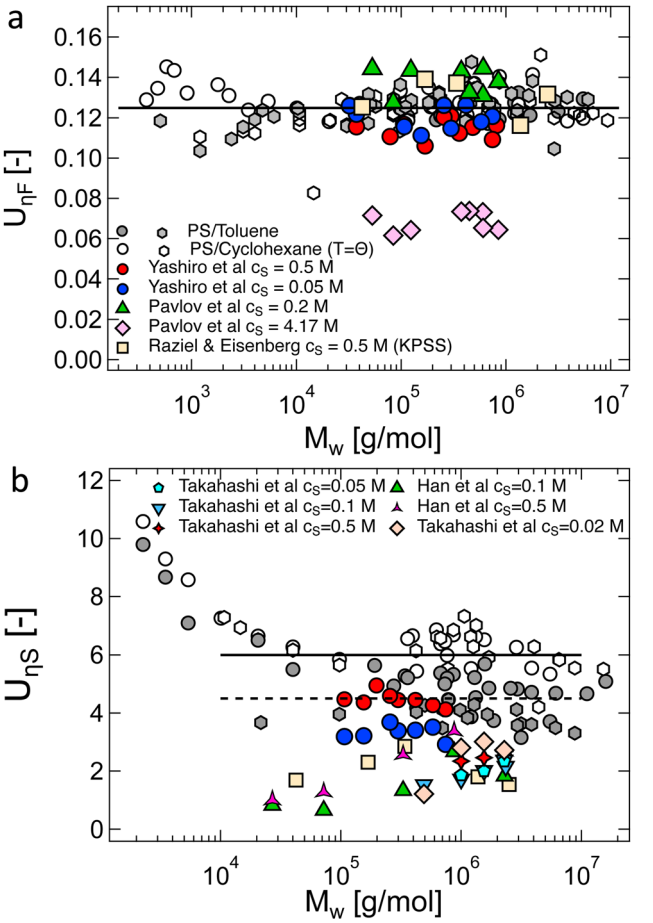

Fig. 27 Comparison of universal ratios $U_{\eta f}$ (top, eqn (50)) and $U_{\eta S}$ (bottom, eqn (48)) for polystyrene in good solvent (grey symbols) and theta solvent (white symbols) and NaPSS in aqueous salt solutions (other symbols). Hexagons are for interpolated values of $[\eta]$ for PS. Data are from ref. 105–107, 193, 301, 475, 487–489, 497 and 590 and references listed in ref. 589. Raziel and Eisenberg's data are for KPSS in KCl solutions. (a) Full line is $U_{\eta f}$ = 0.125. Symbols are listed in the legend. (b) Dashed and full lines in plot (a) are $U_{\eta S}$ = 6 and $U_{\eta S}$ = 4.5, respectively. Symbols are listed in the legends, see also plot (a) for symbols not listed. A plot displaying $U_{\eta S}$ over a wider molar mass range for polystyrene is included in Section S7 of the ESI.†

to a wide range of polymers. The constant value taken by this ratio indicates that hydrodynamic volumes calculated from viscosity and diffusion are proportional or $[\eta] \propto R_H^3/M$.

The Fox–Flory viscosity factor for PS in good solvent takes a value of $\simeq$25% lower than in theta solvent in the high-M limit, as indicated by the full and dashed lines shown in Fig. 27. The data for PSS display a large degree of scatter and therefore a single value for Φ cannot be determined. Studies which consider different added salt concentrations for the same PSS samples find Φ to be dependent on c_s,[109,193,598] a feature also observed for NaPAMS.[518] The trend $U_{\eta S,PS/Cycl} > U_{\eta S,PS/Tol} > U_{\eta S,PSS/NaCl}$ suggests that the Flory–Fox constant decreases with increasing excluded volume strength. For $M_w \lesssim 2 \times 10^4$ g mol^{-1}, the value of $U_{\eta S}$ for polystyrene shows an upturn in good and theta solvents. The data for PSS do not extend over a sufficiently broad range to check whether such ehavior also

Table 4 Comparison of $U_{\eta F}$ (eqn (50)) for different polymer systems. F: flexible, SF: semiflexible, NI: non-ionic, I: ionic, GS: good solvent, θ: theta solvent. Errors are 95% confidence intervals

System	$U_{\eta F}$	Type	Data
PS/Tol	0.125 ± 0.003	F/NI (GS)	Ref. 589 and references therein
PS/CH	0.129 ± 0.003	F/NI (θ)	Ref. 589 and references therein
NaPSS/0.5 M NaCl	0.114 ± 0.003	F/I	Ref. 105–107
NaPSS/0.05 M NaCl	0.120 ± 0.004	F/I	Ref. 105–107
NaPAMS/0.05 M NaCl	0.128 ± 0.004	F/I	Ref. 108, 109 and 112
NaPAMS/0.5 M NaCl	0.122 ± 0.003	F/I	Ref. 108, 109 and 112
NaHy/0.2 M NaCl	0.110 ± 0.005	SF/I	Ref. 565
PHIC/hexane	0.115 ± 0.002	SF/NI (GS)	Ref. 595
PS stars/toluene	0.118 ± 0.003	F/NI (GS)	Ref. 596 and 597
PS stars/cyclohexane	0.111 ± 0.004	F/NI (θS)	Ref. 596 and 597

occurs. The limited data available suggest that $U_{\eta S}$ for PSS in aqueous salt solutions decreases at low M_w.

The ratio of $[\eta]$ to A_2M was compared as a function of molar mass for polystyrene in toluene and PSS in 0.5 M NaCl solutions, as shown in Fig. 28(a). For $M_w \gtrsim 10^5$ g mol^{-1}, NaPSS and PS converge to a value of $[\eta]/A_2M \simeq 0.81$. The only exception are the data from Takahashi *et al.*,[193] which show a pronounced decrease with increasing M_w. At low molar masses, a surprising deviation was observed for Hirose *et al.*'s dataset,[105] where $[\eta]/A_2M$ is seen to decrease by an order of magnitude, in contrast to PS in toluene, which shows a weak increase at low M_w. Additional studies are needed to confirm this unusual feature. As discussed above, it is possible that the large increase in A_2 for low molar masses is caused by the influence of the chain ends, an effect which is observed also for polystyrene, but only for shorter oligomers.[482] The data from Takahashi *et al.*,[193] Yashiro *et al.*,[107,109] and Han *et al.*[301] for 0.05 M $< c_s <$ 0.1 M consistently show $[\eta]/A_2M$ values below those of polystyrene in toluene, even at intermediate molar masses. Understanding these differences is important because both A_2M and $[\eta]^{-1}$ are widely used as measures for the overlap concentration. For neutral polymers in good solvent, this appears to be justified but for polyelectrolytes in excess salt, the assumption appears questionable in light of the results discussed.

The interpenetration function of NaPSS in NaCl and KCl solutions of different concentrations is compared to that of polystyrene in toluene in Fig. 28(b). The datasets from Norisuye and co-workers show a particularly good agreement with the polystyrene values. Despite the relatively large scatter, the value of Ψ for the PS/Tol and PSS/water/NaCl systems broadly agree. The data from Han *et al.* suggest a possible drop in Ψ at low molar masses, as opposed to the increase seen for PS/Tol, but this cannot be confirmed without more data for $M_w <$ 10^5 g mol^{-1}. This feature would be particularly interesting to investigate because it could provide a hint as to whether the unusual behaviour observed for $[\eta]/A_2M$ discussed above arises from excluded volume or hydrodynamic factors.

The ratio X (eqn (52)) is plotted as a function of M_w in Fig. 28(c). Fairly consistent results are found between the various systems, which approach a value of $X \simeq 1.1$ in the high M_w limit, although the number of datapoints for the PSS system is quite limited. The three lowest molar masses for Yashiro *et al.*'s results[107] in 0.05 M NaCl suggest an increase in X with decreasing molar mass, which is the opposite of what is observed for PS/Tol. We note that other systems display values of X differently from that of polystyrene. For example, results from Murakami *et al.*[595] for PHIC in hexane show a constant value of $X \simeq 0.5$ in the 66 kg mol^{-1} $< M_w <$ 7200 kg mol^{-1} range. Sodium hyaluronate at 0.2 M NaCl also displays a somewhat lower value of $X \simeq 0.8$. This suggests that X may depend to some extent on backbone flexibility, meaning it should not be a universal parameter for polyelectrolytes, where flexibility is a function of c_s.

The ratio $\rho = R_g/R_H$, which is dependent on the solvent quality,[603,604] can be calculated from the parameters discussed so far as: $\rho = X/\left(1.61\sqrt[3]{\psi}\right)$. Considering the high M limit of the datasets in Fig. 28(b) and (c), we obtain $\rho \simeq 1.5$, which is in reasonable agreement with the Zimm prediction.[605] A more robust estimate was made by evaluating the R_g and R_H power-laws at high M, as described in Section S7 (ESI†). The results are summarised in Table 5. For NaPSS and other polyelectrolytes, ρ was observed to decrease with c_s, see Fig. S25 and S26 (ESI†).

A comparison of the 'universal ratios' of flexible neutral polymers with those of a flexible polyelectrolyte shows many similarities and also significant differences between ionic and non-ionic polymers. The only truly universal ratio appears to be $U_{\eta F}$, which takes a constant value for all systems considered over a very wide molar mass range and for different solvent qualities, see Table 4. In general, we observe the largest discrepancies for ratios which combine excluded volume or conformational parameters with hydrodynamic parameters, *e.g.* $U_{A\eta}$ or Φ. In contrast, parameters combining only hydrodynamic parameters ($U_{\eta F}$) or conformational/thermodynamic parameters (Ψ) display closer agreement between neutral polymers and polyelectrolytes.

3.13 Scattering properties of polyelectrolyte solutions

Small-angle scattering techniques are among the most powerful experimental methods for investigating the structure of polymer solutions.[606] An overview of the scattering properties of polyelectrolytes in salt-free solution can be found in ref. 69, 125, 391 and 607. In excess salt, calculating the scattering contrast for X-rays and neutrons typically requires knowledge of salt-exclusion factors as discussed by Eisenberg and co-workers.[481,608–610] This rigorous calculation is usually replaced

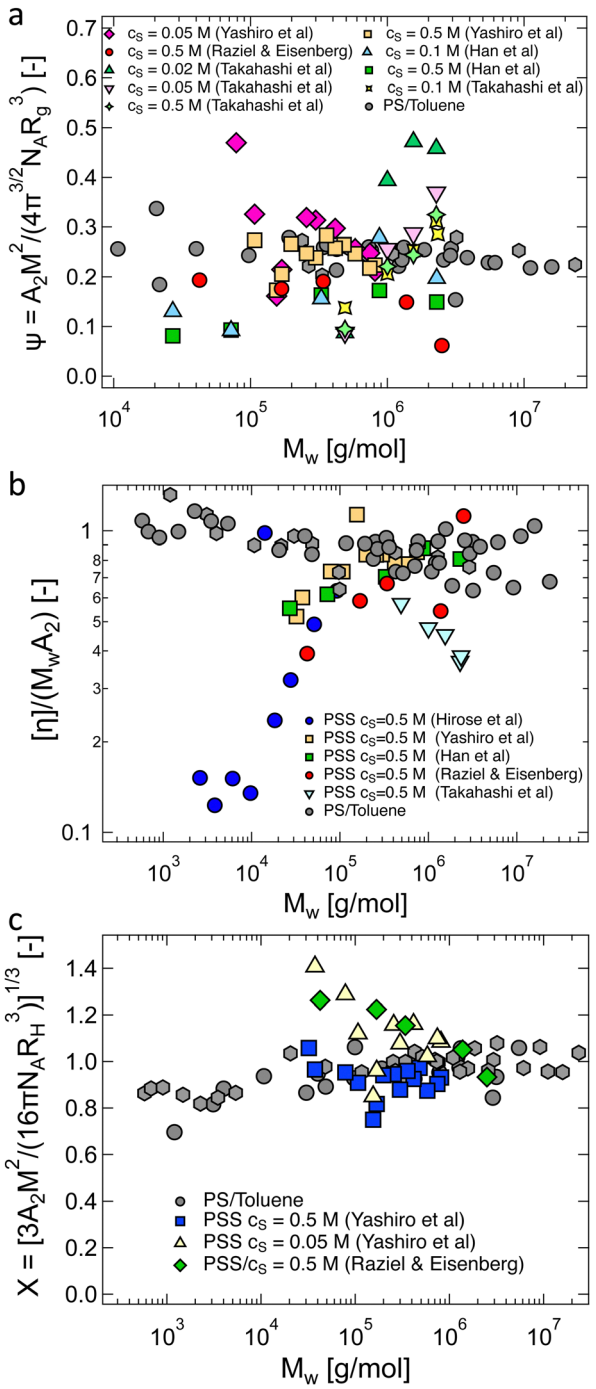

Fig. 28 Comparison of the universal ratios $U_{\eta A}$ (a), Ψ (b) and X (c) for polystyrene in good solvent (grey symbols) and NaPSS in aqueous salt solutions (other symbols). Data are from ref. 105–107, 193, 301, 475, 487–489, 531, 590 and 599–602 and references listed in ref. 589. Raziel *et al.*'s data are for KPSS in KCl aqueous solution.

by a simpler approach that approximates the salt and the solvent as a single component.[19,209,234,236,611]

3.13.1 The form factor. The form factor $P(q)$ contains information on the spatial correlations between the monomers of a single chain. Experimentally, it can be obtained by use of the zero-average contrast (ZAC) technique for solutions with or without added salt.[125,611–614] In solutions with excess added salt, $P(q)$ at infinite dilution can also be obtained by extrapolating the reduced scattering intensity $[I(q)/c]$ to the $c \to 0$ limits and normalising the resulting values by $I(q)/c$ extrapolated to $c \to 0$ and $q \to 0$.[615]

Table 5 Ratio $\rho = R_g/R_H$ for polystyrene and polystyrene sulfonate. Errors are 95% confidence intervals. For polystyrene, the values are for the high N limit

System	ρ	Ref.
PS/toluene (good solvent)	1.44 ± 0.04	See ESI
PS/cyclohexane (θ solvent)	1.32 ± 0.04	See ESI
PSS/0.5 M NaCl	1.32 ± 0.03	105–107
PSS/0.05 M NaCl	1.5 ± 0.05	105–107

In Fig. 29(a), the form factor of TMAPSS with N = 40 ($c^* \simeq 1$ M from Fig. 11(a)) in salt-free aqueous solution is plotted, measured by the zero-average contrast technique. The TMA counterions are contrast-matched and hence do not contribute to the coherent scattering signal.[125,616] The form factor for c = 0.1 and 0.2 M agrees well, suggesting that the solutions are sufficiently diluted that the chain conformation is independent of the polymer concentration. The form factor displays a region where $P(q) \propto q^{-1}$ as expected for rigid objects. The steeper dependence in the high-q region arises from the finite lateral dimensions of the chain, and the flattening at low q corresponds to the Guinier region ($qR_g \lesssim 1$), where the $P(q) \simeq 1 - q^2R_g^2/3$. For fully stretched configurations (B = 1), the PSS chain is expected to have an effective contour length of $L \simeq 10$ nm. As we expect the chain to be stretched in salt-free D_2O below c^*, the form factor of the particle should be that of a cylinder. Using a cross-sectional radius of 0.4 nm, the form factor of a cylinder with L = 10 nm is shown as a blue line, which clearly does not fit the experimental data. If L = 5.9 nm is assumed instead, corresponding to an effective monomer size of 0.17 nm (B = 1.5), an excellent fit is obtained. This is in reasonable agreement with the value of B = 1.8 obtained from correlation length data in semidilute solutions of NaPSS.[96] The high q region of the form factor of NaPSS from other studies yields effective monomer length values of 0.22–0.25 nm,[96,611,613,617] while Kassapidou *et al.*'s[125] data are an exception in this regard, and the reason remains unclear.

The form factor of TMAPSS in 0.19 M TMACl/D_2O solution is shown in Fig. 29(b) using data by Ragnetti and Oberthür.[615] At high-q, the form factor of a worm-like chain (or a cylinder) is

$$P(q) \simeq \frac{\pi}{qb'} P_{CS}(q), \tag{53}$$

where b' is the effective monomer size (b/B) and $P_{CS}(q)$ is a function that accounts for the finite cross-sectional dimensions of the chain. P_{CS} is given by the Hankel transform of the radial density profile of the chain.[125] Fixing the chain cross-sectional radius at r_C = 0.6 nm, and leaving the background scattering as a fit parameter, we obtain a monomer unit length of $b' \simeq 2.5$ Å ($B \simeq 1$), relatively close to Ragnetti and Obhertür's value of $b' \simeq 2.2$ Å ($B \simeq 1.1$). This corresponds to an effective contour length of L = 270 nm. At this added salt concentration, the persistence length of the chain is smaller than the contour

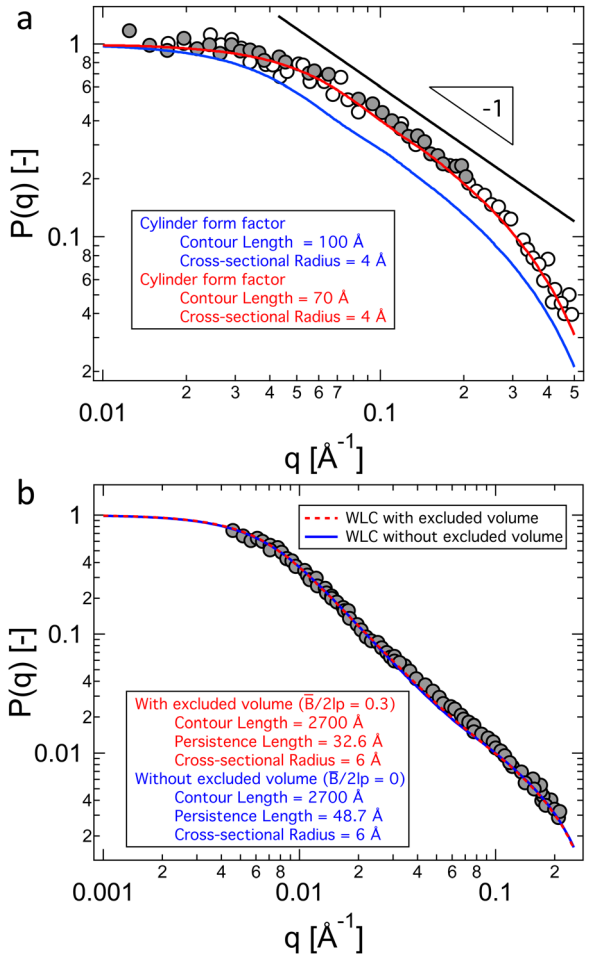

Fig. 29 Form factor of TMAPSS in (a) salt-free aqueous solution (grey circles c = 0.2 M, white circles c = 0.1 M, $c^* \simeq 1$ M based on Fig. 11) and (b) 0.19 M TMACl solution. Lines are fit to the cylinder form factor for (a) and to the worm-like chain form factor with and without excluded volume for (b). The fit parameters are indicated in the legend. The black line in the top panel represents the power law of −1. Cylinder form factors and WLC with excluded volume are calculated using SASView v 5.0.6. Data are from ref. 125 and 615.

length and therefore the chains are coiled. The dashed red line shown in Fig. 29(b) is the form factor of worm-like chain without excluded volume, calculated according to method 2 of ref. 618, leaving the persistence length as the only fit parameter, which yields $l_p \simeq 4.9$ nm. This value is much larger than $l_p \simeq 2$ nm estimated for NaPSS at the same ionic strength by Norisuye and co-workers, see Fig. 26.

As PSS chains with N = 1070 in c_s = 0.19 M salt solution are expected to be perturbed by the excluded volume, we next try to fit the form factor in Fig. 29(b) to an expanded worm-like chain form factor. Unfortunately, there is no analytical expression for the worm-like chain form factor with arbitrarily excluded volume (Sharp and Bloomfield developed a form factor for WLC with excluded volume,[619] errors in this model are noted in ref. 618). Pedersen and Schurtenberger[618] worked out the form factor of worm-like chains with a reduced binary cluster integral of $\bar{B}/(2l_p)$ = 0.3. This value is appropriate for many polymers in good solvent systems, but if we trust the values of B and l_p plotted in Fig. 26, it does not work generally for polyelectrolytes in excess salt. Specifically, for NaPSS in c_s = 0.19 M, we expect $\bar{B}/(2l_p) \simeq 0.5$. Lacking a better approximation, we fit the Pedersen-Schurtenberger form factor (model 3 of ref. 618, implemented in SASView as a "flexible cylinder model"). The result is shown as a dashed red line in Fig. 29(b). The quality of the fit is identical to that of the form factor without excluded volume, but the obtained persistence length now takes a lower value of $l_p \simeq 3.3$ nm.

The fits to Ragnetti and Oberthür's data show that the form factor of a polyelectrolyte cannot, in general, be used to extract the excluded volume and persistence length simultaneously. As with the global chain properties discussed earlier (R_g, D, $[\eta]$...), $P(q)$ for a chain in a solution of a given ionic strength must be fitted to a pair of l_p and $\bar{B}$ values. Fitting of chains of varying molar mass with the assumption that l_p and $\bar{B}$ are N-independent may allow for independently extracting these two parameters.

Because the reduced binary cluster integral $\bar{B}/(2l_p)$ is a function of the solution's ionic strength, it will be important for the field that forms factors for worm-like chains with arbitrarily excluded volume are developed. Some theories[9] propose that dilute polyelectrolytes adopt a directed random walk conformation. As the form factor for directed random walks has not been calculated, it is difficult to test these predictions. As discussed above, simulation studies have found that, under certain conditions, the bond orientation correlation function of polyelectrolytes is bimodal. Again, no form factor is available to check when or if this is observed experimentally.

3.13.2 Intermolecular structure factor. A major difficulty in treating scattering data from polyelectrolyte solutions is the lack of a theory that can predict the intermolecular structure factor accurately for low ionic strength solvents. The random phase approximation, which works well for neutral polymer solutions and polyelectrolytes in excess salt,[207,209,611] is not suitable for polyelectrolytes in low ionic strength media, failing to reproduce experimentally observed peak phenomena.[611,614,620] The PRISM theory, developed for polyelectrolytes primarily by Yethiraj and co-workers[61,621,622] correctly captures most features of the scattering function of dilute and semidilute solutions. However, calculations of the structure factor are rather involved and a comparison with experimental data has not been carried out. Simplified versions of the PRISM theory have been applied to experimental data, but the best-fit structural parameters such as the persistence length, do not yield reasonable results.[623,624] The theory of Muthukumar[427] calculated the static scattering properties of polyelectrolytes in the low-q limit and was found to describe experimental results for a weakly charged polyelectrolyte.[428]

3.13.3 The low-q upturn and the slow mode. The total structure factor of a two-component solution in the q = 0 limit (sometimes known as the thermodynamic limit) is related to the osmotic pressure (Π) of the solution as:

$$S(0) = k_B T \frac{dc}{d\Pi}. \quad (54)$$

Further, the osmotic pressure of polyelectrolytes is given by:

$$\Pi \simeq k_B T f c, \quad (55)$$

where we approximate the osmotic coefficient of polyelectrolyte solutions as $\phi \simeq f$, which is valid at $c \gtrsim c^*$.

Combining eqn (54) and (55), we get:

$$S(0) \simeq f^{-1}. \tag{56}$$

This may be compared to a neutral polymer solution where $S(0) \sim N$ at $c = c^*$. The scattering of polyelectrolytes in salt-free solutions at low q is therefore expected to be extremely weak compared to that of neutral polymers. The reason for this is that the high osmotic pressure created by the counterions suppresses long-ranged concentration fluctuations. Experimentally however, a large upturn at low wave vectors is found and the values of $S(0)$ are several orders of magnitude higher than expected by eqn (56). Most of the experimental data for this phenomenon are for semidilute solutions[92,233,625] and they are not reviewed here.

The intermediate scattering function of polyelectrolytes, as measured by dynamic light scattering, was shown to be bimodal in solvents of low ionic strength. For some systems, it has been observed that bimodal behaviour emerges when $fc/c_s \gtrsim 0.03$–0.1,[103,396] but this is not always the case.[422,626] The fast mode arises from the counterions, the motions of which are strongly coupled to those of the polyelectrolyte backbone.[65] The slow mode is thought to have the same physical origin as the low-q upturn. The presence of the slow mode, sometimes referred to as 'extraordinary' behaviour, has been extensively studied[65,103,396,422,627–629] and hotly debated in the literature.[630,631] There exists at present no consensus about its origin.

This slow mode and low-q upturn have often been interpreted as arising from multichain clusters with a size of $\sim$100 nm.[632] Such interpretations are considered unsatisfactory by some because it is not clear how highly incompressible systems can withstand such long-ranged concentration fluctuations. Possible explanations are that the entities responsible for the upturn are either not at equilibrium with the rest of the solution (*e.g.*, undissolved polymer residues) or that they are non-permeable to the solution (*e.g.*, dust particles).[630,633,634] These explanations have generally been rejected on the basis of experimental tests.[631,635–640]

In our view, the main challenge is to reconcile the following three statements: (1) osmotic pressure and conductivity data show that eqn (55) is correct;[68,424,641] (2) eqn (54) should be applied generally to two-component systems;[642] (3) scattering measurements show that eqn (56) does not hold. A satisfactory account to the upturn/slow mode problem must be able to explain both the high values of $S(0)$ and the low osmotic compressibility of the systems.

When polyelectrolyte diffusion is measured using techniques such as pulsed field gradient NMR[19,301,410,643] or fluorescence photobleaching recovery,[644,645] no slow mode or otherwise abnormal diffusion is apparent.[631] Electrophoretic mobility measurements also do not show any abnormal behaviour.[644,646,647] The viscosity of polyelectrolyte solutions also appears to be independent of the amplitude of the slow mode.[648] This leads to the conclusion that whatever entities are responsible for the slow mode and low-q upturn involve only a very small number of chains and/or occupy a very small fraction of the solution volume.

3.13.4 The intermediate scattering function. We next turn to the dynamic scattering properties of polyelectrolyte solutions. The intermediate scattering function $F(q,t)$ contains information about the scale-dependent dynamic processes of polymer chains. At small times, $F(q,t)$ can usually be modelled by an exponential decay so that

$$-\frac{\mathrm{d}\,\ln[F(q,t)]}{\mathrm{d}t} \simeq \Gamma, \tag{57}$$

where Γ is a decay rate. An apparent diffusion coefficient can be calculated as: $D_{\mathrm{app}} = \Gamma/q^2$. For diffusive processes in dilute solution, in the low q limit, the apparent diffusion coefficient can be expressed as

$$D_{\mathrm{app}}(q,c) \simeq D(1 + k_{\mathrm{D}}c)\left(1 + C'q^2R_{\mathrm{g}}^2\right), \tag{58}$$

where D is the translational diffusion of the chains, k_{D} is a parameter for which there is no standard name but is sometimes referred to as the 'diffusion virial coefficient' and C' is a constant which depends on the particle size and shape.[649] Note that the apparent diffusion coefficient obtained by dynamic light scattering at finite concentrations is different from the translational diffusion coefficient of the chains. These two quantities only match in the $c = 0$ limit.[650]

The variation of k_{D} with molar mass and added salt concentration for polyelectrolytes has been reported in many literature studies.[106–109,112,113,474,477,499,500,519–523] The results are compiled in the ESI,† where it is shown to be approximately proportional to the overlap concentration of the system under high excluded volume conditions, see Section S6 (ESI†). This agrees with results for neutral polymers in good solvents.[651] For constant C', the available datasets[474] do not allow us to draw any clear conclusions.

In the $R_{\mathrm{g}}^{-1} \lesssim q \lesssim (2l_{\mathrm{p}})^{-1}$ region, eqn (58) does not apply and instead, the so-called q^3 asymptote ($\Gamma \propto q^3$ or $D_{\mathrm{app}} \propto q$) is predicted by several theories, in agreement with experimental observations for neutral polymers.[116,652] The Zimm model with full hydrodynamic interactions predicts:

$$\Gamma(q) = A_0\frac{k_{\mathrm{B}}T}{\eta_{\mathrm{s}}}q^3, \tag{59}$$

where the dimensionless pre-factor of A_0 takes a value of 0.0788 for the good solvent limit and 0.0625 for theta solvents.

The apparent diffusion coefficient of DNA in NaCl and LiCl solutions normalised to its value at $q = 0$ is plotted as a function of qR_{g} in Fig. 30. The datasets for different added salt concentrations approximately collapse onto a single curve. The exception is the $c_{\mathrm{s}} = 0.005$ M NaCl sample, which at intermediate qR_{g} shows higher D_{app}/D than the other samples. The Zimm prediction (eqn (59)) for good solvents ($A_0 = 0.0788$, $\rho = 1.41$) is shown as a dashed line. It correctly captures the scaling of $D_{\mathrm{app}} \propto q$ (or equivalently $\Gamma \propto q^3$) displayed by the DNA data, although the pre-factor to the power-law is over-predicted by around 30%. For $qR_{\mathrm{g}} \gtrsim 6$, the D_{app}/D_0 data approach a plateau, which has been observed for $ql_{\mathrm{K}} \gtrsim 5$ for various polymer-solvent systems.[116,653] Note that for the present system $ql_{\mathrm{K}} = 5$ corresponds to $qR_{\mathrm{g}} \simeq 12$–$18$. The plateau is seen more clearly

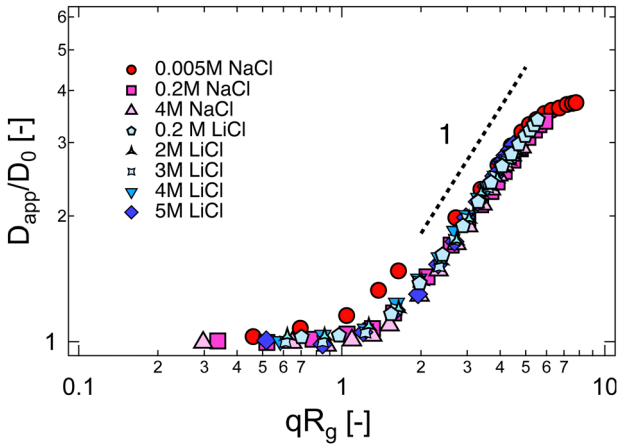

Fig. 30 Apparent diffusion coefficient normalised to its value at q = 0 as a function of qR_g for NaDNA and LiDNA in NaCl and LiCl solutions. Data are from ref. 502, 503 and 655. Line is the prediction of the Zimm model: eqn (59), no free parameters (A_0 = 0.0788).

for higher molar mass DNA samples, see for example ref. 654. The height of the plateau depends on the friction coefficient of the Kuhn segment and on the strength of the hydrodynamic interactions.[591,653,654]

3.14 Transition from salt-free to excess salt regimes

The preceding discussion has shown that, despite some open questions, the scaling theory largely captures the essential static and dynamic properties of polyelectrolytes in the salt-free and in excess added salt limits. We next consider the cross-over between these two regimes. The aim is to determine at which added salt concentration polyelectrolytes become flexible. The hydrodynamic radius of NaPSS in aqueous solutions at infinite polymer dilution is plotted as a function of the added salt in Fig. 31. The data of Jia *et al.*[211] for a single NaPSS sample with M_w = 66 kg mol^{-1} are considered in Fig. 31(a), and a broader set of samples from different literature reports with $M_w \simeq 20$ kg mol^{-1} are compared in Fig. 31(b). At low added salt concentrations, $R_H \sim c_s^0$ is observed. Such a regime is often observed in polyelectrolyte systems, such as gels.[350,352] At high added salt concentrations, the scaling prediction $R_H \sim {c_s}^{-1/5}$ works for the limited added salt concentration range studied. The critical added salt concentration (c_s') separating the two regimes can be identified from the intercept of the two power-laws or by fitting a crossover function, given in the caption. Both methods yield nearly identical results: $c_s' \simeq 0.02$ M ($\kappa^{-1} \simeq 2$ nm) and $c_s' \simeq 0.1$ M ($\kappa^{-1} \simeq 1$ nm) for the 66 and 20 kg mol^{-1} polymers, respectively.

The scaling model predicts that chains become flexible when the screening length (eqn (10)) is of the order of the chain size. Since, as shown in Section 3.5 in the infinite dilution limit NaPSS are fully stretched in DI water, R is of the order of the contour length of the chain. Thus, we find $R/\kappa^{-1} \simeq L/\kappa^{-1} \simeq$ 20–30, which is larger than the prediction of the Dobrynin model ($r_{scr} \simeq 3.5\kappa^{-1}$ for NaPSS in water).[89] In order to test the scaling prediction for the flexible-to-rod

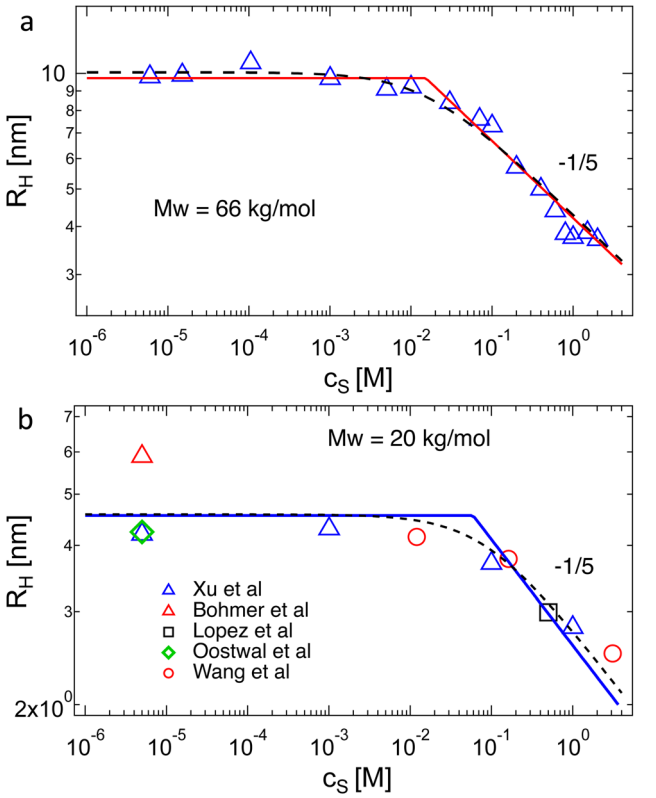

Fig. 31 Hydrodynamic radius of NaPSS in aqueous salt solutions at infinite dilution showing crossover between rod-like and flexible coil. Solid lines are fitted to $R_H = R_H(0)$ for $c_s < c_s^*$ to $R_H = R_H(0)\left(c_s/c_s'\right)^{-1/5}$ at high c_s. Dashed lines are fit to crossover function $R_H(c_s) = R_H(0)/\left(1 + c_s/c_s'\right)^{-1/5}$. The value of R_H at low salt and the cross-over salt concentration $\left(c_s'\right)$ are left as fitting parameters. Data for panel (a) are from ref. 211 and for panel (b) from ref. 19, 383, 386, 410, 496 and 656. Xu *et al.*'s values are interpolated.

transition, a study of the molar mass dependence of c_s' is needed. Chains become flexible when the screening length is of the order of their end-to-end distance. For longer chains, the screening length for which chains become flexible is therefore larger, corresponding to a lower value of c_s'. Specifically, the scaling model predicts $c_s' \propto N^{-2}$. A cursory examination of the available experimental data for NaPSS suggests they may be compatible with this prediction, but lacking more extensive datasets, no clear conclusion can be drawn at this point.

3.15 Specific ions effects on polyelectrolyte conformation

As discussed in Section 3.1, the phase behaviour of polyelectrolytes in excess added salts reveals that salt ions interact with polyelectrolytes in ways that cannot be explained by simple electrostatics.[657] For example, chaotropic or hydrophobic ions may bind to non-ionic sites on the polyelectrolyte backbone because the resulting change in the structure of water is enthalpically or entropically favourable.[658] In addition, Collins' concept of matching water affinities[659] and ion-pair formation can be extended to soft matter interfaces: Malikova *et al.*[660] proposed that there can be a hydration match between

counter-ions that favors ion pairing on polyelectrolytes. These solvent-mediated effects are well-known and have been studied for a variety of soft matter systems,[213–215,661] but the physical origin of the observed behaviour remains controversial.[662] Neutral polymers in solutions of ionic liquids are known to display associative properties,[663–665] a phenomenon often attributed to interactions between the ionic liquid ions and the dipoles along the polymer backbone. Such interactions may also be important for polyelectrolytes in concentrated salt solutions.

Studies by potentiometry and other methods have shown that the nature of counterions can influence the thermodynamic and transport properties of polyelectrolytes in solution,[660,666–669] but a framework to understand and predict these interactions is lacking.[78,662] Calorimetric techniques[670–672] show a strong influence of the counterion type on the enthalpy of dilution of polystyrene sulfonate. Such data are difficult to interpret but for PSS, several authors concluded that the strength of counterion binding to the backbone increases with increasing counterion size. These trends are not clearly observed for the conformational and hydrodynamic properties of PSS. For example, the static structure factor of different alkaline salts shows only minor differences[673] and the viscosity and diffusion coefficient of the sodium and cesium salts of PSS have been found to be identical.[301]

The importance of specific ion effects in relatively simple systems such as concentrated electrolyte solutions or neutral polymer solutions with added salts[220] is recognised but poorly understood, despite important progress in recent years.[662,674] As discussed in Section 3.1, polyethylene oxide is the most studied system in this regard. Depending on the solvent, addition of salt can either deteriorate solvent quality or lead to significant ion binding along the backbone, thereby inducing polyelectrolyte-like behavior. For polyelectrolyte solutions, where additional layers of complexity are present due to the importance of electrostatic screening, ion pairing, *etc.*, it seems unlikely that a full understanding of these phenomena will be reached any time soon. It might therefore be advisable to focus part of our attention on systems where such interactions are expected to be minimised, for example, polyelectrolyte solutions in polar solvents with low hydrogen bonding. Unfortunately, experimental data for such systems are sparse. Finding polyelectrolyte/solvent/salt solutions where ion-specific are not important would be helpful, as it would allow us to work with systems for which interpretation of experimental data becomes comparatively simpler. The lack of ion-specific effects can be established if conformational or hydrodynamic properties of polyelectrolytes are found to be independent of the ion-type added.

Lacking a theoretical framework with which to interpret the influence of ion type on the conformational and hydrodynamic properties of polyelectrolytes, we limit ourselves here to introducing a few interesting results, which will hopefully draw attention to the complexity of this topic. The data of Kagawa and Fuoss[210] for the intrinsic viscosity of sodium polyacrylate is plotted as a function of added salt concentration for three different monovalent salts in Fig. 32(a). At low c_s, $[\eta]$ is largely unaffected by the salt type but beyond $c_s \simeq 0.5$ M, qualitatively different behaviour is observed. Particularly striking is the case

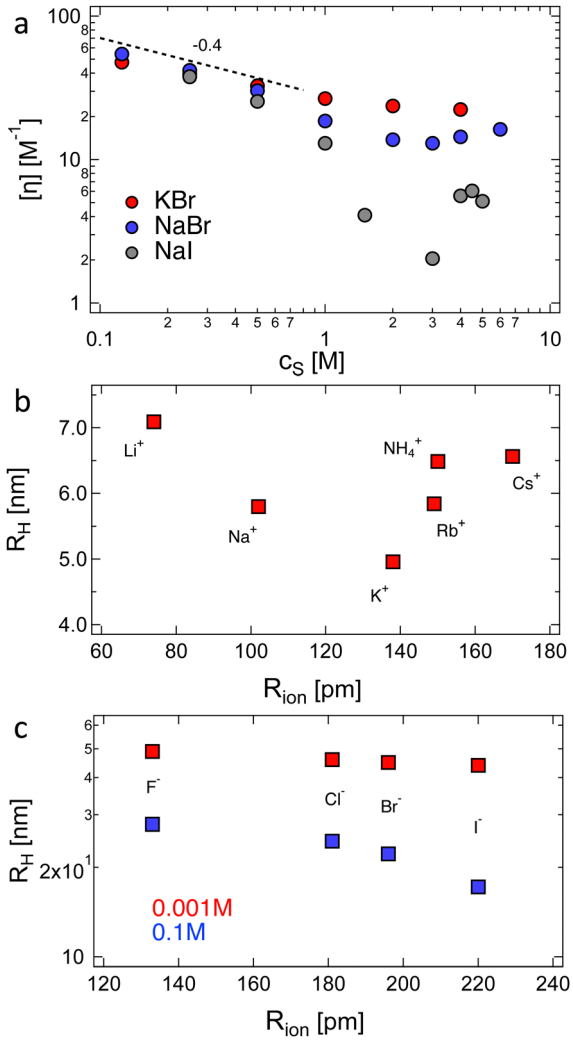

Fig. 32 (a) Intrinsic viscosity of sodium polyacrylate as a function of added salt for different concentrations of monovalent salts. Data are from ref. 210. (b) Hydrodynamic radius of PVS in 0.5 M salt solutions of X^+Cl, where $X^+ = Li^+$, Na^+, K^+, Rb^+, Cs^+ and NH_4^+, plotted as a function of cation radius. R_H values are estimated from intrinsic viscosity using eqn (50) with $U_{\eta F} = 0.12$. Data are from ref. 194. (c) Hydrodynamic radius of quaternised P2VP in 0.001 M and 0.1 M salt solution as a function of the anion radius. Data are from ref. 103.

of NaI, where chain re-expansion above $c_s \simeq 3$ M is apparent. The influence of counterion radius on the hydrodynamic radius of polyvinyl sulfate and quaternised polyvinyl pyridine in excess added salt is shown in Fig. 32(b) and (c), respectively. The data from Beer *et al.*[103] show that R_H is almost independent of anion radius (R_{ion}) in low added salt (c_s = 1 mM) but decreases significantly with R_{ion} at c_s = 0.1 M. The dependence of R_H on counterion size for PVS is more complicated, as it goes through a minimum. Qualitatively similar behaviour has also been observed for polyphosphates[675,676] and dextran sulfate.[677,678]

3.16 Charge screening in concentrated electrolyte solutions

Here, we introduce a unique charge screening behaviour observed recently for PILs in ionic liquid solutions. Ionic

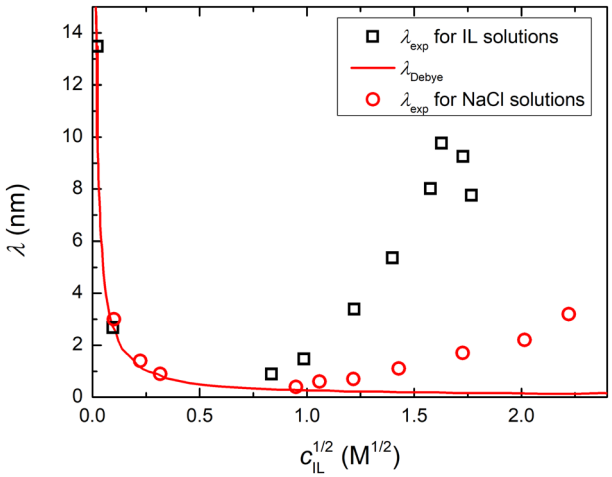

Fig. 33 The dependence of the measured screening length λ_{exp} on the square root of the concentration c_{IL} for an ionic liquid, 1-butyl-1-methylpyrrolidinium bis(trifluoromethanesulfonyl)imide ([C_4C_1 Pyrr][TFSI]), in propylene carbonate (black squares) and NaCl solutions (red circles). The red solid curve represents the screening length λ_{Debye} predicted by the Debye–Hückel theory. The λ_{exp} and λ_{Debye} are taken from Fig. 2 of ref. 682.

liquids (ILs) are a type of salts that exist in a liquid state at room temperature.[37] As a result, ILs have been used as plasticizers for polymeric materials.[679] In this context, the mixture of PILs and ILs could be utilized as electrolytes in batteries[680] and membranes for molecular separation.[681] Consequently, understanding the conformation and the polymer dynamics of PILs in IL solutions is of great importance because they are intimately related to the properties of PIL-based materials.

In the previous sections, we showed that PILs behave as polyelectrolytes when dissolved in organic solvents. The physical properties of polyelectrolytes are regulated by the addition of salts because of the charge screening. Accordingly, one may intuitively assume that any charge effects are completely screened in ionic liquids because the concentration of ions is extremely high. Namely, the screening length is small enough that polyelectrolyte chains can behave as a neutral polymer in ionic liquids. However, recent experimental studies on the screening length showed that the charge screening behaviour in ionic liquid solutions was much more complicated than those predicted by the classical Debye–Hückel model.[57,442,683] Fig. 33 shows a typical example of the experimentally determined screening length in ionic liquid solutions, showing a non-monotonic dependence against the increasing ionic liquid concentration.[682] In the plot, symbols are the screening length estimated using a surface force apparatus, while the line represents the Debye length. The surface apparatus works by measuring the force between two smooth mica surfaces as a function of separation distance, for inter-surface distances in the range $\simeq$2–15 nm. In particular, the measured screening length increased with increasing concentration of salts in the high-salt regime, which was attributed to the charge underscreening.[684] The Debye–Hückel theory predicts a monotonic decrease of the screening length with the increasing salt concentration. Note that the region where the measured screening length and the Debye–Hückel prediction disagree corresponds to $\kappa^{-1} < l_B$. Holm and co-workers argued, on the basis of simulation work, that experimental results pointing to under-screening are likely the result of confinement effects and do not reflect the properties of ionic liquids in the bulk.[685,686] This topic remains controversial,[687] with several apparently conflicting results being reported over the last few years.[688–693]

The apparent hydrodynamic radius, measured at c = 0.01 M and scattering angle 40°, for a PIL (PC_4-TFSI) in DMF solution is plotted as a function of added ionic liquid (Bmim-TFSI: 1-butyl-3-methylimidazolium bis(trifluoromethanesulfonyl)imide) concentration, c_{IL} in Fig. 34. For $c_{IL} \gtrsim 1$ M, the apparent hydrodynamic radius is seen to increase with increasing ionic strength. Using the scaling laws of Lee *et al.*,[694] the screening length of the polyelectrolyte solution can be expressed as follows:

$$r_{scr}^{mod} \sim r_{scr}\left(1 + \frac{a^3}{r_{scr}^3}\right), \quad (60)$$

where a is the ion diameter of salt ions. The modified screening length decreases with increasing salt concentrations at low concentrations, similar to r_{scr}, but starts to increase with increasing salt concentrations when r_{scr} is comparable to a. The size of a dilute polyelectrolyte chain in excess salt is related to the screening length as $R \propto r_{scr}^{0.4}$. Replacing eqn (60) with r_{scr}, the dependence of the hydrodynamic radius ($R_H \simeq R$) on the c_{IL} is shown as a dashed blue line in Fig. 34. The calculation is seen to track experimental data reasonably well. Note also that the increase in the apparent R_H at $c_{IL} \simeq 1$ M coincides with the increase in the specific viscosity of the solutions.[57] While data in dilute solution for PILs are sparse, a systematic investigation of their semidilute properties has been conducted by Matsumoto *et al.*[57,442,683] The specific viscosity and the longest relaxation time of PILs dissolved in mixtures of organic solvents and ionic liquids can be described by applying the scaling model of Dobrynin *et al.*[89] using eqn (60) as the screening length.

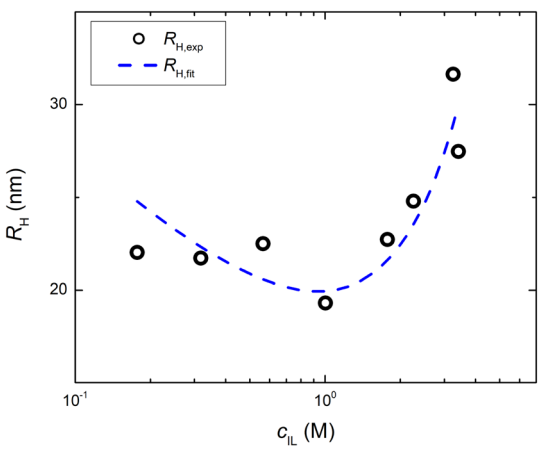

Fig. 34 Variation of the apparent hydrodynamic radius of PC_4-TFSI in DMF solution at c = 0.01 M as a function of added ionic liquid (Bmim-TFSI) concentration c_{IL}. The line is calculated assuming $R_H \propto r_{scr}^{0.4}$, leaving the proportionality constant as a free parameter. The data are taken from ref. 57.

Chain expansion at high added salt concentrations has also been observed for linear and grafted polyelectrolytes in aqueous media.[211,246,695] These results have been interpreted in terms of the underscreening theory.[696] A major problem for this type of interpretation is that for many polyelectrolyte systems, chain expansion is not observed at high-added salt. The most prominent example of this is NaPSS in aqueous NaCl solutions, which have been studied for c_s up to 4.17 M. The results of Smith *et al.*[682] for the screening length of concentrated electrolyte solutions expect that underscreening occurs not only for concentrated ionic liquid solutions but also for simple salts. For example, their measurements showed that λ for NaCl in water, shown in Fig. 33, increases for $c_s \gtrsim 1$ M. Extensive datasets on the variation of the static and hydrodynamic sizes of NaPSS with added NaCl and KCl concentrations (up to 4.17 M) in aqueous media have been reported by several groups.[105,193,475,477] These did not show any evidence of chain re-expansion in the high c_s region, as would be expected from the results of Smith *et al.*

The curve fit shown in Fig. 34 relies on the assumptions that (1) the charge fraction on the PIL chain remains the same as that in DMF, *i.e.*, f is independent of c_{IL}, (2) the non-electrostatic excluded volume effect does not change with respect to the increasing c_{IL}, (3) the scaling law of r_{scr}^{mod}, found by surface force measurements (2-D screening process), holds for the charge screening in polyelectrolyte systems, and (4) the solvent dynamics does not change by the addition of PILs. Unless these assumptions are justified, we cannot conclude that the charge underscreening is attributed to the increase of R_H.

4 Conclusions & outstanding questions

Polyelectrolytes are ubiquitous in our daily life. The conformation and properties of polyelectrolytes are strongly influenced by the electrostatic interactions acting between charged monomers. We re-visited literature reports in the polyelectrolyte field and combined them to know the current level of understanding of the conformation and dynamics of polyelectrolyte solutions, in particular in the dilute regime. Key research challenges requiring further investigations are summarized as follows.

1. The conformation of polyelectrolytes in low ionic strength solvents at infinite dilution limit is challenging to assess experimentally. This is because of the extreme dilution required for chains to be weakly interacting. Intrinsic viscosity data for polyelectrolytes in DI water or other low ionic strength solvents could serve as a valuable measure of chain conformation, but the extrapolation of the reduced viscosity to the $c \to 0$ limit is challenging. In this regime, the technique which appears to yield the most robust results is fluorescence correlation spectroscopy (see Fig. 10a). The available R_H and $[\eta]$ data for NaPSS exceed the theoretical prediction for fully stretched chains, suggesting the influence of the primary electroviscous effect.

2. The overlap concentration data for various systems agrees with theoretical predictions that in dilute salt-free solutions, polyelectrolytes are highly stretched ($R \sim N$). Data for NaPSS in DI water suggest that its end-to-end distance at $c = c^*$ is significantly shrunken with respect to its value at infinite dilution, in agreement with simulation work.[98] Discrepancies with respect to the scaling with dielectric constant and charge fraction are observed. The data suggest deviations from Manning's condensation theory and/or the scaling calculation of the electrostatic blob may be responsible for these discrepancies but current experimental evidence does not allow us to reach a firm conclusion. Data for c^* as a function of dielectric constant along with independent estimates for the fraction of free counterions, for example, based on osmometry, conductivity or dielectric spectroscopy data, would help resolve this outstanding question. Weakly charged polyelectrolytes ($Ab \gg l_B$), where no condensation is expected, are understudied systems. Systematic data for c^* (or other conformational parameters) as a function of charge fraction, solvent permittivity and molar mass would be particularly useful to resolve open questions regarding the nature of the electrostatic blob.

3. The phenomenon of counterion condensation is key to understanding virtually every property of highly charged polyelectrolytes in solution because the charge fraction has a large influence on the conformational and thermodynamic properties of chains. Estimates for the fraction of free counterions obtained from overlap concentration data reveal two surprising trends. First, f increases with increasing added salt content (Fig. 13c). Second, the dependence of f on solvent permittivity follows a power-law of $f \propto \varepsilon^{1.6}$ (Fig. 13d), in contrast to the linear relationship predicted by the Manning model. Both findings deserve additional work using different experimental techniques such as membrane osmometry and conductivity, which provide more direct measures of counterion condensation.

4. The scaling theory's prediction for the size of the electrostatic blob was checked against viscosity and radius of gyration data for several polyelectrolyte systems. In salt-free and excess salt, the scaling prediction is partially supported by current experimental evidence, but several experimental observations (*e.g.*, Fig. 11(c) and Fig. S8, ESI†) do not agree with the scaling predictions. Further experimental work is needed in two regards: first, systematic work on the conformational and hydrodynamic properties as a function of charge fraction in salt-free solution is at present limited to two studies,[97,399] extension to other systems is vital if we are to understand the discrepancies between theory and experiment. Second, the scaling predicts $\xi_{el} < l_K$ for polyelectrolytes with more than one dissociated charge per Kuhn segment, but experimental evidence (see Fig. 12, 22(b) and 23) suggests $\xi_{el} > l_B$. To further understand this problem, conformational and hydrodynamic data for polyelectrolytes in solvents with a broad range of dielectric constants are required.[697]

5. The N-scaling of the radius of gyration, diffusion coefficient and intrinsic viscosity of polyelectrolytes in excess salt agreed well with the scaling predictions. The c_s scaling of these quantities showed stronger departures from theory. This is not unexpected since our understanding of the electrostatic excluded volume in polyelectrolyte solutions remains relatively thin.

6. Several experimental observations, such as the solubility of polyelectrolytes in organic media, the ionomer to polyelectrolyte crossover in solution, or the temperature induced conformational transition observed in Fig. 15 suggest that understanding the solvation of the polymer backbone, ionic groups and counterions will be critical to fully account for the behaviour of ionic polymers in solution.

7. Modelling polyelectrolytes in excess salt as expanded worm-like chains can reproduce many of their dilute solution properties, including the form-factor, radius of gyration, diffusion coefficient and intrinsic viscosity. The extracted parameters for the persistence length and excluded volume strength suggest an approximately linear variation of these two quantities with the Debye screening length. The range of applicability of this model to polyelectrolytes remains unclear, with experiments suggesting that the WLC model applies over a broader range than expected by several polyelectrolyte theories and simulations. A related question is the lengthscale at which electrostatic interactions become screened in polyelectrolyte solutions. The data analysed in this review broadly support the validity of eqn (10). However, it is of interest to note that eqn (10) appears to hold over a broader c_s range than the conditions for which it was derived.

8. A comparison of several ''universal ratios'' for flexible neutral polymers and polyelectrolytes in excess salt revealed significant differences between the two types of systems. Only one of the ratios considered $U_{\eta F} = 6\pi\sqrt[3]{[\eta]M/(N_A R_H{}^3)}$, appeared to be truly universal, and may offer a way to estimate the molar mass of polyelectrolytes from diffusion and intrinsic viscosity data, which could be useful when refractive index increment values at constant chemical potential are not available. It is possible that replacing $R_H{}^3$ with a combination of R_g and R_H, as expected by various theories, may yield a more robust universal ratio.

9. The transition between rod-like and flexible chain behavior was examined on the basis of diffusion data in the infinite dilution limit. The data showed departures from the predictions of the scaling model of Dobrynin *et al.* Here, obtaining additional datasets as a function of molar mass should provide insightful tests to theoretical ideas on screening in polyelectrolyte solutions.

10. Poly(ionic liquid)s in ionic liquid solutions exhibited an unusual upturn in the plot of the hydrodynamic radius with respect to the increasing ionic liquid concentration. This phenomenon appears to be similar to the increase in specific viscosity with increasing ionic liquid content, primarily observed for semidilute solutions. The mechanism of such counter-intuitive screening behaviour remains elusive. More generally, the topic of underscreening in concentrated electrolyte solutions is a controversial one. The dimensions of polyelectrolyte chains are highly sensitive to the screening length of the solvent media. Therefore, studying polyelectrolytes in concentrated electrolyte solutions could offer interesting insights into the underlying phenomenon.

11. Theoretical models to treat scattering data from polyelectrolyte solutions lag behind those available for neutral polymers. For example, the calculation of form factors of worm-like chains for arbitrary values of the excluded volume strength and for directed random walks will be important. Simulation work has shown that under certain conditions, polyelectrolytes display bimodal bond-orientation correlation functions. Form factors to describe the scattering of polymer chains with these configurations are also lacking. Approximate analytical expressions for the form factors of chains with bimodal orientational correlation functions might allow experimentalists to test simulation results.

12. Several experimental results make it clear that in solutions containing monovalent salts in high concentrations, the ion type can have a large influence on the properties of polyelectrolytes. Ion-specific effects, despite being very widely studied in other contexts, have not received sufficient attention in the polyelectrolyte literature. The importance of ion-specific effects is a major hindrance to understanding basic phenomena, such as the chain conformation or phase behaviour of polyelectrolytes in concentrated salt solutions. As ion-specific effects arise largely (though not exclusively) from hydrogen bonding, work in organic solvents, especially aprotic ones, should be addressed in the future. Poly(ionic liquid)s with hydrophobic counterions, which exhibit good solubility in these systems, are good systems for such studies.

13. The importance of accurately evaluating the concentration of residual salts in polyelectrolyte solutions is of crucial importance if we are to understand their solution in low ionic strength media. Many experimental techniques may introduce residual salt ions into polyelectrolyte solutions, for example, if these come in contact with glass. Therefore, it is important to evaluate the residual salt content of samples after rheological measurements are completed, which only a few studies[320] have attempted. Cohen *et al.* noted the importance of devising ''*a standard procedure for cleaning and preparing the glass surface*''; yet, there remains a deficit in such standardized methods. While there are accounts of cleaning capillary viscometers using concentrated acid solutions,[299,323] the implications of these practices on the results are not well-defined.

Experimental work on several of the open questions discussed above would benefit from studies of polyelectrolyte behaviour in non-aqueous solvents. While water is undoubtedly the most important polyelectrolyte solvent, experimental work in aqueous solutions is often confounded by pronounced ion-specific effects at high salt concentrations and the inadvertent presence of residual salts in low ionic strength environments. Employing organic solvents could significantly enhance our understanding of how the solvent media's dielectric constant affects polyelectrolyte behavior, an area where existing research is limited.

We hope that the subjects discussed in this article will help readers to grasp an overview of the current research progress on the conformation and dynamics of polyelectrolytes in dilute solutions. We also highlight open research questions to be answered. It is envisioned that in the not-too-distant future, many of the existing puzzles in polyelectrolyte physics will be solved, providing more accurate predictions for the solution properties of polyelectrolytes.

Appendix: nomenclature

a	Ion diameter of salt ions
A_0	Pre-factor in eqn (59), given by the Zimm model
A_2	Second virial coefficient
$\bar{B}$	Excluded volume strength
$\overline{B_0}$	Intrinsic excluded volume strength
$\overline{B_{\mathrm{el}}}$	Electrostatic excluded volume strength
$\overline{B_{\mathrm{A}}}$	Attractive contribution to excluded volume strength
$\overline{B_{\mathrm{HC}}}$	Hard-core repulsive excluded volume strength
b	Length of a chemical monomer
B	Stretching parameter
b'	Effective (z-projected) monomer size
b_{c}	Distance between neighboring two point charges on a line charge
c	Polymer concentration (number per unit volume)
$c_{\max}$	Polymer concentration at which the reduced viscosity is maximum
c^*	Overlap concentration
c_{IL}	Concentration of ionic liquid
c_{s}	Added salt concentration (number of salt molecules per unit volume)
c_{s}^{**}	Critical salt concentration for precipitation
$c_{\mathrm{s}}^{\mathrm{D}}$	Critical salt concentration at re-entrant phase boundary
c_{s}'	Added salt concentration at which chains become flexible
C'	Dimensional constant for D_{app} in eqn (58)
D	Translational diffusion coefficient
D_0	Translational diffusion coefficient of a worm-like chain without excluded volume
D_{app}	Apparent diffusion coefficient
d_{C}	Chain's cross-sectional diameter
e	Electrostatic unit of charge
f	Fraction of charged monomers bearing a dissociated charge
$F(q,t)$	Intermediate scattering function
F_η	Function given in ref. 384
G	Function given in ref. 365
G'	Storage modulus
G''	Loss modulus
g_{K}	Number of chemical monomers per Kuhn segment
g_{T}	Number of chemical monomers in a thermal blob
g_{el}	Number of chemical monomers in an electrostatic blob
g_{scr}	Number of chemical monomers in a segment of length of r_{scr}
H	Function in eqn (43)
$I(q)$	Intensity of scattered light
i	Degree of ionisation
J	Dimensional constant in eqn (33)
K	Function in eqn (16)
K_{B}	Pre-factor in eqn (22)
K_{I}	Pre-factor in eqn (23)
K_η	Product given in eqn (35)
k_{B}	Boltzmann's constant
k_{D}	Diffusion second virial coefficient
k_{H}	Huggins constant
L	Contour length of chain
l	Distance along the chain contour
l_{B}	Bjerrum length
$l_{\mathrm{K},0}$	Length of bare Kuhn monomer
l_{p}	Persistence length
$l_{\mathrm{p,e}}$	Electrostatic persistence length
$l_{\mathrm{p},0}$	Intrinsic persistence length
M_{w}	Weight averaged molar mass
M_0	Molar mass of a monomer
M_{L}	Mass per unit length
n	Refractive index of solutions
N	Degree of polymerisation (number of chemical monomers)
N_{A}	Avogadro's constant
N_{n}	Number-averaged degree of polymerisation (in number of chemical monomers)
N_{w}	Weight-averaged degree of polymerisation (in number of chemical monomers)
N_z	z-Averaged degree of polymerisation (in number of chemical monomers)
$N_{\mathrm{K},0}$	Degree of polymerisation (in number of bare Kuhn monomers)
O	Function in eqn (42)
$P(q)$	Form factor (by definition $P(0) = 1$)
q	Scattering wavevector
R	End-to-end distance of a chain
$\bar{R}$	Gas constant
R_0	End-to-end distance of a WLC without excluded volume
R_{g}	Radius of gyration of a chain
$R_{\mathrm{g},0}$	Radius of gyration of a chain without electrostatic effects (variational theory)
R_{H}	Hydrodynamic radius
R_{ion}	Counterion radius
r_{scr}	Electrostatic screening length (scaling theory)
$r_{\mathrm{scr}}^{\mathrm{mod}}$	Modified screening length
r_{C}	Chain's cross-sectional radius
$S(q)$	Total structure factor
$s(l)$	Bond–bond orientational correlation function
T	Temperature
T_{p}	Phase separation temperature
T_{c}	Critical temperature
u	Ratio of Bjerrum length to monomer size (l_{B}/b)
u_{M}	Ratio of Bjerrum length to charge distance ($l_{\mathrm{B}}/b_{\mathrm{c}}$)
U_{el}	Coulomb energy of an electrostatic blob
$U_{\mathrm{A}\eta}$	Universal ratio given by eqn (47)
$U_{\eta\mathrm{S}}$	Universal ratio given by eqn (48)
U_{AS}	Universal ratio given by eqn (49)
$U_{\eta\mathrm{F}}$	Universal ratio given by eqn (50)
W	Dimensional constant in eqn (33)
X	Universal ratio given by eqn (52)
z	Excluded volume parameter
$\tilde{z}$	Function given by eqn (16) – scaled excluded-volume parameter
Z_{p}	Valence of a side-chain ion
Z_{c}	Valence of a counterion
α	Expansion factor (QTP theory)
α_{R}	Expansion factor for end-to-end distance ($\alpha_{\mathrm{R}}^2 \equiv R/R_0$)

α_S'	Expansion factor in variational theory
α_D	Expansion factor for diffusion coefficient
α_η	Expansion factor for intrinsic viscosity
β_1	Exponent in eqn (23)
β_B	Exponent in eqn (22)
χ	Flory–Huggins solubility parameter
χ_0	Intrinsic (non-electrostatic) contribution to the Flory–Huggins solubility parameter
χ_{el}	Electrostatic contribution to the Flory–Huggins solubility parameter
δ	Fraction of monomers bearing an ionic group
ε_0	Vacuum permittivity
ε_r	Relative dielectric constant of solvents
Φ	Flory viscosity factor
Γ	Initial decay rate of intermediate scattering function
γ	Polymer/solvent interfacial tension
$\dot{\gamma}$	Shear rate
$\dot{\gamma}_C$	Critical shear rate for the onset of shear thinning of
γ_η	Power-law exponent describing N-dependence of intrinsic viscosity
γ_R	Power-law exponent describing N-dependence of radius of gyration
γ_D	Power-law exponent describing N-dependence of diffusion coefficient
$[\eta]_0$	Intrinsic viscosity of WLC without excluded volume
$[\eta_0]$	Intrinsic viscosity of non-ionic polymer
$[\eta]_{rod}$	Intrinsic viscosity of rod-like objects
$[\eta]$	Intrinsic viscosity
η	Zero-shear viscosity of polymer solutions
η_s	Viscosity of solvent
η_{sp}	Specific viscosity ($\eta_{sp} = (\eta - \eta_s)/\eta_s$)
η_{red}	Reduced viscosity (η_{sp}/c)
κ^{-1}	Debye screening length
λ	Screening length in electrolyte solutions
μ	Dipole moment of a solvent molecule
ν	Solvent quality exponent
ρ	Ratio R_g/R_H
θ	Theta temperature
τ	Reduced temperature ($\tau \equiv T - \theta/T$)
τ_Z	Longest relaxation time (Zimm model)
ξ_T	End-to-end distance of thermal blob
ξ_{el}	End-to-end distance of electrostatic blob
$\xi_{T,el}$	Thermal blob, incorporating electrostatic contribution to excluded volume
Ψ	Interpenetration function
Π	Osmotic pressure

Conflicts of interest

The authors declare no conflict of interest.

Acknowledgements

C. G. L. acknowledges the Deutsche Forschungsgemeinschaft project GO 3250/2-1, and the Theodore von Karman Fellowship (GSO070) from the RWTH Aachen. C. G. L. thanks prof. Takaichi Watanabe for hosting his stay at the University of Okayama, during which most of the work for this manuscript was carried out, and Prof. Ralph Colby (Penn State) for many useful discussions and for providing feedback on an early version of the manuscript. We also thank Dr Max Hohenschutz (RWTH) for useful discussions and for proofreading the manuscript. A. M. acknowledges funding from the Japanese Society for the Promotion of Science (Grants-in-Aid for Early-Career Scientists, Grant No. 21K14686; Grant-in-Aid for Scientific Research(B), Grant No. 22H02139). A. Q. S. acknowledges the support of the Okinawa Institute of Science and Technology Graduate University with subsidy funding from the Cabinet Office, Government of Japan. Much of the graphical extraction of data extraction was carried out with the aid of WebPlotDigitizer.[698]

References

1 H. Staudinger, *Ber. Dtsch. Chem. Ges.*, 1920, **53**, 1073–1085.
2 **https://iupac.org/polymer-edu/what-are-polymers/**.
3 A. S. Abd-El-Aziz, M. Antonietti, C. Barner-Kowollik, W. H. Binder, A. Boker, C. Boyer, M. R. Buchmeiser, S. Z. D. Cheng, F. D'Agosto, G. Floudas, H. Frey, G. Galli, J. Genzer, L. Hartmann, R. Hoogenboom, T. Ishizone, D. L. Kaplan, M. Leclerc, A. Lendlein, B. Liu, T. E. Long, S. Ludwigs, J.-F. Lutz, K. Matyjaszewski, M. A. R. Meier, K. Mullen, M. Mullner, B. Rieger, T. P. Russell, D. A. Savin, A. D. Schluter, U. S. Schubert, S. Seiffert, K. Severing, J. B. P. Soares, M. Staffilani, B. S. Sumerlin, Y. Sun, B. Z. Tang, C. Tang, P. Theato, N. Tirelli, O. K. C. Tsui, M. M. Unterlass, P. Vana, B. Voit, S. Vyazovkin, C. Weder, U. Wiesner, W.-Y. Wong, C. Wu, Y. Yagci, J. Yuan and G. Zhang, *Macromol. Chem. Phys.*, 2020, **221**, 2000216.
4 R. M. Fuoss and U. P. Strauss, *J. Polym. Sci.*, 1948, **3**, 246–263.
5 A. Eisenberg and J.-S. Kim, *Introduction to ionomers*, Wiley, 1998.
6 A. Eisenberg and M. Rinaudo, *Polym. Bull.*, 1990, 671.
7 Q. Chen, N. Bao, J.-H. H. Wang, T. Tunic, S. Liang and R. H. Colby, *Macromolecules*, 2015, **48**, 8240–8252.
8 L. Nova, F. Uhlik and P. Košovan, *Phys. Chem. Chem. Phys.*, 2017, **19**, 14376–14387.
9 A. V. Dobrynin and M. Rubinstein, *Prog. Polym. Sci.*, 2005, **30**, 1049–1118.
10 A. V. Dobrynin, *Polymer*, 2020, **202**, 122714.
11 A. J. Konop and R. H. Colby, *Macromolecules*, 1999, **32**, 2803–2805.
12 S. Joly, R. Kane, L. Radzilowski, T. Wang, A. Wu, R. E. Cohen, E. L. Thomas and M. F. Rubner, *Langmuir*, 2000, **16**, 1354–1359.
13 G. S. Manning, *J. Chem. Phys.*, 1969, **51**, 924–933.
14 R. H. Colby, *Rheol. Acta*, 2010, **49**, 425–442.
15 M. Muthukumar, *Macromolecules*, 2017, **50**, 9528–9560.
16 G. Chen, A. Perazzo and H. A. Stone, *J. Rheol.*, 2021, **65**, 507–526.

17 G. Chen, A. Perazzo and H. A. Stone, *Phys. Rev. Lett.*, 2020, **124**, 177801.
18 A. H. Slim, W. H. Shi, F. Safi Samghabadi, A. Faraone, A. B. Marciel, R. Poling-Skutvik and J. C. Conrad, *ACS Macro Lett.*, 2022, **11**, 854–860.
19 C. G. Lopez, J. Linders, C. Mayer and W. Richtering, *Macromolecules*, 2021, **54**, 8088–8103.
20 A. V. Walter, L. N. Jimenez, J. Dinic, V. Sharma and K. A. Erk, *Rheol. Acta*, 2019, **58**, 145–157.
21 L. N. Jimenez, C. D. MartiInez NarvaIez and V. Sharma, *Macromolecules*, 2022, **55**, 8117–8132.
22 L. N. Jimenez, J. Dinic, N. Parsi and V. Sharma, *Macromolecules*, 2018, **51**, 5191–5208.
23 C. G. Lopez, R. H. Colby and J. T. Cabral, *Macromolecules*, 2018, **51**, 3165–3175.
24 C. Robin, C. Lorthioir, C. Amiel, A. Fall, G. Ovarlez and C. Le Coeur, *Macromolecules*, 2017, **50**, 700–710.
25 P. Komorowska, S. Różańska and J. Różański, *Cellulose*, 2017, **24**, 4151–4162.
26 A. Matsumoto, C. Zhang, F. Scheffold and A. Q. Shen, *ACS Macro Lett.*, 2022, **11**, 84–90.
27 F. Del Giudice, V. Calcagno, V. Esposito Taliento, F. Greco, P. A. Netti and P. L. Maffettone, *J. Rheol.*, 2017, **61**, 13–21.
28 J.-M. Carrillo, Y. Wang, R. Kumar and B. G. Sumpter, *Eur. Phys. J. E: Soft Matter Biol. Phys.*, 2023, **46**, 92.
29 E. Buvalaia, M. Kruteva, I. Hoffmann, A. Radulescu, S. Forster and R. Biehl, *ACS Macro Lett.*, 2023, **12**, 1218–1223.
30 K. Akkaoui, M. Yang, Z. A. Digby and J. B. Schlenoff, *Macromolecules*, 2020, **53**, 4234–4246.
31 Q. Wang and J. B. Schlenoff, *Macromolecules*, 2014, **47**, 3108–3116.
32 A. M. Rumyantsev, N. E. Jackson and J. J. De Pablo, *Annu. Rev. Condens. Matter Phys.*, 2021, **12**, 155–176.
33 B. Ghosh, R. Bose and T. D. Tang, *Curr. Opin. Colloid Interface Sci.*, 2021, **52**, 101415.
34 S. Shah and L. Leon, *Curr. Opin. Colloid Interface Sci.*, 2021, **53**, 101424.
35 H. Ohno and K. Ito, *Chem. Lett.*, 1998, 751–752.
36 J. Yuan and M. Antonietti, *Polymer*, 2011, **52**, 1469–1482.
37 R. Hayes, G. G. Warr and R. Atkin, *Chem. Rev.*, 2015, **115**, 6357–6426.
38 L. N. Wong, S. D. Jones, K. Wood, L. De Campo, T. Darwish, M. Moir, H. Li, R. A. Segalman, G. G. Warr and R. Atkin, *Phys. Chem. Chem. Phys.*, 2022, **24**, 4526–4532.
39 U. H. Choi, A. Mittal, T. L. Price, M. Lee, H. W. Gibson, J. Runt and R. H. Colby, *Electrochim. Acta*, 2015, **175**, 55–61.
40 D. S.-d la Cruz, M. D. Green, Y. Ye, Y. A. Elabd, T. E. Long and K. I. Winey, *J. Polym. Sci., Part B: Polym. Phys.*, 2012, **50**, 338–346.
41 K. Nakamura, K. Fukao and T. Inoue, *Macromolecules*, 2012, **45**, 3850–3858.
42 T. Inoue, A. Matsumoto and K. Nakamura, *Macromolecules*, 2013, **46**, 6104–6109.
43 U. H. Choi, Y. Ye, D. Salas de la Cruz, W. Liu, K. I. Winey, Y. A. Elabd, J. Runt and R. H. Colby, *Macromolecules*, 2014, **47**, 777–790.
44 M. M. Obadia, B. P. Mudraboyina, A. Serghei, T. N. T. Phan, D. Gigmes and E. Drockenmuller, *ACS Macro Lett.*, 2014, **3**, 658–662.
45 F. Fan, Y. Wang, T. Hong, M. F. Heres, T. Saito and A. P. Sokolov, *Macromolecules*, 2015, **48**, 4461–4470.
46 Z. Wojnarowska, J. Knapik, J. Jacquemin, S. Berdzinski, V. Strehmel, J. R. Sangoro and M. Paluch, *Macromolecules*, 2015, **48**, 8660–8666.
47 F. Fan, W. Wang, A. P. Holt, H. Feng, D. Uhrig, X. Lu, T. Hong, Y. Wang, N.-G. Kang, J. Mays and A. P. Sokolov, *Macromolecules*, 2016, **49**, 4557–4570.
48 C. Iacob, A. Matsumoto, M. Brennan, H. Liu, S. J. Paddison, O. Urakawa, T. Inoue, J. Sangoro and J. Runt, *ACS Macro Lett.*, 2017, **6**, 941–946.
49 Z. Wojnarowska, H. Feng, Y. Fu, S. Cheng, B. Carroll, R. Kumar, V. N. Novikov, A. M. Kisliuk, T. Saito, N.-G. Kang, J. W. Mays, A. P. Sokolov and V. Bocharova, *Macromolecules*, 2017, **50**, 6710–6721.
50 A. Matsumoto, C. Iacob, T. Noda, O. Urakawa, J. Runt and T. Inoue, *Macromolecules*, 2018, **51**, 4129–4142.
51 E. W. Stacy, C. P. Gainaru, M. Gobet, Z. Wojnarowska, V. Bocharova, S. G. Greenbaum and A. P. Sokolov, *Macromolecules*, 2018, **51**, 8637–8645.
52 P. Kuray, T. Noda, A. Matsumoto, C. Iacob, T. Inoue, M. A. Hickner and J. Runt, *Macromolecules*, 2019, **52**, 6438–6448.
53 Q. Zhao, P. Bennington, P. F. Nealey, S. N. Patel and C. M. Evans, *Macromolecules*, 2021, **54**, 10520–10528.
54 H. Chen and Y. A. Elabd, *Macromolecules*, 2009, **42**, 3368–3373.
55 R. Marcilla, J. Alberto Blazquez, J. Rodriguez, J. A. Pomposo and D. Mecerreyes, *J. Polym. Sci., Part A: Polym. Chem.*, 2004, **42**, 208–212.
56 A. Matsumoto, R. Ukai, H. Osada, S. Sugihara and Y. Maeda, *Macromolecules*, 2022, **55**, 10600–10606.
57 A. Matsumoto, F. Del Giudice, R. Rotrattanadumrong and A. Q. Shen, *Macromolecules*, 2019, **52**, 2759–2771.
58 J. Barrat and J. Joanny, *Adv. Chem. Phys.*, 1996, **94**, 1–66.
59 C. Holm, J. Joanny, K. Kremer, R. Netz, P. Reineker, C. Seidel, T. A. Vilgis and R. Winkler, *Polyelectrolyte theory*, Springer, 2004.
60 A. V. Dobrynin, *Curr. Opin. Colloid Interface Sci.*, 2008, **6**, 376–388.
61 A. Yethiraj, *J. Phys. Chem. B*, 2009, **113**, 1539–1551.
62 S. Forster and M. Schmidt, *Phys. Prop. Polym.*, 2005, 51–133.
63 J. Landsgesell, L. Nova, O. Rud, F. Uhlik, D. Sean, P. Hebbeker, C. Holm and P. Košovan, *Soft Matter*, 2019, **15**, 1155–1185.
64 K.-H. Shen, M. Fan and L. M. Hall, *Macromolecules*, 2021, **54**, 2031–2052.
65 M. Sedlak, *Langmuir*, 1999, **15**, 4045–4051.
66 T. Miyajima, *Physical Chemistry of Polyelectrolytes*, CRC Press, 2001, pp. 851–896.
67 U. Scheler, *Curr. Opin. Colloid Interface Sci.*, 2009, **14**, 212–215.
68 F. Bordi, C. Cametti and R. Colby, *J. Phys.: Condens. Matter*, 2004, **16**, R1423.
69 J. Combet, P. Lorchat and M. Rawiso, *Eur. Phys. J.: Spec. Top.*, 2012, **213**, 243–265.

70 C. Holm, M. Rehahn, W. Oppermann and M. Ballauff, *Polyelectrolytes with Defined Molecular Architecture II*, 2004, pp. 1–27.
71 V. M. Prabhu, *Curr. Opin. Colloid Interface Sci.*, 2005, **10**, 2–8.
72 V. Vlachy, *Pure Appl. Chem.*, 2008, **80**, 1253–1266.
73 G. Maurer, S. Lammertz and L. N. Schafer, *Polym. Thermodyn.: Liquid Polymer-Containing Mixtures*, 2011, pp. 67–136.
74 K. Huber and U. Scheler, *Curr. Opin. Colloid Interface Sci.*, 2012, **17**, 64–73.
75 M. Rubinstein and G. A. Papoian, *Soft Matter*, 2012, **8**, 9265–9267.
76 W. F. Reed, *Bunsen-Ges. Phys. Chem., Ber.*, 1996, **100**, 685–695.
77 M. Borkovec, G. J. Koper and C. Piguet, *Curr. Opin. Colloid Interface Sci.*, 2006, **11**, 280–289.
78 J. Smiatek, *Molecules*, 2020, **25**, 1661.
79 P. Ander, *Water-soluble polymers: synthesis, solution properties, and applications (ACS Symposium Series)*, 1991, ch. 13.
80 C. Wandrey, D. Hunkeler, U. Wendler and W. Jaeger, *Macromolecules*, 2000, **33**, 7136–7143.
81 A. Zhang, X. Yang, F. Yang, C. Zhang, Q. Zhang, G. Duan and S. Jiang, *Molecules*, 2023, **28**, 2042.
82 The monograph by Nagasawa[151] provides a very good introduction to the physical chemistry of dilute polyelectrolyte solutions, including many topics not covered here, but deals primarily with studies published before 1980.
83 A. Matsumoto, *Nihon Reoroji Gakkaishi*, 2022, **50**, 43–50.
84 K. G. Wilcox, S. K. Kozawa and S. Morozova, *Chem. Phys. Rev.*, 2021, **2**, 041309.
85 F. Horkay, *Gels*, 2021, **7**, 102.
86 M. Rubinstein and R. H. Colby, *Polymer Physics*, Oxford University Press, New York, 2003.
87 P.-G. De Gennes, P. Pincus, R. Velasco and F. Brochard, *J. Phys.*, 1976, **37**, 1461–1473.
88 P. Pfeuty, *J. Phys., Colloq.*, 1978, **39**, C2–149.
89 A. V. Dobrynin, R. H. Colby and M. Rubinstein, *Macromolecules*, 1995, **28**, 1859–1871.
90 A. V. Dobrynin and M. Jacobs, *Macromolecules*, 2021, **54**, 1859–1869.
91 M. Jacobs, C. G. Lopez and A. V. Dobrynin, *Macromolecules*, 2021, **54**, 9577–9586.
92 C. G. Lopez, S. E. Rogers, R. H. Colby, P. Graham and J. T. Cabral, *J. Polym. Sci., Part B: Polym. Phys.*, 2015, **53**, 492–501.
93 W. N. Sharratt, R. O'Connell, S. E. Rogers, C. G. Lopez and J. T. Cabral, *Macromolecules*, 2020, **53**, 1451–1463.
94 K. Salamon, D. Aumiler, G. Pabst and T. Vuletic, *Macromolecules*, 2013, **46**, 1107–1118.
95 E. Di Cola, N. Plucktaveesak, T. Waigh, R. Colby, J. Tan, W. Pyckhout-Hintzen and R. Heenan, *Macromolecules*, 2004, **37**, 8457–8465.
96 C. G. Lopez, F. Horkay, R. Schweins and W. Richtering, *Macromolecules*, 2021, **54**, 10583–10593.
97 S. Dou and R. H. Colby, *J. Polym. Sci., Part B: Polym. Phys.*, 2006, **44**, 2001–2013.
98 M. J. Stevens and K. Kremer, *J. Chem. Phys.*, 1995, **103**, 1669–1690.
99 Y. Kantor and M. Kardar, *Phys. Rev. Lett.*, 1999, **83**, 745.
100 A. Gulati, M. Jacobs, C. G. Lopez and A. V. Dobrynin, *Macromolecules*, 2023, **56**, 2183–2193.
101 M. Muthukumar, *J. Chem. Phys.*, 1996, **105**, 5183–5199.
102 M. Muthukumar, *Polym. Sci., Ser. A*, 2016, **58**, 852–863.
103 M. Beer, M. Schmidt and M. Muthukumar, *Macromolecules*, 1997, **30**, 8375–8385.
104 A. Katchalsky, O. Kunzle and W. Kuhn, *J. Polym. Sci.*, 1950, **5**, 283–300.
105 E. Hirose, Y. Iwamoto and T. Norisuye, *Macromolecules*, 1999, **32**, 8629–8634.
106 Y. Iwamoto, E. Hirose and T. Norisuye, *Polym. J.*, 2000, **32**, 428–434.
107 J. Yashiro and T. Norisuye, *J. Polym. Sci., Part B: Polym. Phys.*, 2002, **40**, 2728–2735.
108 J. Yashiro and T. Norisuye, *Polym. Bull.*, 2006, **56**, 467–474.
109 J. Yashiro, R. Hagino, S. Sato and T. Norisuye, *Polym. J.*, 2006, **38**, 57–63.
110 K. Hayashi, K. Tsutsumi, F. Nakajima, T. Norisuye and A. Teramoto, *Macromolecules*, 1995, **28**, 3824–3830.
111 K. Hayashi, K. Tsutsumi, T. Norisuye and A. Teramoto, *Polym. J.*, 1996, **28**, 922–928.
112 R. Hagino, J. Yashiro, M. Sakata and T. Norisuye, *Polym. J.*, 2006, **38**, 861–867.
113 S. Chisaka and T. Norisuye, *J. Polym. Sci., Part B: Polym. Phys.*, 2001, **39**, 2071–2080.
114 T. Ishikawa, M. Kikuchi, M. Kobayashi, N. Ohta and A. Takahara, *Macromolecules*, 2013, **46**, 4081–4088.
115 T. Norisuye, *Prog. Polym. Sci.*, 1993, **18**, 543–584.
116 H. Yamakawa, *Helical wormlike chains in polymer solutions*, Springer, 1997, vol. 1.
117 Intrinsic viscosity and diffusion coefficient data for low molar masses are typically required to obtain precise estimates of d_C and/or M_L.
118 R. M. Davis, *Macromolecules*, 1991, **24**, 1149–1155.
119 M. Fixman and J. Skolnick, *Macromolecules*, 1978, **11**, 863–867.
120 K. Kawakami and T. Norisuye, *Macromolecules*, 1991, **24**, 4898–4903.
121 R. Davis and W. Russel, *J. Polym. Sci., Part B: Polym. Phys.*, 1986, **24**, 511–533.
122 T. Odijk, *J. Polym. Sci., Polym. Phys. Ed.*, 1977, **15**, 477–483.
123 J. Skolnick and M. Fixman, *Macromolecules*, 1977, **10**, 944–948.
124 M. Le Bret, *J. Chem. Phys.*, 1982, **76**, 6243–6255.
125 K. Kassapidou, W. Jesse, M. Kuil, A. Lapp, S. Egelhaaf and J. Van der Maarel, *Macromolecules*, 1997, **30**, 2671–2684.
126 H. Yamakawa, T. Yoshizaki and D. Ida, *J. Chem. Phys.*, 2013, **139**, 204902.
127 J.-L. Barrat and J.-F. Joanny, *Europhys. Lett.*, 1993, **24**, 333.
128 Note that this condition is not met for common polyelectrolyte systems such as NaPSS or NaPAMS in water $(l_{p,0}l_B)^{1/2} \simeq 1$ nm and $b/A \simeq 1.2$ nm.
129 R. Everaers, A. Milchev and V. Yamakov, *Eur. Phys. J. E: Soft Matter Biol. Phys.*, 2002, **8**, 3–14.
130 A. V. Dobrynin, *Macromolecules*, 2005, **38**, 9304–9314.

131 M. Fixman, *J. Phys. Chem. B*, 2010, **114**, 3185–3196.
132 T. Odijk and A. C. Houwaart, *J. Polym. Sci., Polym. Phys. Ed.*, 1978, **16**, 627–639.
133 P. J. Flory, *J. Chem. Phys.*, 1953, **21**, 162–163.
134 K. Ghosh and M. Muthukumar, *J. Polym. Sci., Part B: Polym. Phys.*, 2001, **39**, 2644–2652.
135 K. Ghosh, G. A. Carri and M. Muthukumar, *J. Chem. Phys.*, 2001, **115**, 4367–4375.
136 If $\xi_{el} \lesssim l_{K,0}$, chains are rigid on all length scales, hence the d_C of the chain can be used for the cylinder's cross-section. For the $\xi_{el} > l_{K,0}$ case, chains can be modelled as a pole of electrostatic blobs, and ξ_{el} provides a better estimate for the cylinder's diameter.
137 M. M. Tirado and J. G. de la Torre, *J. Chem. Phys.*, 1979, **71**, 2581–2587.
138 M. M. Tirado and J. G. De La Torre, *J. Chem. Phys.*, 1980, **73**, 1986–1993.
139 J. Lapham, J. P. Rife, P. B. Moore and D. M. Crothers, *J. Biomol. NMR*, 1997, **10**, 255.
140 Note that the Flory constant depends on polymer flexibility, see for example ref. 148 and 591.
141 A. Gosteva, A. S. Gubarev, O. Dommes, O. Okatova and G. M. Pavlov, *Polymers*, 2023, **15**, 961.
142 H. Schiessel and P. Pincus, *Macromolecules*, 1998, **31**, 7953–7959.
143 H. Schiessel, *Macromolecules*, 1999, **32**, 5673–5680.
144 M. Muthukumar, *J. Chem. Phys.*, 2004, **120**, 9343–9350.
145 Q. Liao, A. V. Dobrynin and M. Rubinstein, *Macromolecules*, 2006, **39**, 1920–1938.
146 J. Jeon and A. V. Dobrynin, *Macromolecules*, 2007, **40**, 7695–7706.
147 A. V. Dobrynin and M. Rubinstein, *Macromolecules*, 2001, **34**, 1964–1972.
148 H. Yamakawa and M. Fujii, *Macromolecules*, 1974, **7**, 128–135.
149 H. Yamakawa and M. Fujii, *Macromolecules*, 1973, **6**, 407–415.
150 I. Fortelný, J. Kovář, A. Živný and M. Bohdanecký, *J. Polym. Sci., Polym. Phys. Ed.*, 1981, **19**, 181–184.
151 S. A. Rice and A. R. Dinner, *Physical Chemistry of Polyelectrolyte Solutions*, John Wiley & Sons, 2015, vol. 158.
152 A. Popov and D. A. Hoagland, *J. Polym. Sci., Part B: Polym. Phys.*, 2004, **42**, 3616–3627.
153 R. Kakehashi, H. Yamazoe and H. Maeda, *Colloid Polym. Sci.*, 1998, **276**, 28–33.
154 F. Oosawa, *J. Polym. Sci.*, 1957, **23**, 421–430.
155 R. M. Nyquist, B.-Y. Ha and A. J. Liu, *Macromolecules*, 1999, **32**, 3481–3487.
156 E. Trizac and G. Tellez, *Phys. Rev. Lett.*, 2006, **96**, 038302.
157 G. S. Manning, *J. Phys. Chem. B*, 2007, **111**, 8554–8559.
158 R. Kumar, A. Kundagrami and M. Muthukumar, *Macromolecules*, 2009, **42**, 1370–1379.
159 J.-M. Y. Carrillo and A. V. Dobrynin, *Macromolecules*, 2011, **44**, 5798–5816.
160 P. Gonzalez-Mozuelos and M. O. de la Cruz, *J. Chem. Phys.*, 1995, **103**, 3145–3157.
161 E. Raphael and J.-F. Joanny, *EPL*, 1990, **13**, 623.
162 E. Y. Kramarenko, A. R. Khokhlov and K. Yoshikawa, *Macromol. Theory Simul.*, 2000, **9**, 249–256.
163 G. V. Ramanathan and C. P. Woodbury, *J. Chem. Phys.*, 1982, **77**, 4133–4140.
164 M. Deserno, C. Holm and S. May, *Macromolecules*, 2000, **33**, 199–206.
165 A. Deshkovski, S. Obukhov and M. Rubinstein, *Phys. Rev. Lett.*, 2001, **86**, 2341–2344.
166 A. V. Dobrynin, M. Rubinstein and S. P. Obukhov, *Macromolecules*, 1996, **29**, 2974–2979.
167 M. Muthukumar, *Macromolecules*, 2002, **35**, 9142–9145.
168 S. Liu and M. Muthukumar, *J. Chem. Phys.*, 2002, **116**, 9975–9982.
169 R. G. Winkler, M. Gold and P. Reineker, *Phys. Rev. Lett.*, 1998, **80**, 3731.
170 T. Ono, M. Ohta and K. Sada, *ACS Macro Lett.*, 2012, **1**, 1270–1273.
171 S. Ben Mahmoud, W. Essafi, A. Brulet and F. Boue, *Macromolecules*, 2018, **51**, 9259–9275.
172 M. Hara, J. Wu and A. H. Lee, *Macromolecules*, 1988, **21**, 2214–2218.
173 R. Barbucci, A. Magnani and M. Consumi, *Macromolecules*, 2000, **33**, 7475–7480.
174 S. Jousset, H. Bellissent and J. C. Galin, *Macromolecules*, 1998, **31**, 4520–4530.
175 W. J. Horne, M. A. Andrews, K. L. Terrill, S. S. Hayward, J. Marshall, K. A. Belmore, M. S. Shannon and J. E. Bara, *ACS Appl. Mater. Interfaces*, 2015, **7**, 8979–8983.
176 B. Siadat, R. Lundberg and R. Lenz, *Macromolecules*, 1981, **14**, 773–776.
177 R. Weiss, R. Lundberg and S. Turner, *J. Polym. Sci., Polym. Chem. Ed.*, 1985, **23**, 549–568.
178 C. M. Hansen, *Hansen solubility parameters: a user's handbook*, CRC Press, 2007.
179 M.-X. Du, Y.-F. Yuan, J.-M. Zhang and C.-Y. Liu, *Macromolecules*, 2022, **55**, 4578–4588.
180 Y.-F. Yuan, J.-M. Zhang, B.-Q. Zhang, J.-J. Liu, Y. Zhou, M.-X. Du, L.-X. Han, K.-J. Xu, X. Qiao and C.-Y. Liu, *Phys. Chem. Chem. Phys.*, 2021, **23**, 21893–21900.
181 N. Ohtani, Y. Inoue, H. Mizuoka and K. Itoh, *J. Polym. Sci., Part A: Polym. Chem.*, 1994, **32**, 2589–2595.
182 N. Ohtani, Y. Inoue, Y. Kaneko, A. Sakakida, I. Takeishi and H. Furutani, *Polym. J.*, 1996, **28**, 11–15.
183 N. Ohtani, Y. Inoue, Y. Kaneko and S. Okumura, *J. Polym. Sci., Part A: Polym. Chem.*, 1995, **33**, 2449–2454.
184 M. Hara, A. Lee and J. Wu, *J. Polym. Sci., Part B: Polym. Phys.*, 1987, **25**, 1407–1418.
185 R. Lundberg and R. Phillips, *J. Polym. Sci., Polym. Phys. Ed.*, 1982, **20**, 1143–1154.
186 S. Nomula and S. L. Cooper, *Macromolecules*, 2001, **34**, 925–930.
187 G. Gebel, P. Aldebert and M. Pineri, *Polymer*, 1993, **34**, 333–339.
188 Y. Nishiyama and M. Satoh, *J. Polym. Sci., Part B: Polym. Phys.*, 2000, **38**, 2791–2800.

189 Y. Fukunaga, M. Hayashi and M. Satoh, *J. Polym. Sci., Part B: Polym. Phys.*, 2007, **45**, 1166–1175.
190 N. Yasumoto, Y. Hata and M. Satoh, *Polym. Int.*, 2004, **53**, 766–771.
191 A. M. Rumyantsev, A. Pan, S. Ghosh Roy, P. De and E. Y. Kramarenko, *Macromolecules*, 2016, **49**, 6630–6643.
192 R. Buscall and T. Corner, *Eur. Polym. J.*, 1982, **18**, 967–974.
193 A. Takahashi, T. Kato and M. Nagasawa, *J. Phys. Chem.*, 1967, **71**, 2001–2010.
194 H. Eisenberg and G. R. Mohan, *J. Phys. Chem.*, 1959, **63**, 671–680.
195 P. J. Flory and J. E. Osterheld, *J. Phys. Chem.*, 1954, **58**, 653–661.
196 M. O. De La Cruz, L. Belloni, M. Delsanti, J. Dalbiez, O. Spalla and M. Drifford, *J. Chem. Phys.*, 1995, **103**, 5781–5791.
197 A. Ikegami and N. Imai, *J. Polym. Sci.*, 1962, **56**, 133–152.
198 M. A. Axelos, M. M. Mestdagh and J. Francois, *Macromolecules*, 1994, **27**, 6594–6602.
199 M. Delsanti, J. P. Dalbiez, O. Spalla, L. Belloni and M. Drifford, *Phase Diagram of Polyelectrolyte Solutions in Presence of Multivalent Salts*, 1994, pp. 381–392.
200 R. Schweins, G. Goerigk and K. Huber, *Eur. Phys. J. E: Soft Matter Biol. Phys.*, 2006, **21**, 99–110.
201 N. Volk, D. Vollmer, M. Schmidt, W. Oppermann and K. Huber, *Polyelectrolytes with Defined Molecular Architecture II*, 2004, pp. 29–65.
202 M. Hansch, B. Hamisch, R. Schweins, S. Prevost and K. Huber, *J. Chem. Phys.*, 2018, **148**, 014901.
203 M. Hansch, H. P. Kaub, S. Deck, N. Carl and K. Huber, *J. Chem. Phys.*, 2018, **148**, 114906.
204 C. G. Sinn, R. Dimova and M. Antonietti, *Macromolecules*, 2004, **37**, 3444–3450.
205 H. Eisenberg and E. F. Casassa, *J. Polym. Sci.*, 1960, **47**, 29–44.
206 H. Eisenberg and D. Woodside, *J. Chem. Phys.*, 1962, **36**, 1844–1854.
207 W. W. Graessley, *Polymeric liquids & networks: structure and properties*, Garland Science, 2003.
208 S. Kawaguchi, S. Toui, M. Onodera, K. Ito and A. Minakata, *Macromolecules*, 1993, **26**, 3081–3085.
209 C. G. Lopez, F. Horkay, M. Mussel, R. L. Jones and W. Richtering, *Soft Matter*, 2020, **16**, 7289–7298.
210 I. Kagawa and R. M. Fuoss, *J. Polym. Sci.*, 1955, **18**, 535–542.
211 P. Jia and J. Zhao, *J. Chem. Phys.*, 2009, **131**, 231103.
212 H. Yuan and G. Liu, *Soft Matter*, 2020, **16**, 4087–4104.
213 I. Hakem and J. Lal, *EPL*, 2003, **64**, 204.
214 I. F. Hakem, J. Lal and M. R. Bockstaller, *J. Polym. Sci., Part B: Polym. Phys.*, 2006, **44**, 3642–3650.
215 M. Hohenschutz, P. Bauduin, C. G. Lopez, B. Forster and W. Richtering, *Angew. Chem.*, 2022, **62**, e202210208.
216 S. Z. Moghaddam and E. Thormann, *J. Colloid Interface Sci.*, 2019, **555**, 615–635.
217 M. Ataman, *Colloid Polym. Sci.*, 1987, **265**, 19–25.
218 S. Kawaguchi, G. Imai, J. Suzuki, A. Miyahara, T. Kitano and K. Ito, *Polymer*, 1997, **38**, 2885–2891.
219 E. Boucher and P. Hines, *J. Polym. Sci., Polym. Phys. Ed.*, 1978, **16**, 501–511.
220 R. Lundberg, F. Bailey and R. Callard, *J. Polym. Sci., Part A-1: Polym. Chem.*, 1966, **4**, 1563–1577.
221 K. Ono, H. Konami and K. Murakami, *J. Phys. Chem.*, 1979, **83**, 2665–2669.
222 F. Quina, L. Sepulveda, R. Sartori, E. B. Abuin, C. G. Pino and E. A. Lissi, *Macromolecules*, 1986, **19**, 990–994.
223 M. Giesecke, F. Hallberg, Y. Fang, P. Stilbs and I. Furo, *J. Phys. Chem. B*, 2016, **120**, 10358–10366.
224 C. Zhou, C. Ji, Y. Nie, J. Yang and J. Zhao, *Gels*, 2022, **8**, 213.
225 M. Drifford and M. Delsanti, *Polyelectrolyte solutions with multivalent added salts: stability, structure, and dynamics*, CRC Press, 2001, pp. 157–184.
226 A. Ezhova and K. Huber, *Macromolecules*, 2014, **47**, 8002–8011.
227 A. Urbanski, M. Hansch, C. G. Lopez, R. Schweins, Y. Hertle, T. Hellweg, F. Polzer and K. Huber, *J. Chem. Phys.*, 2018, **149**, 163318.
228 I. Michaeli, *J. Polym. Sci.*, 1960, **48**, 291–299.
229 J.-S. Jan and V. Breedveld, *Macromolecules*, 2008, **41**, 6517–6522.
230 I. Sabbagh and M. Delsanti, *Eur. Phys. J. E: Soft Matter Biol. Phys.*, 2000, **1**, 75–86.
231 E. Raspaud, M. O. De La Cruz, J.-L. Sikorav and F. Livolant, *Biophys. J.*, 1998, **74**, 381–393.
232 J. Pelta, F. Livolant and J.-L. Sikorav, *J. Biol. Chem.*, 1996, **271**, 5656–5662.
233 V. M. Prabhu, *Phase behavior of polyelectrolyte solutions*, University of Massachusetts Amherst, 2002.
234 V. Prabhu, M. Muthukumar, G. D. Wignall and Y. B. Melnichenko, *J. Chem. Phys.*, 2003, **119**, 4085–4098.
235 For other carboxylate polyelectrolytes such as NaCMC, heavier alkaline earth cations exhibit much lower values of c_S^{**} ($\sim$10 mM) than Mg^{2+}, which exhibits H-type precipitation.[93].
236 V. Prabhu, M. Muthukumar, G. Wignall and Y. Melnichenko, *Polymer*, 2001, **42**, 8935–8946.
237 S. Kanai and M. Muthukumar, *J. Chem. Phys.*, 2007, **127**, 244908.
238 E. Dubois and F. Boue, *Macromolecules*, 2001, **34**, 3684–3697.
239 W. N. Sharratt, C. G. Lopez, M. Sarkis, G. Tyagi, R. O'Connell, S. E. Rogers and J. T. Cabral, *Gels*, 2021, **7**, 44.
240 R. L. Feddersen and S. N. Thorp, *Sodium carboxymethylcellulose*, Elsevier, 1993, pp. 537–578.
241 D. Ishii, D. Tatsumi and T. Matsumoto, *Nihon Reoroji Gakkaishi*, 2013, **40**, 267–272.
242 C. Hu, W. Lu, A. Mata, K. Nishinari and Y. Fang, *Int. J. Biol. Macromol.*, 2021, **177**, 578–588.
243 D. M. Roquero, A. Othman, A. Melman and E. Katz, *Mater. Adv.*, 2022, **3**, 1849–1873.
244 P.-Y. Hsiao and E. Luijten, *Phys. Rev. Lett.*, 2006, **97**, 148301.
245 P.-Y. Hsiao, *Macromolecules*, 2006, **39**, 7125–7137.
246 Y. Roiter, O. Trotsenko, V. Tokarev and S. Minko, *J. Am. Chem. Soc.*, 2010, **132**, 13660–13662.
247 Y. Hou, G. Liu, Y. Wu and G. Zhang, *Phys. Chem. Chem. Phys.*, 2011, **13**, 2880–2886.
248 P.-Y. Hsiao, *J. Chem. Phys.*, 2006, **124**, 044904.
249 K. Besteman, K. Van Eijk and S. Lemay, *Nat. Phys.*, 2007, **3**, 641–644.
250 W. M. de Vos and S. Lindhoud, *Adv. Colloid Interface Sci.*, 2019, **274**, 102040.

251 T. T. Nguyen, A. Y. Grosberg and B. I. Shklovskii, *Phys. Rev. Lett.*, 2000, **85**, 1568.
252 A. Y. Grosberg, T. Nguyen and B. Shklovskii, *RMP*, 2002, **74**, 329.
253 V. Perel and B. Shklovskii, *Phys. A*, 1999, **274**, 446–453.
254 J. Mattai and J. C. Kwak, *Macromolecules*, 1986, **19**, 1663–1667.
255 E. Nordmeier and W. Dauwe, *Polym. J.*, 1991, **23**, 1297–1305.
256 T. Tamura, N. Kawabata, S. Kawauchi, M. Satoh and J. Komiyama, *Polym. Int.*, 1998, **46**, 353–356.
257 T. Miyajima, M. Mori, S.-i Ishiguro, K. H. Chung and C. H. Moon, *J. Colloid Interface Sci.*, 1996, **184**, 279–288.
258 T. Miyajima, M. Mori and S.-i Ishiguro, *J. Colloid Interface Sci.*, 1997, **187**, 259–266.
259 Z. Iatridi, G. Bokias and J. Kallitsis, *J. Appl. Polym. Sci.*, 2008, **108**, 769–776.
260 I. Pochard, P. Couchot and A. Foissy, *Colloid Polym. Sci.*, 1998, **276**, 1088–1097.
261 T. Miyajima, *Ion Exchange Solvent Extraction*, 1995, 275–351.
262 I. Pochard, A. Foissy and P. Couchot, *Colloid Polym. Sci.*, 1999, **277**, 818–826.
263 W. R. Archer and M. D. Schulz, *Soft Matter*, 2020, **16**, 8760–8774.
264 S. Lages, R. Michels and K. Huber, *Macromolecules*, 2010, **43**, 3027–3035.
265 A. Kundagrami and M. Muthukumar, *J. Chem. Phys.*, 2008, **128**, 244901.
266 The ion bridging phenomenon has been studied most extensively for polyelectrolyte brushes, see ref. 699–703.
267 Y. Ikeda, M. Beer, M. Schmidt and K. Huber, *Macromolecules*, 1998, **31**, 728–733.
268 S. Lages, P. Lindner, P. Sinha, A. Kiriy, M. Stamm and K. Huber, *Macromolecules*, 2009, **42**, 4288–4299.
269 R. Schweins, P. Lindner and K. Huber, *Macromolecules*, 2003, **36**, 9564–9573.
270 R. Schweins and K. Huber, *Eur. Phys. J. E: Soft Matter Biol. Phys.*, 2001, **5**, 117–126.
271 K. Huber, *J. Phys. Chem.*, 1993, **97**, 9825–9830.
272 G. Goerigk, R. Schweins, K. Huber and M. Ballauff, *EPL*, 2004, **66**, 331.
273 S. Lages, G. Goerigk and K. Huber, *Macromolecules*, 2013, **46**, 3570–3580.
274 R. W. Rosser, N. Nemoto, J. L. Schrag and J. D. Ferry, *J. Polym. Sci., Polym. Phys. Ed.*, 1978, **16**, 1031–1040.
275 The data from ref. 704 are in the semidilute non-entangled regime.
276 R. M. Fuoss, *Science*, 1948, **108**, 545–550.
277 R. M. Fuoss and U. P. Strauss, *Ann. N. Y. Acad. Sci.*, 1949, **51**, 836–851.
278 R. M. Fuoss and G. I. Cathers, *J. Polym. Sci.*, 1949, **4**, 97–120.
279 R. M. Fuoss and W. N. Maclay, *J. Polym. Sci.*, 1951, **6**, 305–317.
280 R. M. Fuoss, *Discuss. Faraday Soc.*, 1951, **11**, 125–134.
281 W. N. Maclay and R. M. Fuoss, *J. Polym. Sci.*, 1951, **6**, 511–521.
282 R. M. Fuoss and D. Edelson, *J. Polym. Sci.*, 1951, **6**, 523–532.
283 U. P. Strauss and R. M. Fuoss, *J. Polym. Sci.*, 1952, **8**, 593–598.
284 T. Alfrey Jr, R. M. Fuoss, H. Morawetz and H. Pinner, *J. Am. Chem. Soc.*, 1952, **74**, 438–441.
285 D. C. Boris and R. H. Colby, *Macromolecules*, 1998, **31**, 5746–5755.
286 C. G. Lopez, R. H. Colby, P. Graham and J. T. Cabral, *Macromolecules*, 2017, **50**, 332–338.
287 U. Lohmander and R. Stromberg, *Makromol. Chem.: Macromol. Chem. Phys.*, 1964, **72**, 143–158.
288 T. Yanaki and M. Yamaguchi, *Chem. Pharm. Bull.*, 1994, **42**, 1651–1654.
289 L. Yuan, T. Dougherty and S. Stivala, *J. Polym. Sci., Part A-2*, 1972, **10**, 171–189.
290 H. Trivedi, C. Patel and R. Patel, *Appl. Macromol. Chem. Phys.*, 1981, **95**, 155–170.
291 P. Liberti and S. Stivala, *J. Polym. Sci., Part B: Polym. Lett.*, 1966, **4**, 137–145.
292 J. R. Schaefgen and C. F. Trivisonno, *J. Am. Chem. Soc.*, 1952, **74**, 2715–2717.
293 Other plots, for example η_{red} *vs.* $c^{-1/2}$ or $\eta_{red}/c^{1/2}$ *vs.* $c^{1/2}$ were also found to work well. A discussion of these can be found in ref. 289–292 and 403.
294 H. Inagaki, H. Sakurai and T. Sasaki, *Bull. Inst. Chem. Res., Kyoto Univ.*, 1956, **34**, 74–86.
295 The appearance of a peak was also noted by Fuoss and Cathers for in 1 mM TBABr solvent media.[278].
296 H. Zhang, H. Zheng, Q. Zhang, J. Wang and M. Konno, *Biopolymers*, 1998, **46**, 395–402.
297 J. Cohen, Z. Priel and Y. Rabin, *J. Chem. Phys.*, 1988, **88**, 7111–7116.
298 J. L. Ganter, M. Milas and M. Rinaudo, *Polymer*, 1992, **33**, 113–116.
299 K. Nishida, K. Kaji, T. Kanaya and N. Fanjat, *Polymer*, 2002, **43**, 1295–1300.
300 Fig. 8 of ref. 322 shows the shear rate dependence of NaPSS with a N = 5900 (×2.4 that of Nishida's sample). We expect $\tau \propto N^3$, so that Nishida's η_{red} data should correspond to values 10–20% lower than the zero shear rate limit. Eqn (36) gives $\dot{\gamma}C \simeq 10^3\ s^{-1}$, which is on the order of the shear rate applied by capillary viscometers.
301 A. Han, V. V. S. Uppala, D. Parisi, C. George, B. J. Dixon, C. D. Ayala, X. Li, L. A. Madsen and R. H. Colby, *Macromolecules*, 2022, **55**, 7148–7160.
302 L. Ghimici and F. Popescu, *Eur. Polym. J.*, 1998, **34**, 13–16.
303 L. Ghimici and E. Avram, *J. Appl. Polym. Sci.*, 2003, **90**, 465–469.
304 B. A. Wolf, *Macromol. Rapid Commun.*, 2007, **28**, 164–170.
305 J. Eckelt, A. Knopf and B. A. Wolf, *Macromolecules*, 2008, **41**, 912–918.
306 A. Eich and B. A. Wolf, *ChemPhysChem*, 2011, **12**, 2786–2790.
307 X. Xiong and B. A. Wolf, *Soft Matter*, 2014, **10**, 2124–2131.
308 L. Ghimici, M. Nichifor, A. Eich and B. A. Wolf, *Carbohydr. Polym.*, 2012, **87**, 405–410.
309 B. A. Wolf, *RSC Adv.*, 2016, **6**, 38004–38011.
310 P. Suresha, M. V. Badiger and B. A. Wolf, *RSC Adv.*, 2015, **5**, 27674–27681.

311 M. V. Badiger, N. R. Gupta, J. Eckelt and B. A. Wolf, *Macromol. Chem. Phys.*, 2008, **209**, 2087–2093.
312 M. Bercea and B. A. Wolf, *Int. J. Biol. Macromol.*, 2019, **140**, 661–667.
313 A. Chatterjee and B. Das, *Carbohydr. Polym.*, 2013, **98**, 1297–1303.
314 A. Banerjee, R. De and B. Das, *Carbohydr. Polym.*, 2022, **277**, 118855.
315 J. Cohen and Z. Priel, *J. Chem. Phys.*, 1990, **93**, 9062–9068.
316 M. Kato, T. Nakagawa and H. Akamatu, *Bull. Chem. Soc. Jpn.*, 1960, **33**, 322–329.
317 J. Yamanaka, H. Araie, H. Matsuoka, H. Kitano, N. Ise, T. Yamaguchi, S. Saeki and M. Tsubokawa, *Macromolecules*, 1991, **24**, 6156–6159.
318 H. Vink, *Polymer*, 1992, **33**, 3711–3716.
319 H. Vink, *J. Chem. Soc., Faraday Trans. 1*, 1987, **83**, 801–811.
320 S. Batzill, R. Luxemburger, R. Deike and R. Weber, *Eur. Phys. J. B*, 1998, **1**, 491–501.
321 H. Vink, *Macromol. Chem. Phys.*, 1970, **131**, 133–145.
322 J. Yamanaka, H. Matsuoka, H. Kitano, M. Hasegawa and N. Ise, *J. Am. Chem. Soc.*, 1990, **112**, 587–592.
323 J. Yamanaka, S. Yamada, N. Ise and T. Yamaguchi, *J. Polym. Sci., Part B: Polym. Phys.*, 1995, **33**, 1523–1526.
324 H. Eisenberg, *J. Polym. Sci.*, 1957, **23**, 579–599.
325 Note that for sodium hyaluronate, which is a co-polymer of D-glucuronic acid and *N*-acetyl-D-glucosamine we express the concentration in units of saccharide units, *i.e.* each chain segment with a length of $\simeq 5$ Å is counted as a monomer. This differs from the more usual convention of expressing molar concentration in terms of disaccharide units.
326 D. Ray, R. De and B. Das, *J. Chem. Thermodyn.*, 2016, **101**, 227–235.
327 T. J. Podlas and P. Ander, *Macromolecules*, 1970, **3**, 154–157.
328 R. L. Cleland, *Biopolymers*, 1968, **6**, 1519–1529.
329 M. Rinaudo and M. Milas, *Chem. Phys. Lett.*, 1976, **41**, 456–459.
330 D. Truzzolillo, F. Bordi, C. Cametti and S. Sennato, *Phys. Rev. E: Stat., Nonlinear, Soft Matter Phys.*, 2009, **79**, 011804.
331 J. A. V. Butler, A. Robins and K. Shooter, *Proc. R. Soc. London, Ser. A Sci.*, 1957, **241**, 299–310.
332 I. Roure, M. Rinaudo, M. Milas and E. Frollini, *Polymer*, 1998, **39**, 5441–5445.
333 H. Terayama, *J. Polym. Sci.*, 1956, **19**, 181–198.
334 H. Terayama, *J. Polym. Sci.*, 1955, **15**, 575–590.
335 H. Fujita and T. Homma, *J. Colloid Sci.*, 1954, **9**, 591–601.
336 H. Fujita and T. Homma, *J. Polym. Sci.*, 1955, **15**, 277–295.
337 I. Roure, M. Rinaudo and M. Milas, *Bunsen-Ges. Phys. Chem., Ber.*, 1996, **100**, 703–706.
338 M. Rinaudo, I. Roure, M. Milas and A. Malovikova, *Int. J. Polym. Anal. Charact.*, 1997, **4**, 57–69.
339 H. Zhang, H. Wang, J. Wang, R. Guo and Q. Zhang, *Polym. Adv. Technol.*, 2001, **12**, 740–745.
340 J. Cohen and Z. Priel, *Macromolecules*, 1989, **22**, 2356–2358.
341 W. Essafi, N. Haboubi, C. Williams and F. Boue, *J. Phys. Chem. B*, 2011, **115**, 8951–8960.
342 J. Yang, N. Liu, D. Yu, C. Peng, H. Liu, Y. Hu and J. Jiang, *Ind. Eng. Chem. Res.*, 2005, **44**, 8120–8126.
343 W. F. Reed, *J. Chem. Phys.*, 1994, **101**, 2515–2521.
344 M. Antonietti, A. Briel and S. Forster, *J. Chem. Phys.*, 1996, **105**, 7795–7807.
345 K. Nishida, K. Kaji and T. Kanaya, *Polymer*, 2001, **42**, 8657–8662.
346 B. Ashok and M. Muthukumar, *J. Phys. Chem. B*, 2009, **113**, 5736–5745.
347 R. Borsali, T. Vilgis and M. Benmouna, *Macromolecules*, 1992, **25**, 5313–5317.
348 W. Hess and R. Klein, *Adv. Phys.*, 1983, **32**, 173–283.
349 S. Nojd, P. Holmqvist, N. Boon, M. Obiols-Rabasa, P. S. Mohanty, R. Schweins and P. Schurtenberger, *Soft Matter*, 2018, **14**, 4150–4159.
350 C. G. Lopez, T. Lohmeier, J. E. Wong and W. Richtering, *J. Colloid Interface Sci.*, 2020, **558**, 200–210.
351 A. Fernandez-Nieves, A. Fernandez-Barbero, B. Vincent and F. De Las Nieves, *Macromolecules*, 2000, **33**, 2114–2118.
352 D. Capriles-Gonzalez, B. Sierra-Martin, A. Fernandez-Nieves and A. Fernandez-Barbero, *J. Phys. Chem. B*, 2008, **112**, 12195–12200.
353 T. Lopez-Leon and A. Fernandez-Nieves, *Phys. Rev. E: Stat., Nonlinear, Soft Matter Phys.*, 2007, **75**, 011801.
354 A. Fernandez-Nieves, A. Fernandez-Barbero, B. Vincent and F. De las Nieves, *J. Chem. Phys.*, 2003, **119**, 10383–10388.
355 A. A. Polotsky, F. A. Plamper and O. V. Borisov, *Macromolecules*, 2013, **46**, 8702–8709.
356 R. Borsali, T. A. Vilgis and M. Benmouna, *Macromol. Theory Simul.*, 1994, **3**, 73–77.
357 F. Akkerman, D. Pals and J. Hermans, *Recl. Trav. Chim. Pays-Bas*, 1952, **71**, 56–63.
358 M. Moan and C. Wolff, *Eur. Polym. J.*, 1973, **9**, 1085–1093.
359 W. Brown and D. Henley, *Macromol. Chem. Phys.*, 1964, **79**, 68–88.
360 W. Brown, D. Henley and J. Ohman, *Ark. Kemi*, 1964, **22**, 189–206.
361 H. Eisenberg, *J. Polym. Sci.*, 1957, **25**, 257–271.
362 R. Stromberg, *Non-Newtonian Flow of Dilute Polymethacrylic Acid Solutions at Different Degrees of Neutralization and Ionic Strengths*, Uppsala Univ. (Sweden) Inst. of Physical Chemistry Technical Report, 1966.
363 S. Pan, D. A. Nguyen, B. Dunweg, P. Sunthar, T. Sridhar and J. Ravi Prakash, *J. Rheol.*, 2018, **62**, 845–867.
364 H. Dakhil, S. Basu, S. Steiner, Y. Gerlach, A. Soller, S. Pan, N. Germann, M. Leidenberger, B. Kappes and A. Wierschem, *J. Rheol.*, 2021, **65**, 159–169.
365 M. Fixman, *J. Chem. Phys.*, 1966, **45**, 793–803.
366 T. Kotaka, H. Suzuki and H. Inagaki, *J. Chem. Phys.*, 1966, **45**, 2770–2773.
367 I. Noda, Y. Yamada and M. Nagasawa, *J. Phys. Chem.*, 1968, **72**, 2890–2898.
368 H. Suzuki, T. Kotaka and H. Inagaki, *J. Chem. Phys.*, 1969, **51**, 1279–1285.
369 R. G. Larson, *J. Rheol.*, 2005, **49**, 1–70.
370 J. G. Kirkwood and R. J. Plock, *J. Chem. Phys.*, 1956, **24**, 665–669.

371 N. Saito and M. Sugita, *J. Phys. Soc. Jpn.*, 1952, **7**, 554–559.
372 H. A. Scheraga, *J. Chem. Phys.*, 1955, **23**, 1526–1532.
373 J. T. Yang, *J. Am. Chem. Soc.*, 1958, **80**, 1783–1788.
374 D. Shogin and P. A. Amundsen, *Phys. Fluids*, 2020, **32**, 063101.
375 R. Pamies, J. H. Cifre and J. G. De La Torre, *J. Polym. Sci., Part B: Polym. Phys.*, 2007, **45**, 1–9.
376 S. Pattanayek and J. R. Prakash, *Macromolecules*, 2008, **41**, 2260–2270.
377 S. P. Singh and R. G. Winkler, *J. Rheol.*, 2020, **64**, 1121–1131.
378 K. Jayasree, R. Kumar Manna, D. Banerjee and P. Kumar, *J. Chem. Phys.*, 2013, **139**, 224902.
379 C. Stoltz, J. J. de Pablo and M. D. Graham, *J. Chem. Phys.*, 2007, **126**, 124906.
380 K. Zheng, K. Chen, W. Ren, J. Yang and J. Zhao, *Macromolecules*, 2022, **55**, 1647–1656.
381 O. Borisov, A. Darinskii and E. Zhulina, *Macromolecules*, 1995, **28**, 7180–7187.
382 R. Pamies, J. H. Cifre and J. G. De La Torre, *J. Polym. Sci., Part B: Polym. Phys.*, 2007, **45**, 714–722.
383 G. Xu, S. Luo, Q. Yang, J. Yang and J. Zhao, *J. Chem. Phys.*, 2016, **145**, 144903.
384 H. Yamakawa and T. Yoshizaki, *Macromolecules*, 1980, **13**, 633–643.
385 G. Sitaramaiah and D. Goring, *J. Polym. Sci.*, 1962, **58**, 1107–1131.
386 G. Xu, J. Yang and J. Zhao, *J. Chem. Phys.*, 2018, **149**, 163329.
387 A similar decrease in $[\eta]$ can be observed for NaPVS in DI water and 10^{-4} M NaCl in Fig. 4c.
388 D. Izzo, M. Cloitre and L. Leibler, *Soft Matter*, 2014, **10**, 1714–1722.
389 N. Imai and K. Gekko, *Biophys. Chem.*, 1991, **41**, 31–40.
390 K. Kaji, H. Urakawa, T. Kanaya and R. Kitamaru, *J. Phys.*, 1988, **49**, 993–1000.
391 C. G. Lopez and W. Richtering, *J. Chem. Phys.*, 2018, **148**, 244902.
392 J. Combet, F. Isel, M. Rawiso and F. Boue, *Macromolecules*, 2005, **38**, 7456–7469.
393 J. Combet, M. Rawiso, C. Rochas, S. Hoffmann and F. Boue, *Macromolecules*, 2011, **44**, 3039–3052.
394 K. Nishida, K. Kaji and T. Kanaya, *J. Chem. Phys.*, 2001, **114**, 8671–8677.
395 M. Drifford and J. P. Dalbiez, *J. Phys. Chem.*, 1984, **88**, 5368–5375.
396 S. Forster, M. Schmidt and M. Antonietti, *Polymer*, 1990, **31**, 781–792.
397 C. G. Lopez, *Macromolecules*, 2019, **52**, 9409–9415.
398 M.-W. Kim and D. Peiffer, *EPL*, 1988, **5**, 321.
399 M. Matsumoto and T. Eguchi, *J. Polym. Sci.*, 1957, **26**, 393–396.
400 Q. Ying and B. Chu, *Macromolecules*, 1987, **20**, 362–366.
401 S. S. Vadodaria and R. J. English, *Cellulose*, 2016, **23**, 1107–1121.
402 Z.-G. Wang, *Macromolecules*, 2017, **50**, 9073–9114.
403 C. G. Lopez and W. Richtering, *J. Phys. Chem. B*, 2019, **123**, 5626–5634.
404 C. G. Lopez, *ACS Macro Lett.*, 2019, **8**, 979–983.
405 A. Han, *PhD thesis*, Penn State, 2002.
406 C. G. Lopez, *J. Rheol.*, 2020, **64**, 191–204.
407 We assume a Kuhn segment of 2 nm and three Kuhn segments per chains, and calculate ξ_{el} assuming no excluded volume inside the electrostatic blob.
408 Note that the $\eta_{sp}(c^*) = 1$ criterion is expected to fail for short oligomeric chains, where, based on the general trends observed for electrolytes,705 the $\eta_{sp}(c^*) \simeq 1$ point is reached well below the 'overlap' point.
409 J. A. Bollinger, G. S. Grest, M. J. Stevens and M. Rubinstein, *Macromolecules*, 2021, **54**, 10068–10073.
410 M. Oostwal, M. Blees, J. De Bleijser and J. Leyte, *Macromolecules*, 1993, **26**, 7300–7308.
411 U. P. Strauss and R. M. Fuoss, *J. Polym. Sci.*, 1949, **4**, 457–472.
412 Q. Liao, A. V. Dobrynin and M. Rubinstein, *Macromolecules*, 2003, **36**, 3399–3410.
413 C. Tsimpris, B. Suryanarayanan and K. Mayhan, *J. Polym. Sci., Part A-2*, 1972, **10**, 1837–1839.
414 DMF is a somewhat unusual solvent polystyrene, see ref. 559 and 706 and references therein.
415 Y. Matsushita, K. Shimizu, Y. Nakao, H. Choshi, I. Noda and M. Nagasawa, *Polym. J.*, 1986, **18**, 361–366.
416 M. Matsumoto and T. Eguchi, *J. Polym. Sci.*, 1957, **23**, 617–634.
417 We are currently conducting small angle X-ray/neutron scattering experiments for PC_4-TFSI in various solvents in order to evaluate the local chain conformation in a given solvent. The preliminary results found the correlation length scaled as $\xi \propto c^{0.5}$ over a wide monomer concentration (c) range. The observed scaling is similar to that for polyelectrolytes in either theta or good solvents. The data will be published elsewhere.
418 S. Dou and R. H. Colby, *Macromolecules*, 2008, **41**, 6505–6510.
419 F. Bordi, C. Cametti, J. Tan, D. Boris, W. Krause, N. Plucktaveesak and R. Colby, *Macromolecules*, 2002, **35**, 7031–7038.
420 E. L. Bennett, I. Calisir, X. Yang, Y. Huang and J. Xiao, *J. Phys. Chem. C*, 2023, **127**, 18669–18677.
421 S. Dou, *Synthesis and characterization of ion-containing polymers*, PhD thesis, Pennsylvania State University, 2007.
422 A. Sehgal and T. A. Seery, *Macromolecules*, 1998, **31**, 7340–7346.
423 Z. Alexandrowicz, *J. Polym. Sci.*, 1959, **40**, 91–106.
424 W. Essafi, F. Lafuma, D. Baigl and C. Williams, *EPL*, 2005, **71**, 938.
425 E. Raspaud, M. Da Conceicao and F. Livolant, *Phys. Rev. Lett.*, 2000, **84**, 2533.
426 P. L. Hansen, R. Podgornik and V. A. Parsegian, *Phys. Rev. E: Stat., Nonlinear, Soft Matter Phys.*, 2001, **64**, 021907.
427 M. Muthukumar, *J. Chem. Phys.*, 2012, **137**, 034902.
428 S. Saha, K. Fischer, M. Muthukumar and M. Schmidt, *Macromolecules*, 2013, **46**, 8296–8303.
429 S. Saha, *PhD thesis*, Mainz, Univ., Diss., 2012, 2013.
430 M. Nagasawa and I. Kagawa, *J. Polym. Sci.*, 1957, **25**, 61–76.
431 T. J. Podlas and P. Ander, *Macromolecules*, 1969, **2**, 432–436.
432 M. Rinaudo and M. Milas, *J. Polym. Sci., Polym. Chem. Ed.*, 1974, **12**, 2073–2081.

433 J. Tan and P. Marcus, *J. Polym. Sci., Polym. Phys. Ed.*, 1976, **14**, 239–250.
434 G. Pass, G. Phillips and D. Wedlock, *Macromolecules*, 1977, **10**, 197–201.
435 S. Miura, M. Satoh and J. Komiyama, *Polymer*, 1996, **37**, 1641–1646.
436 H. Maki and T. Miyajima, *Macromolecules*, 2011, **44**, 5027–5035.
437 F. Bordi, R. Colby, C. Cametti, L. De Lorenzo and T. Gili, *J. Phys. Chem. B*, 2002, **106**, 6887–6893.
438 T. Vuletić, S. D. Babić, D. Grgičin, D. Aumiler, J. Radler, F. Livolant and S. Tomić, *Phys. Rev. E: Stat., Nonlinear, Soft Matter Phys.*, 2011, **83**, 041803.
439 R. Buchner, G. T. Hefter and P. M. May, *J. Phys. Chem. A*, 1999, **103**, 1–9.
440 J. R. Huizenga, P. F. Grieger and F. T. Wall, *J. Am. Chem. Soc.*, 1950, **72**, 4228–4232.
441 M. Nagasawa, I. Noda, T. Takahashi and N. Shimamoto, *J. Phys. Chem.*, 1972, **76**, 2286–2294.
442 A. Matsumoto and A. Q. Shen, *Soft Matter*, 2022, **18**, 4197–4204.
443 P. Rodič, M. Bratuša, M. Lukšič, V. Vlachy and B. Hribar-Lee, *Colloids Surf., A*, 2013, **424**, 18–25.
444 T. A. Waigh, R. Ober, C. E. Williams and J.-C. Galin, *Macromolecules*, 2001, **34**, 1973–1980.
445 G. R. Leader and J. F. Gormley, *J. Am. Chem. Soc.*, 1951, **73**, 5731–5733.
446 S. J. Bass, W. I. Nathan, R. M. Meighan and R. H. Cole, *J. Phys. Chem.*, 1964, **68**, 509–515.
447 A. V. Dobrynin and M. Rubinstein, *Macromolecules*, 1999, **32**, 915–922.
448 W. Essafi, W. Raissi, A. Abdelli and F. Boue, *J. Phys. Chem. B*, 2014, **118**, 12271–12281.
449 W. Essafi, A. Abdelli, G. Bouajila and F. Boue, *J. Phys. Chem. B*, 2012, **116**, 13525–13537.
450 A. Chremos and J. F. Douglas, *J. Chem. Phys.*, 2018, **149**, 163305.
451 A. Chremos and J. F. Douglas, *Soft Matter*, 2016, **12**, 2932–2941.
452 A. Chremos and J. F. Douglas, *J. Chem. Phys.*, 2017, **147**, 241103.
453 A. Chremos and J. F. Douglas, *Gels*, 2018, **4**, 20.
454 N. T. Klooster, F. Van der Touw and M. Mandel, *Macromolecules*, 1984, **17**, 2087–2093.
455 G. Gebel, *Macromolecular Complexes in Chemistry and Biology*, 1994, p. 329.
456 A. Pedley, J. Higgins, D. Peiffer and W. Burchard, *Macromolecules*, 1990, **23**, 1434–1437.
457 A. Young, J. Higgins, D. Peiffer and A. Rennie, *Polymer*, 1995, **36**, 691–697.
458 R. Lundberg and H. Makowski, *J. Polym. Sci., Polym. Phys. Ed.*, 1980, **18**, 1821–1836.
459 P. K. Agarwal, R. T. Garner and W. W. Graessley, *J. Polym. Sci., Part B: Polym. Phys.*, 1987, **25**, 2095–2111.
460 D. Kawaguchi, S. Kawauchi, M. Satoh and J. Komiyama, *Polymer*, 1998, **39**, 1387–1392.
461 R. Weiss, J. Fitzgerald, H. Frank and B. Chadwick, *Macromolecules*, 1986, **19**, 2085–2087.
462 S. Nomula and S. L. Cooper, *Macromolecules*, 2001, **34**, 2653–2659.
463 Z. Zhang, C. Liu, X. Cao, J.-H. H. Wang, Q. Chen and R. H. Colby, *Macromolecules*, 2017, **50**, 963–971.
464 E. Penzel and N. Goetz, *Appl. Macromol. Chem. Phys.*, 1990, **178**, 191–200.
465 S. Newman, W. R. Krigbaum, C. Laugier and P. J. Flory, *J. Polym. Sci.*, 1954, **14**, 451–462.
466 T. Ono, T. Sugimoto, S. Shinkai and K. Sada, *Nat. Mater.*, 2007, **6**, 429–433.
467 T. Ono, T. Sugimoto, S. Shinkai and K. Sada, *Adv. Funct. Mater.*, 2008, **18**, 3936–3940.
468 T. Ono, S. Shinkai and K. Sada, *Soft Matter*, 2008, **4**, 748–750.
469 K. Iseda, M. Ohta, T. Ono and K. Sada, *Soft Matter*, 2011, **7**, 5938–5940.
470 T. Ono, M. Ohta, K. Iseda and K. Sada, *Soft Matter*, 2012, **8**, 3700–3704.
471 D. Kawaguchi and M. Satoh, *Macromolecules*, 1999, **32**, 7828–7835.
472 E. Nordmeier and W. Dauwe, *Polym. J.*, 1992, **24**, 229–238.
473 E. Nordmeier, *Polym. J.*, 1993, **25**, 1–17.
474 E. Nordmeier, *Polym. J.*, 1993, **25**, 19–30.
475 A. Raziel and H. Eisenberg, *Isr. J. Chem.*, 1973, **11**, 183–199.
476 N. Borochov and H. Eisenberg, *Macromolecules*, 1994, **27**, 1440–1445.
477 R. M. Peitzsch, M. J. Burt and W. F. Reed, *Macromolecules*, 1992, **25**, 806–815.
478 A. Bose, J. Rollings, J. Caruthers, M. Okos and G. Tsao, *J. Appl. Polym. Sci.*, 1982, **27**, 795–810.
479 R. Davis and W. Russel, *Macromolecules*, 1987, **20**, 518–525.
480 R. Brussau, N. Goetz, W. Machtle and J. Stolting, *Tenside, Surfactants, Deterg.*, 1991, **28**, 396–406.
481 H. Eisenberg, *Q. Rev. Biophys.*, 1981, **14**, 141–172.
482 H. Yamakawa, *Macromolecules*, 1992, **25**, 1912–1916.
483 K. Tsutsumi and T. Norisuye, *Polym. J.*, 1998, **30**, 345–349.
484 T. Sato, T. Norisuye and H. Fujita, *Polym. J.*, 1984, **16**, 341–350.
485 T. Sato, T. Norisuye and H. Fujita, *Macromolecules*, 1984, **17**, 2696–2700.
486 J. Tan and S. Gasper, *J. Polym. Sci., Polym. Phys. Ed.*, 1975, **13**, 1705–1719.
487 F. Abe, Y. Einaga, T. Yoshizaki and H. Yamakawa, *Macromolecules*, 1993, **26**, 1884–1890.
488 K. Huber, S. Bantle, P. Lutz and W. Burchard, *Macromolecules*, 1985, **18**, 1461–1467.
489 Y. Einaga, F. Abe and H. Yamakawa, *Macromolecules*, 1993, **26**, 6243–6250.
490 P. Balding, R. Borrelli, R. Volkovinsky and P. S. Russo, *Macromolecules*, 2022, **55**, 1747–1762.
491 Z. Luo and G. Zhang, *Macromolecules*, 2010, **43**, 10038–10044.
492 A. K. Sen, S. Roy and V. A. Juvekar, *Polym. Int.*, 2007, **56**, 167–174.

493 A. K. Sen, *PhD thesis*, Indian Institute of Technology, Bombay (India), 2005.
494 Extrapolating the R_H data of Serhatli *et al.*[495] for ≃85% sulfonated PSS in 4.17 M to $R_H^2/N \simeq 5$ Å^2 yields a theta temperature for their samples of 35–40°, consistent with a 1–2 °C shift of the theta point per percentage point of sulfonation.
495 E. Serhatli, M. Serhatli, B. M. Baysal and F. E. Karasz, *Polymer*, 2002, **43**, 5439–5445.
496 L. Wang and H. Yu, *Macromolecules*, 1988, **21**, 3498–3501.
497 G. M. Pavlov, O. V. Okatova, A. S. Gubarev, I. I. Gavrilova and E. F. Panarin, *Macromolecules*, 2014, **47**, 2748–2758.
498 A. Raziel, *Excluded volume study of polyelectrolyte solutions: Potassium polystyrenesulfonate*, PhD thesis, The Weizmann Institute of Science (Israel), 1971.
499 R. Schweins, J. Hollmann and K. Huber, *Polymer*, 2003, **44**, 7131–7141.
500 J. Tanahatoe and M. Kuil, *Macromolecules*, 1997, **30**, 6102–6106.
501 N. Plucktaveesak, A. J. Konop and R. H. Colby, *J. Phys. Chem. B*, 2003, **107**, 8166–8171.
502 N. Borochov and H. Eisenberg, *Biopolymers*, 1984, **23**, 1757–1769.
503 Z. Kam, N. Borochov and H. Eisenberg, *Biopolymers*, 1981, **20**, 2671–2690.
504 S. P. Gasper and J. S. Tan, Water-Soluble Polymers: Proceedings of a Symposium held by the American Chemical Society, Division of Organic Coatings and Plastics Chemistry, in New York City on August 30–31, 1972, 1973, pp. 387–400.
505 J. Tan and S. Gasper, *Macromolecules*, 1973, **6**, 741–746.
506 J. Tan and S. Gasper, *J. Polym. Sci., Polym. Phys. Ed.*, 1974, **12**, 1785–1804.
507 H. Edelhoch and J. Bateman, *J. Am. Chem. Soc.*, 1957, **79**, 6093–6100.
508 R. B. Hawkins and A. Holtzer, *Macromolecules*, 1972, **5**, 294–301.
509 H. Ochiai, M. Handa, H. Matsumoto, T. Moriga and I. Murakami, *Macromol. Chem. Phys.*, 1985, **186**, 2547–2556.
510 N. S. Schneider and P. Doty, *J. Phys. Chem.*, 1954, **58**, 762–769.
511 H. Zhang, H. Zheng, Q. Zhang, S. Gao and J. Wang, *Polym. Adv. Technol.*, 1997, **8**, 722–726.
512 K. Vanneste, D. Slootmaekers and H. Reynaers, *Food Hydrocolloids*, 1996, **10**, 99–107.
513 D. Pals and J. Hermans, *Recl. Trav. Chim. Pays-Bas*, 1952, **71**, 458–467.
514 T. Nicolai and M. Mandel, *Macromolecules*, 1989, **22**, 438–444.
515 E. Sobel and J. Harpst, *Biopolymers*, 1991, **31**, 1559–1564.
516 K. A. Strand, A. Boe, P. Dalberg, T. Sikkeland and O. Smidsroed, *Macromolecules*, 1982, **15**, 570–579.
517 I. Morfin, W. F. Reed, M. Rinaudo and R. Borsali, *J. Phys. II*, 1994, **4**, 1001–1019.
518 L. Fisher, A. Sochor and J. Tan, *Macromolecules*, 1977, **10**, 949–954.
519 E. Daniel and Z. Alexandrowicz, *Biopolymers*, 1963, **1**, 473–495.
520 J. Tanahatoe and M. Kuil, *J. Phys. Chem. A*, 1997, **101**, 8389–8394.
521 R. Smits, M. Kuil and M. Mandel, *Macromolecules*, 1993, **26**, 6808–6816.
522 E. Buhler and M. Rinaudo, *Macromolecules*, 2000, **33**, 2098–2106.
523 E. Buhler, O. Guetta and M. Rinaudo, *Int. J. Polym. Anal. Charact.*, 2001, **6**, 155–175.
524 T. Nicolai and M. Mandel, *Macromolecules*, 1989, **22**, 2348–2356.
525 C. Pyun and M. Fixman, *J. Chem. Phys.*, 1964, **41**, 937–944.
526 H. Yamakawa, *J. Chem. Phys.*, 1962, **36**, 2995–3001.
527 M. Nagasawa and Y. Eguchi, *J. Phys. Chem.*, 1967, **71**, 880–888.
528 J. Si, N. Hao, M. Zhang, S. Cheng, A. Liu, L. Li and X. Ye, *ACS Macro Lett.*, 2019, **8**, 730–736.
529 Z. Luo and G. Zhang, *Polymer*, 2011, **52**, 5846–5850.
530 P. M. Budd, *Polymer*, 1985, **26**, 1519–1522.
531 F. Abe, Y. Einaga and H. Yamakawa, *Macromolecules*, 1993, **26**, 1891–1897.
532 H. Zhou, G. Song, Y. X. Zhang, R. Dieing, L. Ma and L. Haeussling, *Chin. J. Chem.*, 2000, **18**, 322–327.
533 U. P. Strauss, N. L. Gershfeld and E. H. Crook, *J. Phys. Chem.*, 1956, **60**(5), 577–584.
534 H. Inoue, *Kolloid-Zeitschrift und Zeitschrift fur Polymere*, 1964, **195**, 102–110.
535 G. Pavlov and A. Gosteva, *Polym. Sci., Ser. A*, 2022, **64**, 586–590.
536 G. M. Pavlov, A. A. Gosteva, O. V. Okatova, O. A. Dommes, I. I. Gavrilova and E. F. Panarin, *Polym. Chem.*, 2021, **12**, 2325–2334.
537 I. Noda, T. Tsuge and M. Nagasawa, *J. Phys. Chem.*, 1970, **74**, 710–719.
538 T. Kato, T. Tokuya, T. Nozaki and A. Takahashi, *Polymer*, 1984, **25**, 218–224.
539 P. J. Kay and F. Treloar, *Macromol. Chem. Phys.*, 1974, **175**, 3207–3223.
540 A. Takahashi and M. Nagasawa, *J. Am. Chem. Soc.*, 1964, **86**, 543–548.
541 G. Staikos and G. Bokias, *Polym. Int.*, 1993, **31**, 385–389.
542 G. Bokias and G. Staikos, *Polymer*, 1995, **36**, 2079–2082.
543 M. Sakurai, T. Imai, F. Yamashita, K. Nakamura and T. Komatsu, *et al.*, *Polym. J.*, 1993, **25**, 1247–1255.
544 These relationships are extracted from Fig. 1 of ref. 11.
545 W. F. Reed, S. Ghosh, G. Medjahdi and J. Francois, *Macromolecules*, 1991, **24**, 6189–6198.
546 W. F. Reed, Results on Polyelectrolyte Conformations, Diffusion, and Interparticle Interactions and Correlations, *Macro-ion Characterization*, ACS Symposium Series, ACS Publications, 1994, ch. 23, vol. 548, pp. 297–314, DOI: 10.1021/bk-1994-0548.ch023.
547 K. Kamide, A. Kataoka and T. Kawai, *Macromol. Chem. Phys.*, 1970, **139**, 221–253.
548 S. Arichi, *Bull. Chem. Soc. Jpn.*, 1966, **39**, 439–446.
549 S. Arichi, H. Matsuura, Y. Tanimoto and H. Murata, *Bull. Chem. Soc. Jpn.*, 1966, **39**, 434–439.

550 For example water is a non-solvent for P2VP while methanol and 1-propanol are good solvents. We are unable to find references for NMF and formamide.
551 T. Orofino, *Recl. Trav. Chim. Pays-Bas*, 1959, **78**, 434–439.
552 T. Orofino and P. Flory, *J. Phys. Chem.*, 1959, **63**, 283–290.
553 Z. Alexandrowicz, *J. Polym. Sci.*, 1962, **56**, 115–132.
554 K. McCarthy, C. Burkhardt and D. Parazak, *J. Appl. Polym. Sci.*, 1987, **33**, 1699–1714.
555 S. Ghosh, X. Li, C. E. Reed and W. F. Reed, *Biopolymers*, 1990, **30**, 1101–1112.
556 C. E. Reed and W. F. Reed, *J. Chem. Phys.*, 1991, **94**, 8479–8486.
557 N. Mizukoshi and T. Norisuye, *Polym. Bull.*, 1998, **40**, 555–562.
558 W. Stockmayer and M. Fixman, *J. Polym. Sci., Part C: Polym. Symp.*, 1963, 137–141.
559 M. Bohdanecky and D. Berek, *Die Makromolekulare Chemie, Rapid Communications*, 1985, **6**, 275–280.
560 S. Bushin, V. Tsvetkov, Y. B. Lysenko and V. Yemel'Yanov, *Polym. Sci. USSR*, 1981, **23**, 2705–2715.
561 F. Abe, Y. Einaga and H. Yamakawa, *Macromolecules*, 1994, **27**, 3262–3271.
562 An exception to this are the A_2 results for NaPSS and NaPAMS at low N. Their unusual behaviour should be validated by further experimental work.
563 C. G. Lopez, A. Scotti, M. Brugnoni and W. Richtering, *Macromol. Chem. Phys.*, 2019, **220**, 1800421.
564 T. C. Laurent, M. Ryan and A. Pietruszkiewicz, *Biochem. Biophys. Acta*, 1960, **42**, 476–485.
565 R. Takahashi, K. Kubota, M. Kawada and A. Okamoto, *Biopolymers*, 1999, **50**, 87–98.
566 R. L. Cleland and J. L. Wang, *Biopolymers*, 1970, **9**, 799–810.
567 R. L. Cleland, *Biopolymers*, 1984, **23**, 647–666.
568 E. Fouissac, M. Milas, M. Rinaudo and R. Borsali, *Macromolecules*, 1992, **25**, 5613–5617.
569 The fits by Tsutsumi and Norisuye,[483] whose best-fit parameters for the l_P, B, M_L and d we adopt, were carried out using the data from ref. 111 and 483 only. The other datasets included in Fig. 25, which extend the molar mass range, are in excellent agreement with their calculation.
570 A. Khokhlov and K. Khachaturian, *Polymer*, 1982, **23**, 1742–1750.
571 T. Sato, S. Kojima, T. Norisuye and H. Fujita, *Polym. J.*, 1984, **16**, 423–429.
572 A. Gubarev, J.-M. Y. Carrillo and A. V. Dobrynin, *Macromolecules*, 2009, **42**, 5851–5860.
573 M. Manghi and R. R. Netz, *Eur. Phys. J. E: Soft Matter Biol. Phys.*, 2004, **14**, 67–77.
574 M. Ullner and C. E. Woodward, *Macromolecules*, 2002, **35**, 1437–1445.
575 H.-P. Hsu, W. Paul and K. Binder, *Macromolecules*, 2010, **43**, 3094–3102.
576 H.-P. Hsu, W. Paul and K. Binder, *EPL*, 2010, **92**, 28003.
577 P. Bacova, P. Košovan, F. Uhlik, J. Kuldova, Z. Limpouchova and K. Prochazka, *Eur. Phys. J. E: Soft Matter Biol. Phys.*, 2012, **35**, 1–10.
578 M. Kurata and W. H. Stockmayer, *Fortschritte der Hochpolymeren-Forschung*, Springer, 2006, pp. 196–312.
579 J. Lindner, W. Wilson and J. Mays, *Macromolecules*, 1988, **21**, 3304–3312.
580 K. Venkataswamy, A. Jamieson and R. Petschek, *Macromolecules*, 1986, **19**, 124–133.
581 B. Dunweg, D. Reith, M. Steinhauser and K. Kremer, *J. Chem. Phys.*, 2002, **117**, 914–924.
582 M. L. Mansfield and J. F. Douglas, *Phys. Rev. E: Stat., Nonlinear, Soft Matter Phys.*, 2010, **81**, 021803.
583 F. Vargas-Lara, M. L. Mansfield and J. F. Douglas, *J. Chem. Phys.*, 2017, **147**, 014903.
584 T. Konishi, T. Yoshizaki and H. Yamakawa, *Macromolecules*, 1991, **24**, 5614–5622.
585 K. S. Kumar and J. R. Prakash, *Macromolecules*, 2003, **36**, 7842–7856.
586 H. Fujita, *Macromolecules*, 1988, **21**, 179–185.
587 Y. Tsunashima, *Polym. J.*, 1992, **24**, 433–436.
588 Y. Oono and M. Kohmoto, *J. Chem. Phys.*, 1983, **78**, 520–528.
589 L. Fetters, N. Hadjichristidis, J. Lindner and J. Mays, *J. Phys. Chem. Ref. Data*, 1994, **23**, 619–640.
590 H. Yamakawa, F. Abe and Y. Einaga, *Macromolecules*, 1993, **26**, 1898–1904.
591 H. Yamakawa, *Modern theory of polymer solutions*, Harper & Row, 1971.
592 K. Huber, W. Burchard and A. Z. Akcasu, *Macromolecules*, 1985, **18**, 2743–2747.
593 A. Z. Akcasu, *Polymer*, 1981, **22**, 1169–1180.
594 A. Z. Akcasu and M. Benmouna, *Macromolecules*, 1978, **11**, 1193–1198.
595 H. Murakami, T. Norisuye and H. Fujita, *Macromolecules*, 1980, **13**, 345–352.
596 N. Khasat, R. W. Pennisi, N. Hadjichristidis and L. J. Fetters, *Macromolecules*, 1988, **21**, 1100–1106.
597 J. Roovers, N. Hadjichristidis and L. J. Fetters, *Macromolecules*, 1983, **16**, 214–220.
598 A. Han and R. H. Colby, *Macromolecules*, 2021, **54**, 1375–1387.
599 T. Arai, F. Abe, T. Yoshizaki, Y. Einaga and H. Yamakawa, *Macromolecules*, 1995, **28**, 3609–3616.
600 J. Rauch and W. Kohler, *J. Chem. Phys.*, 2003, **119**, 11977–11988.
601 T. Yamada, T. Yoshizaki and H. Yamakawa, *Macromolecules*, 1992, **25**, 377–383.
602 J. Szydlowski and W. A. Van Hook, *Macromolecules*, 1998, **31**, 3266–3274.
603 W. Burchard and W. Richtering, *Dynamic light scattering from polymer solutions*, Springer, 1989, pp. 151–163.
604 W. Burchard, *Makromolekulare Chemie*, Macromolecular Symposia, 1988, pp. 1–35.
605 M. Rubinstein, *J. Polym. Sci., Part B: Polym. Phys.*, 2010, **48**, 2548–2551.
606 P.-G. De Gennes, *Scaling concepts in polymer physics*, Cornell University Press, 1979.
607 J. Combet, *EPJ Web Conf.*, 2018, p. 03001.
608 E. F. Casassa and H. Eisenberg, *J. Phys. Chem.*, 1961, **65**, 427–433.

609 H. Eisenberg, *Bunsen-Ges. Phys. Chem., Ber.*, 1989, **93**, 350–356.
610 E. F. Casassa and H. Eisenberg, *J. Phys. Chem.*, 1960, **64**, 753–756.
611 M. N. Spiteri, *PhD thesis*, Universite Orsay - Paris-Sud, 1997.
612 K. Nishida, H. Urakawa, K. Kaji, B. Gabrys and J. S. Higgins, *Polymer*, 1997, **38**, 6083–6085.
613 F. Boue, J. Cotton, A. Lapp and G. Jannink, *J. Chem. Phys.*, 1994, **101**, 2562–2568.
614 K. Nishida, K. Kaji, T. Kanaya and T. Shibano, *Macromolecules*, 2002, **35**, 4084–4089.
615 M. Ragnetti and R. Oberthur, *Colloid Polym. Sci.*, 1986, **264**, 32–45.
616 We calculate $P(q)$ by dividing the $F(q)$ in Kassapidou's paper by 40, the degree of polymerisation of the sample.
617 M. Spiteri, F. Boue, A. Lapp and J. Cotton, *Phys. Rev. Lett.*, 1996, **77**, 5218.
618 J. S. Pedersen and P. Schurtenberger, *Macromolecules*, 1996, **29**, 7602–7612.
619 P. Sharp and V. A. Bloomfield, *Biopolymers*, 1968, **6**, 1201–1211.
620 M. Nierlich, F. Boue, A. Lapp and R. Oberthur, *Colloid Polym. Sci.*, 1985, **263**, 955–964.
621 A. Yethiraj and C.-Y. Shew, *Phys. Rev. Lett.*, 1996, **77**, 3937.
622 A. Yethiraj, *J. Chem. Phys.*, 1998, **108**, 1184–1192.
623 E. Josef and H. Bianco-Peled, *Soft Matter*, 2012, **8**, 9156–9165.
624 Compare for example the values of $l_p \simeq 5$ Å reported by Josef Bianco-Peled[623] for alginate with the more reasonable estimates of $l_p \simeq 50$–150 Å obtained in earlier literature.[339,707–709].
625 B. D. Ermi and E. J. Amis, *Macromolecules*, 1998, **31**, 7378–7384.
626 M. Sedlak, *J. Chem. Phys.*, 1996, **105**, 10123–10133.
627 M. Schmidt, *Die Makromolekulare Chemie, Rapid Communications*, 1989, **10**, 89–96.
628 M. Sedlak and E. J. Amis, *J. Chem. Phys.*, 1992, **96**, 826–834.
629 M. Sedlak and E. J. Amis, *J. Chem. Phys.*, 1992, **96**, 817–825.
630 W. F. Reed, *Macromolecules*, 1994, **27**, 873–874.
631 K. S. Schmitz, *Biopolymers*, 1993, **33**, 953–959.
632 Y. Zhang, J. F. Douglas, B. D. Ermi and E. J. Amis, *J. Chem. Phys.*, 2001, **114**, 3299–3313.
633 R. C. Michel and W. F. Reed, *Biopolymers*, 2000, **53**, 19–39.
634 D. P. Norwood, M. Benmouna and W. F. Reed, *Macromolecules*, 1996, **29**, 4293–4304.
635 M. Sedlak, *Macromolecules*, 1993, **26**, 1158–1162.
636 M. Sedlak, *Macromolecules*, 1995, **28**, 793–794.
637 M. Sedlak, *J. Chem. Phys.*, 2005, **122**, 151102.
638 M. Sedlak, *J. Chem. Phys.*, 2002, **116**, 5246–5255.
639 M. Sedlak, *J. Chem. Phys.*, 2002, **116**, 5236–5245.
640 R. Cong, E. Temyanko, P. S. Russo, N. Edwin and R. M. Uppu, *Macromolecules*, 2006, **39**, 731–739.
641 A. Takahashi, N. Kato and M. Nagasawa, *J. Phys. Chem.*, 1970, **74**, 944–946.
642 J. S. Higgins and H. C. Benoit, *Polymers and Neutron Scattering*, Oxford University Press, 1994.
643 M. Oostwal and T. Odijk, *Macromolecules*, 1993, **26**, 6489–6497.
644 K. Zero and B. Ware, *J. Chem. Phys.*, 1984, **80**, 1610–1616.
645 A. Sehgal and T. A. Seery, *Macromolecules*, 2003, **36**, 10056–10062.
646 J. P. Wilcoxon and J. M. Schurr, *J. Chem. Phys.*, 1983, **78**, 3354–3364.
647 D. Hoagland, E. Arvanitidou and C. Welch, *Macromolecules*, 1999, **32**, 6180–6190.
648 C. G. Lopez and W. Richtering, *Cellulose*, 2019, **26**, 1517–1534.
649 M. Schmidt, *Macromolecules*, 1984, **17**, 553–560.
650 T. Kanematsu, T. Sato, Y. Imai, K. Ute and T. Kitayama, *Polym. J.*, 2005, **37**, 65–73.
651 W. Brown and T. Nicolai, *Colloid Polym. Sci.*, 1990, **268**, 977–990.
652 M. Doi and S. F. Edwards, *The theory of polymer dynamics*, Oxford University Press, 1988, vol. 73.
653 L. Nicholson, J. Higgins and J. Hayter, *Macromolecules*, 1981, **14**, 836–843.
654 S.-C. Lin and J. M. Schurr, *Biopolymers*, 1978, **17**, 425–461.
655 N. Borochov, H. Eisenberg and Z. Kam, *Biopolymers*, 1981, **20**, 231–235.
656 U. Bohme and U. Scheler, *Macromol. Chem. Phys.*, 2007, **208**, 2254–2257.
657 K. D. Collins, *Biophys. Chem.*, 2012, **167**, 43–59.
658 K. I. Assaf and W. M. Nau, *Angew. Chem., Int. Ed.*, 2018, **57**, 13968–13981.
659 K. D. Collins, *Q. Rev. Biophys.*, 2019, **52**, e11.
660 N. Malikova, S. Čebašek, V. Glenisson, D. Bhowmik, G. Carrot and V. Vlachy, *Phys. Chem. Chem. Phys.*, 2012, **14**, 12898–12904.
661 M. Hohenschutz, I. Grillo, O. Diat and P. Bauduin, *Angew. Chem.*, 2020, **132**, 8161–8165.
662 K. P. Gregory, G. R. Elliott, H. Robertson, A. Kumar, E. J. Wanless, G. B. Webber, V. S. Craig, G. G. Andersson and A. J. Page, *Phys. Chem. Chem. Phys.*, 2022, **24**, 12682–12718.
663 F. Lu, J. Song, B.-W. Cheng, X.-J. Ji and L.-J. Wang, *Cellulose*, 2013, **20**, 1343–1352.
664 X. Chen, S. Liang, S.-W. Wang and R. H. Colby, *J. Rheol.*, 2018, **62**, 81–87.
665 K. Aoki, A. Sugawara-Narutaki, Y. Doi and R. Takahashi, *Macromolecules*, 2022, **55**, 5591–5600.
666 A. Sadeghpour, A. Vaccaro, S. Rentsch and M. Borkovec, *Polymer*, 2009, **50**, 3950–3954.
667 A. Gallegos, G. M. Ong and J. Wu, *Soft Matter*, 2021, **17**, 9221–9234.
668 K. Bohinc, D. Kovacevic and J. Požar, *Phys. Chem. Chem. Phys.*, 2013, **15**, 7210–7219.
669 J. Szymczak, P. Holyk and P. Ander, *J. Phys. Chem.*, 1975, **79**, 269–272.
670 J. Požar, K. Bohinc, V. Vlachy and D. Kovačević, *Phys. Chem. Chem. Phys.*, 2011, **13**, 15610–15618.
671 G. Vesnaver, M. Rudez, C. Pohar and J. Skerjanc, *J. Phys. Chem.*, 1984, **88**, 2411–2414.
672 H. Daoust and A. Hade, *Macromolecules*, 1976, **9**, 608–611.
673 K. Kaji, H. Urakawa, T. Kanaya and R. Kitamaru, *Macromolecules*, 1984, **17**, 1835–1839.
674 B. A. Rogers, H. I. Okur, C. Yan, T. Yang, J. Heyda and P. S. Cremer, *Nat. Chem.*, 2022, **14**, 40–45.

675 U. P. Strauss and P. D. Ross, *J. Am. Chem. Soc.*, 1959, **81**, 5299–5302.
676 U. P. Strauss, D. Woodside and P. Wineman, *J. Phys. Chem.*, 1957, **61**, 1353–1356.
677 I. Satake, M. Fukuda, T. Ohta, K. Nakamura, N. Fujita, A. Yamauchi and H. Kimizuka, *J. Polym. Sci., Polym. Phys. Ed.*, 1972, **10**, 2343–2354.
678 W. Bare and E. Nordmeier, *Polym. J.*, 1996, **28**, 712–726.
679 D. M. Correia, L. C. Fernandes, P. M. Martins, C. Garcia-Astrain, C. M. Costa, J. Reguera and S. Lanceros-Mendez, *Adv. Funct. Mater.*, 2020, **30**, 1909736.
680 T. Huang, M.-C. Long, X.-L. Wang, G. Wu and Y.-Z. Wang, *Chem. Eng. J.*, 2019, **375**, 122062.
681 A. S. Gouveia, M. Yanez, V. D. Alves, J. Palomar, C. Moya, D. Gorri, L. C. Tome and I. M. Marrucho, *Sep. Purif. Technol.*, 2021, **259**, 118113.
682 A. M. Smith, A. A. Lee and S. Perkin, *J. Phys. Chem. Lett.*, 2016, **7**, 2157–2163.
683 A. Matsumoto, R. Yoshizawa, O. Urakawa, T. Inoue and A. Q. Shen, *Macromolecules*, 2021, **54**, 5648–5661.
684 A. A. Lee, C. S. Perez-Martinez, A. M. Smith and S. Perkin, *Faraday Discuss.*, 2017, **199**, 239–259.
685 J. Zeman, S. Kondrat and C. Holm, *Chem. Commun.*, 2020, **56**, 15635–15638.
686 J. Zeman, S. Kondrat and C. Holm, *J. Chem. Phys.*, 2021, **155**, 204501.
687 S. A. Safran and P. Pincus, *Soft Matter*, 2023, **19**, 7907–7911.
688 E. Krucker-Velasquez and J. W. Swan, *J. Chem. Phys.*, 2021, **155**, 134903.
689 S. Kumar, P. Cats, M. B. Alotaibi, S. C. Ayirala, A. A. Yousef, R. van Roij, I. Siretanu and F. Mugele, *J. Colloid Interface Sci.*, 2022, **622**, 819–827.
690 Y. C. Fung and S. Perkin, *Faraday Discuss.*, 2023, **246**, 370–386.
691 H. Jager, A. Schlaich, J. Yang, C. Lian, S. Kondrat and C. Holm, *Faraday Discuss.*, 2023, **246**, 520–539.
692 J. Yang, S. Kondrat, C. Lian, H. Liu, A. Schlaich and C. Holm, *Phys. Rev. Lett.*, 2023, **131**, 118201.
693 A. Hartel, M. Bultmann and F. Coupette, *Phys. Rev. Lett.*, 2023, **130**, 108202.
694 A. A. Lee, C. S. Perez-Martinez, A. M. Smith and S. Perkin, *Phys. Rev. Lett.*, 2017, **119**, 026002.
695 M. Biesalski, D. Johannsmann and J. Ruhe, *J. Chem. Phys.*, 2004, **120**, 8807–8814.
696 G. Liu, D. Parsons and V. S. J. Craig, *J. Colloid Interface Sci.*, 2020, **579**, 369–378.
697 We do not consider the data in Fig. 24 and 12 to provide clear tests to the scaling electrostatic blob because in both cases, the fraction of free counterions was not established independently.
698 A. Rohatgi, *Webplotdigitizer: Version 4.6*, 2022, **https://automeris.io/WebPlotDigitizer**.
699 B. Brettmann, P. Pincus and M. Tirrell, *Macromolecules*, 2017, **50**, 1225–1235.
700 T. H. Pial, H. S. Sachar and S. Das, *Macromolecules*, 2021, **54**, 4154–4163.
701 J. Yu, N. E. Jackson, X. Xu, B. K. Brettmann, M. Ruths, J. J. De Pablo and M. Tirrell, *Sci. Adv.*, 2017, **3**, eaao1497.
702 B. K. Brettmann, N. Laugel, N. Hoffmann, P. Pincus and M. Tirrell, *J. Polym. Sci., Part A: Polym. Chem.*, 2016, **54**, 284–291.
703 J. Yu, N. Jackson, X. Xu, Y. Morgenstern, Y. Kaufman, M. Ruths, J. De Pablo and M. Tirrell, *Science*, 2018, **360**, 1434–1438.
704 D. F. Hodgson and E. J. Amis, *J. Chem. Phys.*, 1989, **91**, 2635–2642.
705 H. D. B. Jenkins and Y. Marcus, *Chem. Rev.*, 1995, **95**, 2695–2724.
706 T. Spychaj, M. Bohdanecky and D. Berek, *Acta Polym.*, 1986, **37**, 93–96.
707 B. Maciel, C. Oelschlaeger and N. Willenbacher, *Colloid Polym. Sci.*, 2020, **298**, 791–801.
708 M. Rinaudo and D. Graebling, *Polym. Bull.*, 1986, **15**, 253–256.
709 F. G. D. Banos, A. I. D. Pena, J. G. H. Cifre, M. C. L. Martinez, A. Ortega and J. G. de la Torre, *Carbohydr. Polym.*, 2014, **102**, 223–230.